# IR WINDOW STUDIES

Ferdinand A. Kroger, et al

University of Southern California

Prepared for:

Air Force Cambridge Research Laboratories
Defense Advanced Research Projects Agency

15 June 1974

UNCLASSIFIED

SECURITY CLASSIFICATION OF THIS PAGE (When Data Entered)

AD/A-003 393

# REPORT DOCUMENTATION PAGE

READ INSTRUCTIONS BEFORE COMPLETING FORM

| | |
|---|---|
| 1. REPORT NUMBER: AFCRL-TR-74-0441 | 2. GOVT ACCESSION NO. |
| 3. RECIPIENT'S CATALOG NUMBER | |
| 4. TITLE (and Subtitle): IR WINDOW STUDIES | 5. TYPE OF REPORT & PERIOD COVERED: Scientific - Interim. Quarterly Report No. 8 |
| 6. PERFORMING ORG. REPORT NUMBER: USCEE Report 476 | |
| 7. AUTHOR(s): Ferdinand A. Kroger, John H. Marburger | 8. CONTRACT OR GRANT NUMBER(s): F19628-72-C-0275 |
| 9. PERFORMING ORGANIZATION NAME AND ADDRESS: University of Southern California, Electronic Sciences Laboratory, Los Angeles, California 90007 | 10. PROGRAM ELEMENT, PROJECT, TASK AREA & WORK UNIT NUMBERS: Project #2055, DoD Element 61101D |
| 11. CONTROLLING OFFICE NAME AND ADDRESS: Air Force Cambridge Research Laboratories (LQ), Hanscom AFB, Massachusetts 01731, Contract Monitor: A. Kahan/LQO | 12. REPORT DATE: 15 JUNE 1974 |
| | 13. NUMBER OF PAGES: 101 |
| 14. MONITORING AGENCY NAME & ADDRESS (if different from Controlling Office) | 15. SECURITY CLASS. (of this report): UNCLASSIFIED |
| | 15a. DECLASSIFICATION/DOWNGRADING SCHEDULE |

16. DISTRIBUTION STATEMENT (of this Report)

A--Approved for public release; distribution unlimited

17. DISTRIBUTION STATEMENT (of the abstract entered in Block 20, if different from Report)

18. SUPPLEMENTARY NOTES

This Research was sponsored by Defense Advanced Research Projects Agency, ARPA Order No. 2055

19. KEY WORDS (Continue on reverse side if necessary and identify by block number)

IR Windows
Alkali Halides
III-V Semiconductors
II-VI Semiconductors
Thermal Lensing
IR Absorption



20. ABSTRACT (Continue on reverse side if necessary and identify by block number)

A sixth melt-grown GaAs sample showed the same absorption characteristic as before. Oxygen regulation in $H_2$ and in liquid gallium with the aid of electrochemical pumping was found to favorably affect epitaxial growth. A first run was made with the high-temperature epitaxial growth apparatus. Twinning does not represent a deformation mechanism for GaAs at room temperature. CdTe shows extra diffuse reflections and anomalous streaks in electron diffraction due to thermal diffuse scattering. Comparison of electron concentrations in CdTe in

DD FORM 1 JAN 73 1473 EDITION OF 1 NOV 65 IS OBSOLETE

UNCLASSIFIED

SECURITY CLASSIFICATION OF THIS PAGE (When Data Entered)

equilibrated and quenched samples show that excess cadmium precipitates during cooling. Annealing of indium doped crystals close to the conductivity cut-off lead to low 10.6μm absorption for thin, but not for thick samples. Work on the defect structure of ZnSe and ZnSe-Al has started. Free electron absorption is $\lambda^3$. The high 10.6μm absorption of KBr is probably due to $BrO_3^-$ or other oxygen containing species. Attempts to reduce absorption by reduction have so far failed. Y-cut quartz is a satisfactory piezoelectric material for studies of KCl by surface waves. The diffraction theory of thermal lensing was extended to anisotropic materials. A method is developed to determine experimentally the contributions of non-linear dipole moments and anharmonic forces to multi-phonon absorption. The new TEA laser for damage studies was tested, and calculations were made of the dependence of bulk damage on spot-size for random inclusions.

AFCRL-TR-74-0441

USCEE Report 476

# IR WINDOW STUDIES

Ferdinand A. Kroger
John H. Marburger

Electronic Sciences Laboratory
University of Southern California
Los Angeles, California 90007

15 June 1974

Quarterly Technical Report No. 8



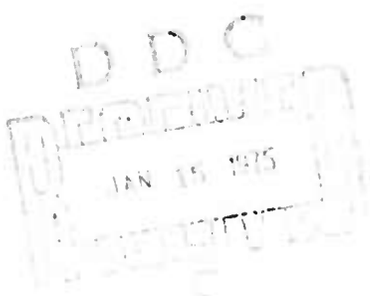


Sponsored By:

Defense Advanced Research Projects Agency
ARPA Order No. 2055

Monitored by

AIR FORCE CAMBRIDGE RESEARCH LABORATORIES
AIR FORCE SYSTEMS COMMAND
UNITED STATES AIR FORCE
HANSCOM AFB, MASSACHUSETTS 01731

ARPA Order No. 2055

Program Code No. 3D10

Effective Date of Contract 1 June 1972

Contractor: University of Southern California

Contract No. F19628-72-C-0275

Principal Investigator and Phone No.
Prof. F. A. Kroger/213 746-6224
Prof. John H. Marburger/213 746-2227/9

AFCRL Project Scientist and Phone No.
Alfred Kahan/617 861-4014

Contract Expiration Date 30 November 1973

CONTENTS

# 1. INTRODUCTION

The format of this report follows closely that of the first quarterly report in which projects are identified by codes keyed to the contract work statement.

The various categories are briefly:

a) Crystal growth
b) Polycrystalline window fabrication
c) Mechanical properties of window materials
d) Window material defect characterization
e) Theory of residual IR optical absorption
f) Absorption measurement techniques
g) Theoretical evaluation of optical performances of windows

## a.1 Epitaxial Growth of Semi-Insulating GaAs from Ga Solutions

P.S. Vijaykumar and J. M. Whelan

The final fabrication of two quartz slider assemblies for the epitaxial growth experiments were completed. One of these was intended for use in a system in which the $H_2$ atmosphere purity could be monitored and adjusted by use of calcia stabilized zirconia tubes used as oxygen gages and pumps. This latter system was tested extensively. The major conclusions were that $H_2$ from a Pd diffusion and a gas manifold system could be readily adjusted so that its water content varied from 0.2 to 80 ppm for flow rates between 100 and 300 ssc/min. Water contents of the $H_2$ supplied to the zirconia gage/pump section varied from 3 to 6 ppm, the higher concentrations following increases in the room temperature by up to 10°C. These fluctuations suggest that the background water concentration is due to outgassing.

The ratio of $H_2O/H_2$ increased from the minimal value of 0.2 ppm to the 2-6 ppm range when the $H_2$ passed through the epitaxy quartz envelope at 700°C. Several growths at 700°C demonstrated that this purity was not degraded by introducing the Ga melt to the system. However, if the nominal growth temperature was raised to 800°C the exhaust $H_2$ increased in $H_2O$ content to 40 ppm. This is due to the original oxides on the melt being reduced to $Ga_2O$ (g) which decomposes to Ga (1) and $Ga_2O_3$ (s) at $\sim$ 550° and these products then determine the $H_2O$ concentration. This is about the maximum concentration allowable if Cr as a dopant is not to be oxidized and hence lost from the melt.

The above system has also a provision for pumping oxygen directly from the melt. Several trial runs indicated that the advantages do appear in that better growths are achieved at lower temperatures with than without pumping.

In our systems and in others used elsewhere Cajon type O-ring joints are used to slide the melt assembly into the growth furnace. The use of the fast responding zirconia tubes has demonstrated that these seals can leak seriously unless great care is taken to adjust the compression on the O-ring and to maintain good alignment of the tube transversing the seal.

The second liquid phase epitaxial system was completed. It differs from the first in that it is designed for use at higher temperature and provides for the introduction of a vertical gradient during growth. Operation of this system will benefit greatly from the experience with the first one.

## a.2 Optimization of Alkali Halide Window Materials

P. J. Shlichta and James Yee

a.2.1 Objectives and Approach: At the beginning of 1974, this part of the program was redirected toward resolving the thousandfold discrepancy between the theoretically predicted and experimentally observed 10.6μ absorptivity of KBr cyrstals. Earlier work had shown that our purification techniques -- ion exchange, fractional crystallization, and treatment of the molten salt with $Br_2$ and HBr -- although previously successful in reducing the absorptivity of KCl, resulted in KBr crystals having 10.6μ absorptivities no lower than those of commercial crystals (i.e., about $10^{-3}cm^{-1}$). Attempts at treatment with organic bromides, such as $CBr_4$ and $C_2H_5Br$, were invariably unsuccesful because of the spontaneous decomposition of these reagents with formation of carbon.

Absorption in the region near 10.6μ is usually due to vibrational modes of polyatomic ions. A recent review (ref. 1) has suggested that the observed excess absorption could be caused by parts-per-million concentrations of anions such as $HCO_3^-$, $NO_2^-$, $SO_4^=$, or $CrO_4^=$. It seems likely, however, that our purification procedures would substantially eliminate, or at least greatly reduce, the concentrations of these ions. The inefficacy of ion exchange and HBr treatment in eliminating this impurity suggest either a momovalent anion with a nonvolatile acid anhydride or else a product of reaction of molten KBr with residual air or water and/or with the crucible material. Since crystals grown from $KBrO_3$-doped KBr have shown a fiftyfold enhancement in 10.6μ absorptivity (ref. 2), it has been tentatively assumed that the principal infrared-absorbing impurity in KBr is either bromate ion or some decomposition product thereof. Therefore, our present program is directed toward the goals of (a) unambiguously identifying the impurity (or impurities) responsible for the excess 10.6μ absorption and (b) developing a purification technique which will completely remove it.

The attainment of the first objective is complicated by the possibility that bromate ions in molten KBr may be unstable enough to decompose to some other species of impurity. At high temperatures, $KClO_3$ either decomposes into KCl and oxygen or disproportionates into KCl and $KClO_4$ (ref. 3). It is possible that similar reactions occur in KBr:$BrO_3$; on the other hand, the stabilization of isolated $BrO_3^-$ ions in the KBr matrix may be strong enough to prevent this. To resolve this ambiguity, bromate-doped KBr powders are being prepared by

solution evaporation and pressed into polycrystalline disks for infrared absorption spectrophometry.

Our approach to the second objective is based on a distinction between metathesis and reduction as methods of removing impurities from alkali halides. Reagents such as HBr, $Br_2$, and $CCl_4$ are effective in removing oxide or hydroxide ions because (as shown in the left-hand column of Table 1) these ions can be converted to volatile molecules without oxidation or reduction. The bromate ion, however, has no stable volatile anhydride and, judging from its effect on 10.6μ absorptivity, is too stable to break down into a bromide ion and gaseous oxygen. It can apparently be removed only by reduction to bromide and either oxide or oxygen bound in a volatile reaction product. Therefore (as shown in the right-hand column of Table 1), free bromine has no effect and HBr or $CCl_4$ can only react by a thermodynamically improbable oxidation to form free halogen. It seems likely that bromate can only be removed by a strong reducing agent. Thus far, two have been suggested and are now being tried.

The most powerful non-contaminating reducing agent would presumably be potassium vapor which, at least in molten KBr, would be expected to reduce all bromate ions to bromide and oxide (Table 1). In solid KBr, however, the reaction must be written

$$6K(g) \longrightarrow 6K_K + 6V_{Br} \quad ;$$

$$6V_{Br} + (BrO_3)_{Br} \longrightarrow 3(O_{Br}^{-}V_{Br}^{+}) + Br_{Br}$$

The indicated charges are effective charges; $V_{Br}$ is an F center, $V_{Br}^{+}$ a bromine ion vacancy. Thus six F-centers must react with the bromate ion (in a single anion site) to produce three oxide ions with associated anion vacancies. Since the creation of an oxide-vacancy complex entails the local loss of lattice energy, it is not obvious which way this reaction would go. Moreover, it is perhaps possible that the oxide-vacancy complex might itself have an infrared absorption. Therefore, treatment with potassium vapor is less likely to remove bromate from solid KBr than from the molten salt and, in any case, it would probably be desirable to remove the oxide thus formed by subsequent treatment with HBr.

An alternative procedure, suggested by A. Kahan of AFCRL, would be treatment of either molten or solid KBr with $C_2F_4$, which can be generated by the pyrolysis of teflon (ref. 4). This reagent has been reported to be

extremely effective in removing oxygen from fluorite crystals (ref. 5, 6) and has even been used for purifying NaCl (ref. 7). As shown in Table 1, $C_2F_4$ is not only effective for the metathetic replacement of oxide by fluoride, but it is also, because of its carbon-carbon double bond, a strong reducing agent which can be expected to reduce bromate to bromide by reacting with the oxygen to form carbonyl fluoride. This approach, however, has several potential disadvantages. It might lead to the formation of anions such as fluorocarbonate

$$COF_2 + O^{=} \longrightarrow (FCOO)^{-} + F^{-}$$

which, if incorporated into the KBr lattice, would certainly cause some form of infrared absorption. Moreover, the spontaneous decomposition of $C_2F_4$ to form $CF_4$ and carbon, although reported to occur only above 1200° C (ref. 5), might nonetheless occur at lower temperatures to a sufficient extent to contaminate the melt with carbon particles. For this reason, treatment with $C_2F_4$ is perhaps more attractive for KBr crystals than as a pretreatment for the molten salt. It should also be noted that this procedure is extremely hazardous, not only because of the toxicity of $C_2F_4$ and its reaction products but also because high concentrations of $C_2F_4$ are potentially explosive. Another disadvantage -- the incorporation of fluoride ions into the KBr lattice -- is regarded as trivial since these ions would presumably have no effect on the infrared absorption and, in any case, could easily be removed by subsequent treatment with HBr. Despite all these possible disadvantages, treatment with $C_2F_4$ is probably the most promising approach to KBr purification that has been suggested thus far.

The incorporation of these approaches into our revised research program is shown schematically in Figure 1. Summaries of our activities during the last three months are detailed in the following paragraphs. Thus far, our preliminary attempts at treatment of KBr with potassium vapor and $C_2F_4$, although inconclusive, have indicated that we may have to revise our approaches substantially.

a.2.2 Evaluation of Purification Techniques*: The use of ion exchange and

*This part of our project was carried out by Mr. Dal-Oong Park, of the USC Chemical Engineering Department, as part of his directed research requirements for a Master's degree.

fractional crystallization for purifying alkali halides has received considerable study (ref. 8) and most of the specific procedures now used at USC have previously been successfully used elsewhere (ref. 9). Nonetheless, it has seemed prudent to make use of all available analytical facilities to check the efficiency and reliability of our procedures. In particular, we wished to determine whether our ion exchange columns were operating at maximum efficiency, whether our handling procedures were introducing any contaminants into the purified salt, whether our two-stage fractional crystallization -- the most tedious part of our procedure -- was really necessary, and whether our purified salt was comparable to the best available commercially purified KBr (i.e., "Suprapur" KBr from E. Merck).

The ions analyzed thus far -- calcium, magnesium, and sodium -- were chosen because they can readily be determined by means of our atomic absorption apparatus (Perkin Elmer model 306) using light sources presently available to us. Calcium and magnesium can be used to characterize the efficiency with which the ion exchange system removes divalent cations. Sodium is expected to be unaffected by passage through ion exchange columns but should be concentrated in the solution fractions of the fractional cyrstallization process.

Figure 2 illustrates the sampling procedure employed. Experiment 1 followed the complete process, as detailed in our earlier reports, from reagent-grade solution to moist crystals. Experiment 2 used the same starting solution in an abreviated process in which the first fractional crystallization was eliminated. Experiment 3 used a heavily doped starting solution in order to investigate the effect of extremely high impurity concentrations on the performance of the ion exchange column.

Only one analytical difficulty was encountered. The high concentrations of KBr in the sample solutions (15 to 36 weight %) hindered reproducible atomic absorption measurements. During sample vaporization, some solid KBr crystallized out, partially clogging the burner so that particles of dried salt entered the flame and caused erratic measurements. Moreover, attempts to calibrate the system with standard solutions containing varying concentrations of KBr resulted in irreproducible low values. Therefore, in order to achieve reproducibility, at some sacrifice of sensitivity, all sample and calibration solutions were diluted to 5 wt. % KBr.

The results of these analyses are shown in Table 2. The calcium concentration was reduced by ion exchange to less than the limit of detection in experiments 1 and 2 and reduced by a factor of nearly 4000 in experiment 3. The magnesium concentration was reduced by a factor of about 60 in all ion

exchange experiments and was essentially unchanged by fractional crystallization. The sodium concentration, as expected, was unaffected by ion exchange but was reduced by a factor of 15 to 30 by fractional crystallization. The difference between the sodium concentrations of the E fractions of experiments 1 and 2 is consistent with earlier observations (ref. 8) that the rejection of sodium during KBr crystallization is extremely sensitive to the rate of crystal growth.

On the basis of these data, we have tentatively concluded that:

(A) our ion exchange columns are operating efficiently and are satisfactorily removing all polyvalent cations except magnesium, which is probably the most difficult divalent cation to remove in this manner,

(B) there is no evidence of recontamination during fractional crystallization and solution transfer,

(C) the fractional crystallization process is probably unnecessary for removing polyvalent cations and useful but inadequate for removing sodium, whose concentration might profitably be reduced (e.g., by precipitation with zinc uranly acetate) prior to ion exchange, and

(D) with the exception of sodium, the cation concentrations are comparable to or lower than those of Merck "suprapur" KBr.

In the future, if time and funding permit, our analytical studies will be extended to include analyses of gas-treated melts, determination of silicon concentrations -- particularly to determine whether melting KBr in fused silica crucibles causes contamination with silicate -- and, most important of all, determination of anion concentrations. The last is, however, contingent upon our obtaining access to facilities for potentiometric electrode analysis.

a.2.3 Crystal Pulling: During the present report period, we suffered a loss of both equipment and personnel. Early in May, the Lepel crystal pulling apparatus, which has been on load to us from another project, ceased to be available. Fortunately, we acquired an obsolete Futurecraft crystal puller, donated to USC by the Wacker Corporation. This has now been sufficiently reconditioned (using the growth chamber, pull rod, and transparent furnace described in previous reports) to be operational, and crystals of KBr have recently been pulled from this apparatus at rates of up to 5cm/hr.

Simultaneously, Dr. Robert E. Chaney left USC for the Motorola Coporation and was replaced on the project by Dr. James Yee.

At present, we are trying to grow KBr crystals, from both purified and bromate-doped melts, in sufficient quantity to provide samples for our experiments with $C_2F_4$ and potassium vapor. During recent attempts to grow

heavily bromate-doped KBr crystals by melting a mixture of KBr and $KBrO_3$ -- rather than by first crystallizing KBr from a bromate-doped solution, as in previous experiments -- it was noted that gas evolved copiously from the heated mixture well below the melting point of KBr. As will be discussed below, this observation may be of considerable significance.

a.2.4 Annealing in $C_2F_4$: Our first experiments with the pyrolysis of teflon were aimed at determining the feasibility of using teflon itself to purify molten KBr, e. g. by using expendable teflon crucible liners. We therefore wished to determine the approximate rate of teflon decomposition at 750°C and the likelihood of carbon formation.

In the first experiment, a 0.5 gram sample of teflon was placed in an 8" silica tube, which was then evacuated to $10^{-2}$ torr, sealed and placed in a furnace so that the end containing the teflon was at 750°C, while the other end, sticking out of the furnace, was at about 200°C. After ten minutes, when the tube was removed from the furnace, the teflon had disappeared and a coating of carbon had formed in all portions of the tube but especially at the cold end.

The second experiment made use of a silica tube in a temperature gradient sealed at the hot (700°C) end and connected to a vacuum pump, vacuum gauge, and sliding thermocouple at the cold (100°) end. A teflon cylinder was attached to the end of the sliding thermocouple, so that it could be positioned at any temperature in the tube. The furnace was provided with a window so that any carbon deposition at the hot end could be immediately observed. After outgassing at 200°C, the teflon was placed in the 700°C while the vacuum pump continued to evacuate the tube. Within 30 seconds, the pressure in the tube rose to 5 Torr and a brown deposit was observed on the tube in the vicinity of the sample. The teflon was then withdrawn to the cold end but the teflon sample fell off in the 500-600°C zone, where, within 60 seconds (when the tube was withdrawn from the furnace) another region of carbon deposition was formed. The teflon cylinder had by then swelled into a rigid foam (Figure 3) and had lost 27% of its original weight.

These observations suggest that:

(A) At temperatures above 600°C, teflon decomposed too rapidly to be useful for processing KBr; these observations are consistent with extrapolations of the weight loss data in Reference 4, which indicate that at 750°C, a teflon sample should disappear completely within a few minutes.

(B) $C_2F_4$ can decompose to form carbon at temperatures well below 700°C. The latter conclusion contradicts ref. 5, which claims that carbon is not observed below 1200°C, and ref. 4, which does not report any evidence of carbon formation at 600°C or 700°C. On the other hand, a representative of E. I.

du Pont de Nemours & Co. advised us that $C_2F_4$ can decompose explosively to form carbon and $CF_4$ at almost any temperature. This tends to be confirmed by thermodynamic calculations which indicate that the reaction

$$C_2F_4 \longrightarrow CF_4 + C$$

is exhothermic to the extent to the extent of about 70 Kcal/mole. It would appear that this aspect of the use of $C_2F_4$ needs further study.

The question of safety is also a formidable one. In confirmation of the warnings from du Pont, ref. 10 lists $C_2F_4$ as an explosive gas. Even more important is the toxicity of carbonly fluroide ($COF_4$), the probable reaction product of $C_2F_4$ and oxygen-containing KBr. According to ref. 10, the toxicity of this compound is presumed to be high but is not well understood. We may infer, however, by analogy to the toxic activity of phosgene ($COCl_2$) that carbonyl fluoride acts by hydrolyzing in the lung tissue to form HF. It is therefore probably at least as toxic as phosgene (56 p.p.m. short-term lethal) and is likely also to be an insidious chronic and even cumulative poison.

We would therefore make the following tentative recommendations to anyone contemplating the use of $C_2F_4$ for purifying either alkali halides or alkaline earth fluorides:

(1) The use of cylinder $C_2F_4$*, suitably diluted with inert gas is

---

*Commercially available.

---

probably perferable to the pyrolysis of teflon, but extreme caution should be observed to prevent possible explosion.

(2) Unusual safety precautions should be taken to prevent possible escape of the $C_2F_4$ itself and especially of any reaction products such as carbonyl fluoride; specifically, alkali scrub towers should be used on the waste gas.

At USC, we have for the present suspended all use of teflon and $C_2F_4$, because of inadequate safety facilities and are studying the possible use of other unsaturated halocarbons such as $C_2Cl_4$.

a.2.5 Treatment with Potassium Vapor: Cleaved specimens of KBr, having various prior treatments, were suspended at the end of a thermocouple, in the center of a vertical evacuated stainless steel tube having a small resevoir of potassium metal at the bottom (sealed) end, to which was attached a second thermocouple. The specimen thermocouple was used to control the furnance, while, by adjusting the position of the tube in the furnace, the potassium resevoir could be maintained at any desired lower temperature. In this manner, it is possible to control the specimen temperature and potassium

vapor pressure as independent variables. In all the experiments reported below, the specimens were kept at 650°C for 20 hours while the potassium was maintained at 445°C, corresponding to a vapor pressure of 10 Torr. All of these specimens became a uniform transparent deep blue with no indication of light scattering due to inclusions. Their spectrum has not yet been studied. In a parallel set of control experiments, specimens were annealed in a static argon atmosphere for 28 hrs. at 650°C.

The untreated potassium-vapor-treated, and argon-annealed KBr cleaved specimens were then measured, by $CO_2$ laser calorimetry, as described previously to determine their 10.6μ absorptivity. The results are shown in Table 3. The customarily reported absorptivity of KBr ($10^{-3}cm^{-1}$) appears to be substantially unaffected by prolonged annealing in $O_2$ or water-saturated $CO_2$ or even (with the possible exception of the $O_2$ treated samples) by annealing in argon. Treatment with potassium vapor, however, instead of lowering the absorptivity as expected, appears to have increased it by an order of magnitude.

This disconcerting result admits of several interpretations. It may indicate the existence of a color center (or a color center-impurity complex which absorbs in the vicinity of 10.6μ . If so, the absorptivity would probably be lowered by subsequent treatment with HBr. Alternatively, this result may indicate that the oxide ion itself can cause 10.6μ absorption. It has been suggested (ref. 11) that whereas the thermal decomposition of $KBrO_3$ appears to proceed by the reaction

$$2KBrO_3 \longrightarrow 2KBr + 3O_2$$

the decomposition of other bromates may proceed by the evolution of bromine an oxygen to form oxide. It is perhaps possible that bromate ions isolated in a KBr matrix decompose in a similar manner and that the enhanced 10.6μ absorptivity previously reported for bromate-doped KBr is actually due to oxide ions. Future work will therefore include the study of oxide-doped KBr, formed by the sequential treatment of as-received or purified crystals with potassium vapor and then with oxygen.

References


1. C. J. Duthler, J. Applied Physics 45, (1974) p. 2668-71
2. P. J. Shlichta and R. E. Chaney, IR Window Studies Quarterly Report #7 (March 1974) University of Southern Calif. Electronic Sciences Laboratory.
3. Wendall M. Latimer and Joel H. Hildebrand, Reference Book of Inorganic Chemistry, revised ed. (McMillan, New York, 1940), p. 174
4. E. E. Lewis and M. A. Naylor, J. Amer. Chem. Soc., 69 (1967), p. 1968; see also 'Teflon Fluorocarbon Resins - Safety in Handling and Use", (E.I. du Pont de Nemours & Co.) copyright 1970.
5. E. G. Chernevskaya and Z. N. Kovneva, Optical Technology, (english translation) 39 (4) (April 1972) pp. 213-5; see also ibid 38 (11) (November 1971) p. 704.
6. Y. K. Voron'ko, V. V. Osiko, V. T. Udovenchik and M. M. Fursikov, Soviet Physics - Solid State (English translation) 7 (1) (July 1965) p. 204-9.
7. V. F. Pissarenko and S. V. Vonopaeva, Physica Status Solidi 15 (1966), p. 95-6.
8. For a review see F. Rosenberger in Techniques of Ultrapurity, ed. by M. Zey and B. Speights (Marcel Dekker, 1972)
9. W. J. Fredericks, L. W. Schuerman, and L. C. Lewis An Investigation of Crystal Growth Processes (report of Chemistry, Oregon State University 1966) Report AF-AFOSR-217-63 and -66.
10. N. I. Sax, Dangerous Properties of Industrial Materials, 3rd. ed. (Van Nostrand, New York, 1968).
11. G. M. Bancroft and H. D. Gesser, J. Inorg. Nucl. Chem. 27, 1545 (1965).

TABLE 1

| METATHESIS OF OXIDE ION | REDUCTION OF BROMATE ION |
|---|---|
| $2HBr + O^{=} \leftrightarrow H_2O + 2Br^{-}$ | $6HBr + BrO_3^{-} \leftrightarrow 3H_2O + 3Br_2 + Br^{-}$ |
| $2Br_2 + 2O^{=} \leftrightarrow O_2 + 4Br^{-}$ | $Br_2 + BrO_3^{-} \leftrightarrow$ N.R. |
| $CCl_4 + O^{=} \leftrightarrow COCl_2 + 2Cl^{-}$ | $3CCl_4 + BrO_3^{-} \leftrightarrow 3COCl_2 + 3Cl_2 + Br^{-}$ |
| $C_2F_4 + 2O^{=} \leftrightarrow 2CO + 4F^{-}$ | $3C_2F_4 + 2BrO_3^{-} \leftrightarrow 6COF_2 + 2Br^{-}$ |
| $K + O^{=} \leftrightarrow$ N.R. | $6K + BrO_3^{-} \leftrightarrow 6K^{+} + 3O^{=} + Br^{-}$ |

TABLE 2

Chemical Analysis of KBr Solutions

| | CALCIUM | | | MAGNESIUM | | | SODIUM | | |
|---|---|---|---|---|---|---|---|---|---|
| | EXPER. 1 | EXPER. 2 | EXPER. 3 | EXPER. 1 | EXPER. 2 | EXPER. 3 | EXPER. 1 | EXPER. 2 | EXPER. 3 |
| A. Original KBr Solution | 5.37 | 5.37 | 4436. | 6.34 | 6.34 | 6646. | 82.5 | 82.5 | 781. |
| B. After Ion Exchange and Filtration | N.D. | N.D. | 1.07 | .85 | .85 | 104. | 82.9 | 82.9 | 783. |
| C. Primary Crystals | N.D. | - | - | 1.27 | - | - | 29. | - | - |
| D. Primary Filtrate | - | - | - | - | - | - | - | - | - |
| E. Secondary Crystals | N.D. | N.D. | - | 1.10 | .95 | - | 58. | 31. | - |
| F. Secondary Filtrate | N.D. | N.D. | - | 1.27 | 1.69 | - | 262. | 211. | - |
| Estimated Precision | | ± .01 | | | ± .01 | | | ± 1 | |

N.B. All concentration units are molar p.p.m. = moles(impurity)/moles(KBr) × $10^6$.

TABLE 3

10.6 μm Absorption of KBr After Various Treatments

| | BEFORE TREATMENT | | AFTER ANNEALING IN ARGON | | AFTER K VAPOR TREATMENT | |
|---|---|---|---|---|---|---|
| | L [cm] | β [$cm^{-1}$] | L [cm] | β [$cm^{-1}$] | L [cm] | β [$cm^{-1}$] |
| OPTOVAC 9: cleaved rods, as-received | 0.98 | $1.6\times10^{-3}$ | 0.72 | $2.9\times10^{-3}$ | 0.38 | $22.9\times10^{-3}$ |
| OPTOVAC 10: annealed 200 hrs. @ 600°C in $H_2O$-saturated $CO_2$ | 0.68 | 3.4 " | 0.59 | 2.6 " | 0.42 | 11.3 " |
| OPTOVAC 11: annealed 150 hrs. @ 600°C in dry $O_2$ | 0.68 | 2.8 " | 0.39 | 12.4 " | 0.49 | 22.5 " |

FIGURE 1

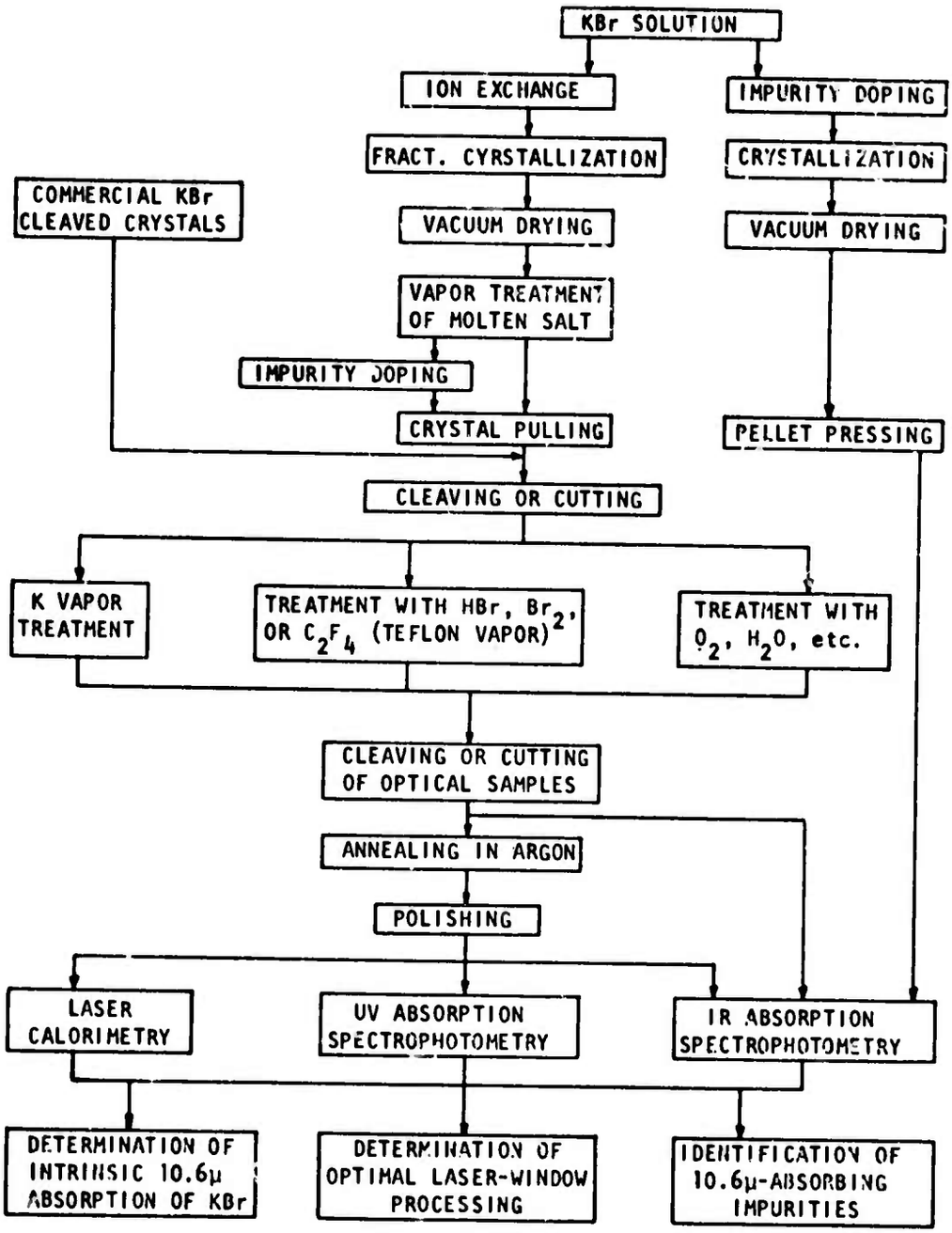
KBr SOLUTION
ION EXCHANGE
IMPURITY DOPING
FRACT. CYRSTALLIZATION
CRYSTALLIZATION
COMMERCIAL KBr CLEAVED CRYSTALS
VACUUM DRYING
VACUUM DRYING
VAPOR TREATMENT OF MOLTEN SALT
IMPURITY DOPING
CRYSTAL PULLING
PELLET PRESSING
CLEAVING OR CUTTING
K VAPOR TREATMENT
TREATMENT WITH HBr, $Br_2$, OR $C_2F_4$ (TEFLON VAPOR)
TREATMENT WITH $O_2$, $H_2O$, etc.
CLEAVING OR CUTTING OF OPTICAL SAMPLES
ANNEALING IN ARGON
POLISHING
LASER CALORIMETRY
UV ABSORPTION SPECTROPHOTOMETRY
IR ABSORPTION SPECTROPHOTOMETRY
DETERMINATION OF INTRINSIC 10.6μ ABSORPTION OF KBr
DETERMINATION OF OPTIMAL LASER-WINDOW PROCESSING
IDENTIFICATION OF 10.6μ-ABSORBING IMPURITIES

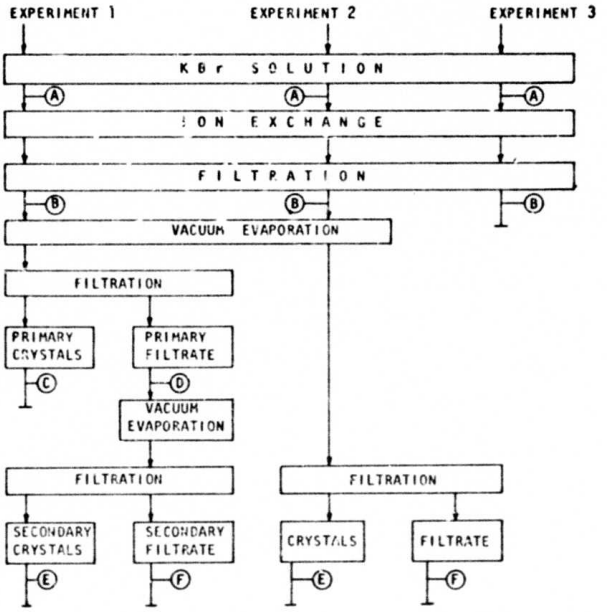


Figure 2

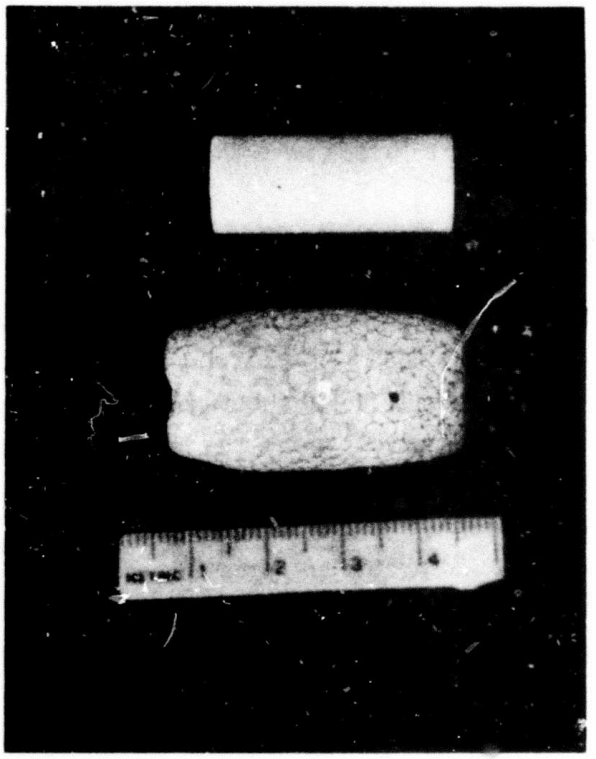

Figure 3

## b.1 Fabrication of Polycrystalline IR Window Materials

S. M. Copley, J. M. Whelan and V. Rana

The aim of this part of the program is to produce CdTe laser window material in polycrystalline form by hot pressing the CdTe powder in the presence of a stable sintering aid.

Experiments have been carried out by hot pressing the CdTe powder with $CdCl_2$ as a sintering aid.

Starting Materials: CdTe used for hot pressings was synthesized from elemental Cd and Te. Both Cd and Te used for this purpose were 99.999% pure, as obtained from Cominco American Incorporated. Procedure for synthesizing CdTe has been described in the earlier report.

This CdTe obtained in the bulk form was crushed and ball milled in WC Jars using WC balls. The resulting powder was separated into different particle sizes by means of a vibrating sieve technique.

$CdCl_2$ used as sintering aid was obtained by purifying Baker analyzed reagent grade $CdCl_2$. Purification was accomplished by subliming in vacuum and recondensing the $CdCl_2$.

The desired amount of $CdCl_2$ was thoroughly mixed with CdTe powder, by dissolving the $CdCl_2$ in deionized water or ethanol and tumbling the resultant solution with CdTe powder. The slurries were then dried at about 110°C and kept in a dessicator before use.

Hot Pressing Operation: Hot pressings were carried out in graphite dies in vacuum using a hot press described in earlier reports.

For some hot pressings the top recess of the graphite die was filled with LiCl-KCl eutectic (melting point 355°C). Utilizing the chill it is possible to have a temperature gradient of 20 to 30°C between the powder and the eutectic. The eutectic melts and seals the powder while the hot pressing is still not complete. Using the seal it has been possible to prevent the vapor loss of the low temperature liquid formed in the hot pressing mixture, thereby observing the role the liquid plays in aiding the hot pressing operation.

Some runs were made using no seal at the top. This allows the volatile liquid phase to slowly escape by effusion leaving behind a highly dense CdTe compact.

Results:

1. CdTe + 50 Vol % $CdCl_2$: Obviously the $CdCl_2$ content was too high to give a high purity CdTe. During preliminary experiments it was observed that

that the effect of $CdCl_2$ on hot pressing of CdTe was different in different temperature ranges. It was decided to carry out experiments using an excess of $CdCl_2$ to facilitate the observation of certain aspects of the compaction process.

A typical result is shown in Figure 1 (graph 1). The densification curve shown is for a powder of particle size less than 32μ , pressed under a pressure of 3500 psi, pressure being maintained as the powder was continuously heated at the rate of 2 to 3°C/min to the final temperature.

There are three stages of compaction:

(i) In the temperature range of 200-350°C, $CdCl_2$ seems to form a liquid phase around CdTe particles at this low temperature, probably by reacting with the surface films present around the particles. There was no measurable grain growth.

(ii) In the temperature range 435 to 475°C during this stage $CdCl_2$ chemically reacts with CdTe forming a liquid phase. There is tremendous grain growth.

(iii) The unreacted $CdCl_2$ melts at 568°C leading to some extra compaction at this temperature.

2. CdTe + 5 Vol % $CdCl_2$: It has been possible to obtain highly dense polycrystalline CdTe samples using 5 vol % $CdCl_2$ and heating the mixture through the first stage only. It yields a very fine grain sized material. If the chemical reaction between CdTe and $CdCl_2$ is slow in this range, then there are chances of obtaining high purity CdTe by suitably evaporating the liquid phase at low temperatures.

(a) Hot Pressing Done Using the Seal: Hot pressings were done either first heating the powder rapidly to 380°C and then applying the pressure of 3500 psi, or first applying this pressure and then heating the powder continuously at the rate of 2 to 3°C/min to 380°C. Both procedures yield highly dense compacts. Starting with a CdTe powder of size less than 32μ, it is possible to obtain a compact having a density of 98.6% of the theoretical density of CdTe.

Evaporation of the liquid was suppressed using the eutectic seal. SEM pictures show CdTe particles coated with the liquid phase. (Figure 2) It seems that the particles are more heavily coated at the edge of the compact than at the center. (Figure 3)

(b) Hot Pressings Done Without Using the Seal: High volatility of the liquid phase was apparent as most of it left the compacts during these runs. Figure 1, Graph 2 shows a typical densification curve. Figure 5, 6, 7 shows the microstructure of the resulting compact.

Annealing experiments are being carried out currently to completely remove

the liquid phase from the compacts, in such a manner that there is no grain growth and the liquid closes all the channels behind it as it escapes.

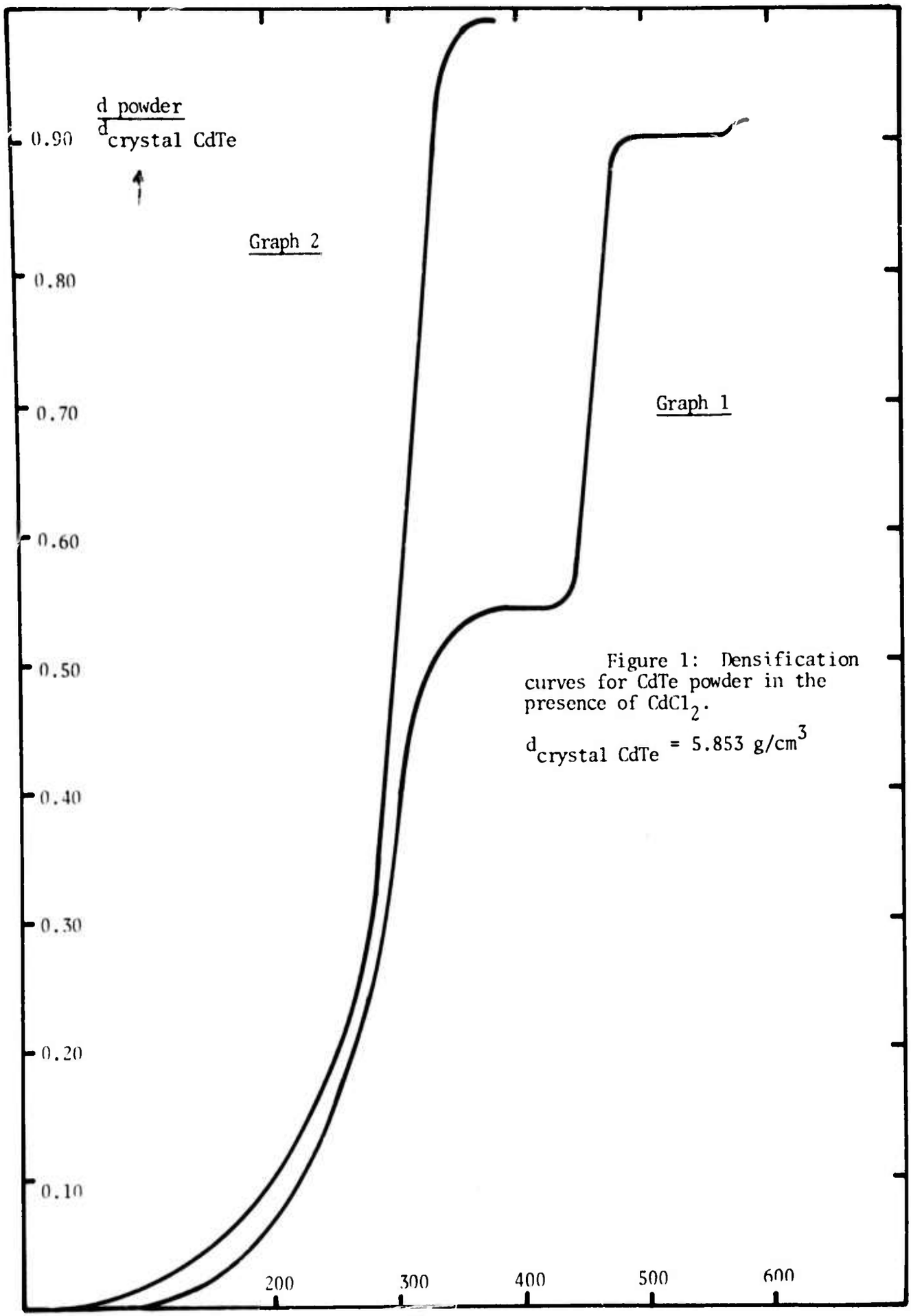


Figure 1: Densification curves for CdTe powder in the presence of $CdCl_2$.

$d_{crystal\ CdTe} = 5.853\ g/cm^3$

Figure 2: Hot pressed CdTe with 5 vol % $CdCl_2$. Powder was first heated to 380°C and then pressured at 3500 psi while the molten seal in the top recess of the die prevents the volatiles from escaping. Micrograph near the center of the compact.

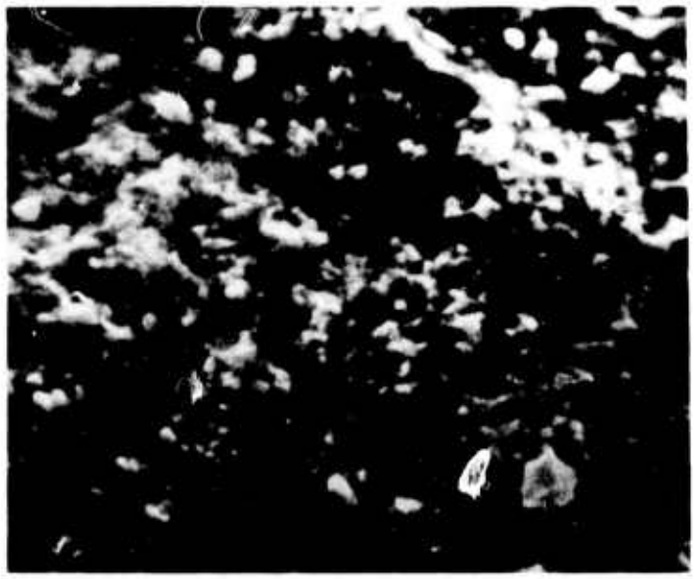

Figure 3: Same compact as in Figure 2. This micrograph shows the area near the surface of the compact.

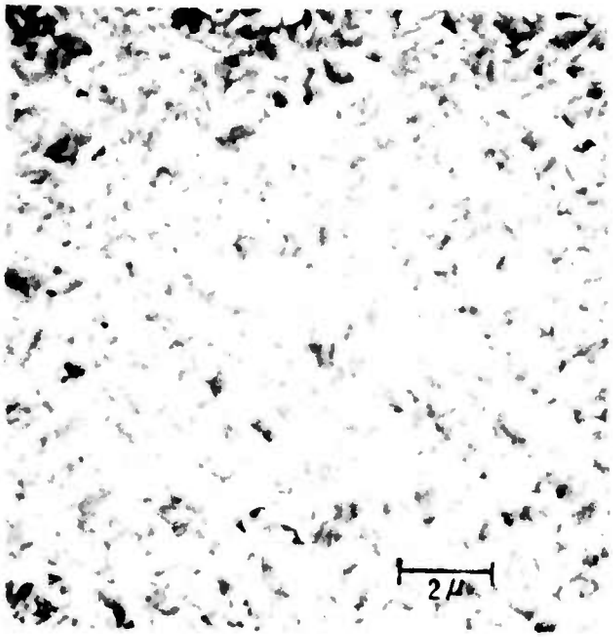


Figure 4

Hot pressed CdTe with 5 vol % $CdCl_2$. A pressure of 3500 psi was applied and maintained while the temperature was continuously raised at the rate of 2 to 3°C/min.

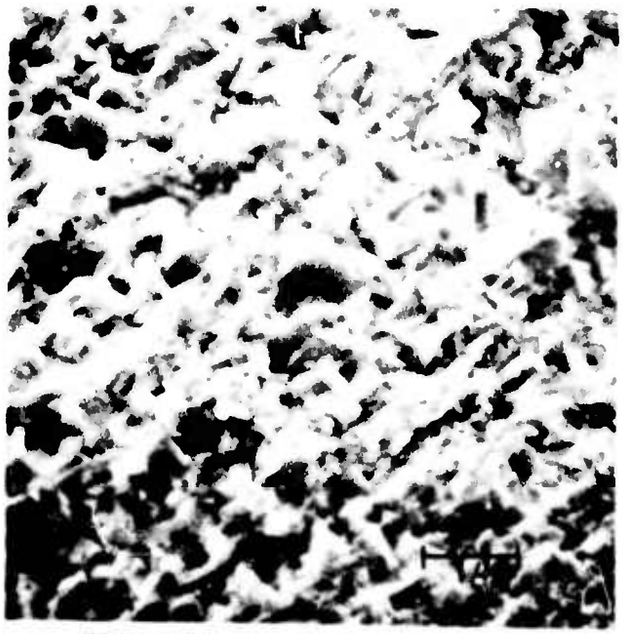

Figure 5

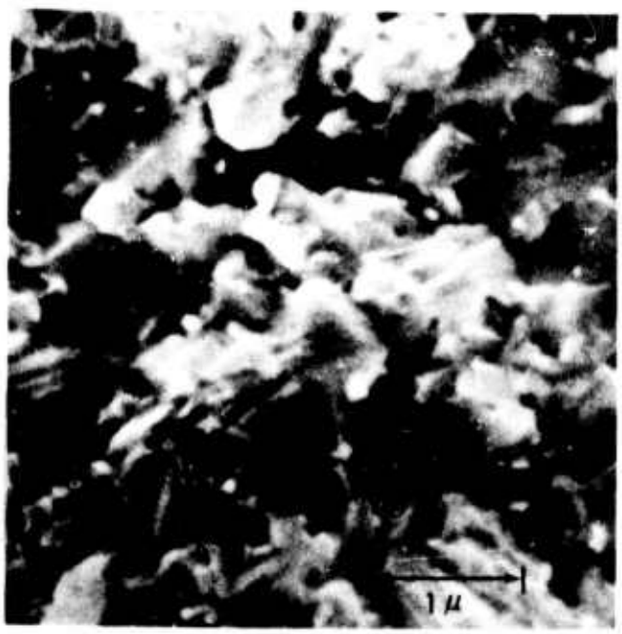


Figure 6

## C.1 Mechanical Behavior of III-V and II-VI Compounds

S. M. Copley, and V. Swaminathan

In this report, we will present the results of room temperature deformation of GaAs and the micro-structural characterization of CdTe.

Room Temperature Deformation of GaAs: In previous quarterly reports we presented the stress-strain curves of GaAs single crystals between 250°C and 550°C. GaAs like other semiconductors becomes brittle at low temperatures. However, the possibility of twinning as a low temperature deformation mechanism. has not been investigated before. With this in mind, we carried out compression tests on Si-doped GaAs single crystals at room temperature. To avoid any problem of misalignment during testing, a spherically aligned loading head was used. No twinning or slip was observed and the samples were found to break into several columnar fragments with their long dimensions parallel to the stress axis. On examining the fracture surface, cleavage facets were observed. The orientation of several of these facets was determined by the electron channeling technique. Fig. 1 shows a series of micrographs taken from adjacent areas of the crystal. The columnar nature of fracture is designated by arrows. A typical cleavage facet denoted by A and the corresponding electron channeling pattern are shown in Fig. 2. In all cases the cleavage facet was found to be within ± 5° of {110}.

Microstructural Characterization of CdTe: A microstructural characterization was carried out on In-doped CdTe single crystals. Samples were annealed at 700, 800, and 900°C at different partial pressures of cadmium ($p_{Cd}$). After annealing the samples were quenched to room temperature (see section by Kroger & Selim). They were then examined for evidence of point defects condensing either as vacancy or interstitial dislocation loops for evidence of precipitation.

Samples for transmission electron microscope were prepared by a jet polishing technique using a solution 40 HCl-4$H_2O_2$-1$H_2O$. Figure 3 is a bright field photo micrograph obtained from a sample annealed for 100 hrs. at 700°C and $5 \times 10^{-2}$ atm $p_{Cd}$ and then quenched. The dislocation loops are marked by arrows. Following the contrast analysis outlined by Edmondson and Williamson (Phil. Mag. 9, 277, 1964) these loops are identified as interstitial loops.

Figure 4 is a brightfield photo micrograph obtained from a sample annealed for 100 hrs. at 800°C and $5 \times 10^{-2}$ atm $p_{Cd}$ and then quenched. Precipitates designated by arrows can be seen in the photomicrograph. The volume fraction

of these precipitates is not sufficient for them to give rise to additional reflections in the electron diffraction patterns and thus their structure has not been identified. It is believed that the point defect most likely to condense upon quenching from high temperature is the cadmium interstitial (see section by Kroger and Selim). Figure 3 suggests that the concentration of Cd interstitials is not sufficient after annealing at 700°C for them to condense as precipitates. Instead, these defects condense as loops. On further increasing the temperature of annealing more cadmium interstitials are available for precipitation. It is concluded that the precipitates in Figure 4 are most probably cadmium. More experiments are being carried out to verify this conclusion.

Anomalous Diffraction from CdTe: As observed in GaAs (see Narayanan and Copley, Phys. Stat. Solidi, May 1974) electron diffraction patterns from CdTe exhibit diffuse streaks and extra reflections. These streaks and extra reflections are explained on the basis of thermal diffuse scattering. It was shown previoulsy (Narayanan, Copley) that the intensity of the streaks increases with increasing temperature further proving the thermal origin of the streaks. We carried out in situ cooling experiment on CdTe and observed the changes in the intensity of the streaks. Figure 5 is an electron diffraction pattern taken at room temperature showing diffuse streaks and extra spots indicated by arrows. Figure 6 is the electron diffraction pattern taken at 140°K for the same orientation. It is clearly seen that the intensity of the streaks is lower than that of Figure 5. Diffuse streaks were observed in both samples containing precipitates with high absorption and those that did not contain precipitates with low absorption. This clearly indicates that the diffuse streaks and spots are of thermal origin and are not due to any precipitated phase.

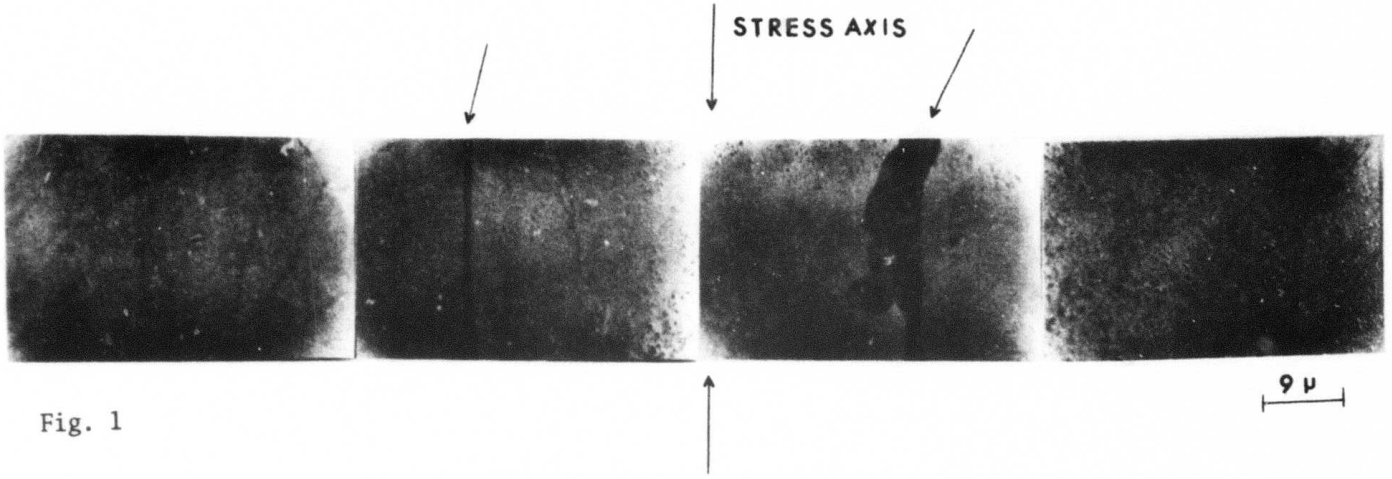


Fig. 1

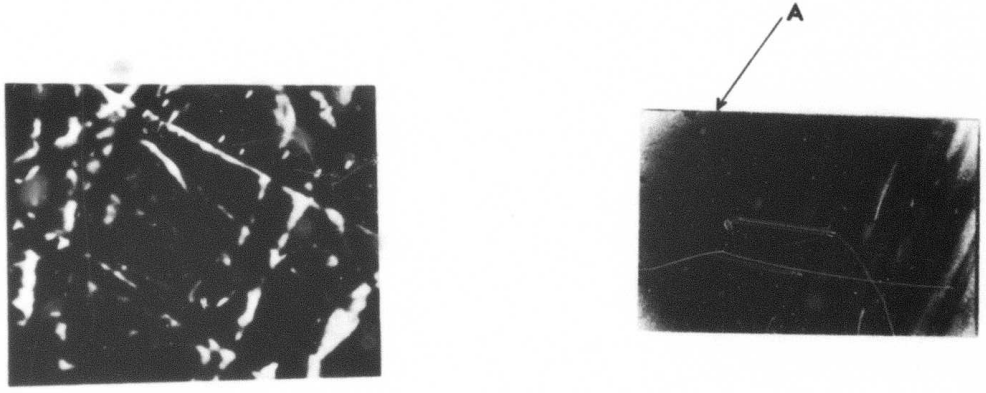


Fig. 2


Fig. 4

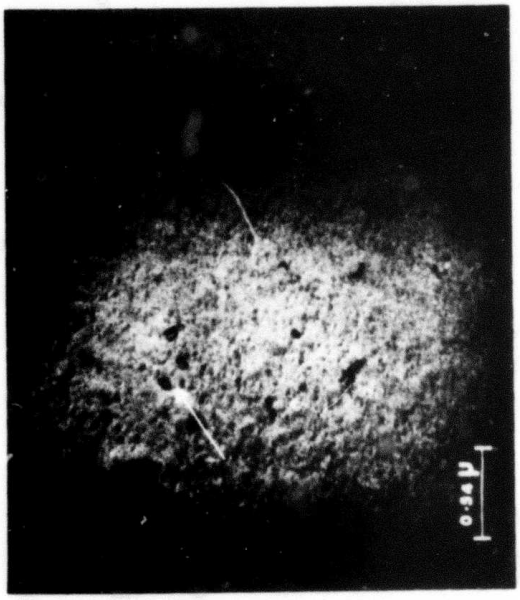


Fig. 3

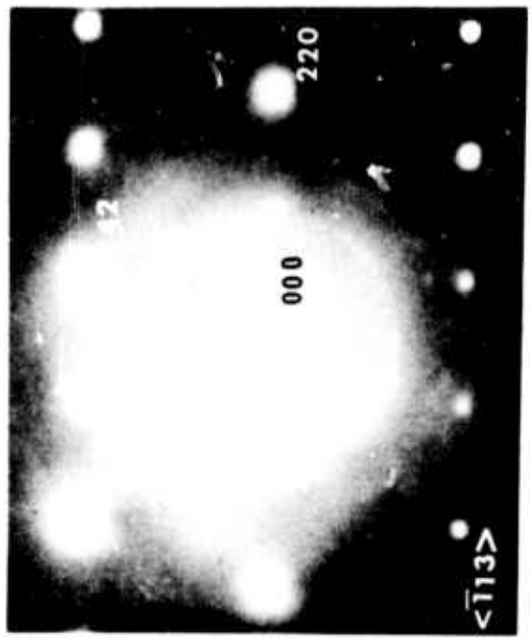


Fig. 6

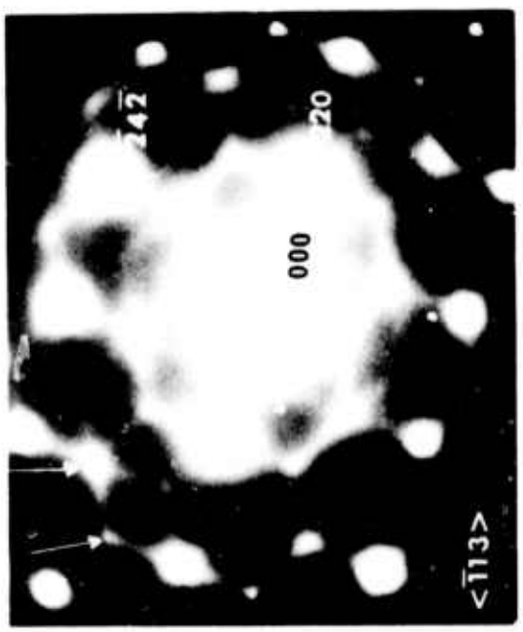


Fig. 5

d.1 Dielectric Constant Measurements

C. R. Crowell and I. Strzalkowski

Work on the determination of the dielectric constants of GaAs, CdTe and ZnSe has continued. Sample preparation of all three materials now seem adequate. Steps required to complete this program are measurements of the temperature dependence of the capacitance; an estimate of the edge corrections, and a determination of the absolute accuracy of the bridges used for the measurements. It is anticipated that these steps will be completed within the next reporting period.

d.2 Study of Defects in II-VI Compounds

F. A. Kroger and F. Selim

CdTe: During this period, the work was concentrated on the relation between the equilibrium state reached in annealing at a high temperature under well-defined cadmium pressures and the properties of crystals quenched to room temperature. Two types of crystals were used, both purchased from the II-VI Company:

1) CdTe + $5 \times 10^{16}$ Cl $cm^{-3}$
2) CdTe + $1 \times 10^{17}$ In $cm^{-3}$

The electron concentrations as $f(p_{Cd})$ determined from the Hall effect at 700°, 800° and 900°C are practically the same for both types of samples, and very similar to those expected for undoped CdTe (Figure 1a, 2a). After cooling marked differences occur. Crystals of the first group show free electrons at higher $p_{Cd}$, free holes at lower $p_{Cd}$, with a narrow high resistance range in between. (Figure 1 b) This behavior is again similar to that expected for undoped CdTe. Note in particular the negative dependence of the electron concentration on the annealing temperature at high $p_{Cd}$.

Cooled crystals of the second group show free electrons at high and medium $p_{Cd}$, but have a high resistance at low $p_{Cd}$ (figure 2 b). The electron concentrations found at high $p_{Cd}$ are 1 to $2 \times 10^{16} cm^{-3}$; 5 to 10 times smaller than the concentration expected on the basis of the indium content (de Nobel found in cooled crystals electrons in a concentration equal to the indium content).

This, together with the fact that no effect was found for the $5 \times 10^{16}$ Cl $cm^{-3}$ of the samples of crystal 1 indicates that either the donor concentrations are lower than reported by the suppliers of the crystals, or they contain considerable amounts of compensating acceptors. In view of the care we are taking in handling the samples and in cleaning our quartz ware we do not think that these acceptors are introduced in the annealing run. A third possibility would be that the indium solubility at low temperature is $\approx 10^{16} cm^{-3}$ so that most of the indium precipitates during cooling. Since precipitation involves nucleation, the difference between our results and those of de Nobel then could be that in his case nucleation did not occur, whereas in ours it does. This possibility will be tested by investigating the behavior of more strongly doped samples grown by us.

As reported in the previous report, absorption of the cooled crystals at 10.6μm is almost entirely due to free carriers. This is largely corroborated by our present results shown in Figure 1 c and 2c.

For samples prepared at 700°C, $\alpha_{10.6} \propto$ carrier concentration, indicating that the absorption is almost exclusively free carrier absorption.

For samples prepared at 800° and 900°C, there is some scatter, indicating that other factors are involved in the absorption, probably scattering at precipitates.

The lowest 10.6μm absorption, with $\alpha_{10.6} = 9.9 \times 10^{-4} cm^{-1}$, was found in 1.72mm thick crystals of the 2nd group quenched from 700°C at $p_{Cd} = 5 \times 10^{-3}$ atm. In order to see whether thicker crystals with a similarly low absorption can be made, we measured the 10.6μm absorption for cyrstals of various thickness annealed at 700°C at $p_{Cd} = 5 \times 10^{-3}$ atm and all quenched in the same manner.

The 10.6μ absorption coefficient is found to increase with thickness (Figure 3). Measuring of the absorption strength of the thickest crystal (a cube of 10 × 10 × 10 mm) showed the absorption to be highest at the center lowest at the surface (Figure 4). The $\alpha_{10.6\mu m}$ near the center is $\approx 10^{-2} cm^{-1}$, i.e. approximately the absorption of the crystals as-received.

A transmission photograph made by Swaminathan using an IR microscope showed a cloudy absorption pattern in the central area, whereas the transmitting regions near the surface are clear. This indicates that precipitation occurs in the central region.

A resistivity measurement on a bar cut from the cube in such a way that it connects the centers of two opposite surface planes showed that the central part of the cube has a lower resistivity than the regions near the surface.

Assuming a mobility of $640 cm^2 V^{-1} sec^{-1}$ and an absorption cross section per electron $K'_e = 1.4 \times 10^{-16} cm^2$ as determined in the previous report, we can calculate from the resistivity the expected free carrier absorption at 10.6μm. The result is shown in Figure 4 (dashed line). It is seen that the free carrier absorption is within a factor 3 equal to the measured absorption coefficient, indicating that free carriers are probabably responsible for the increased absorption in the center of the cube.

These effects must be attributed to the difference in the cooling rates; thin crystals are cooled more rapidly than thick ones, and in the latter, cooling near the surface is faster than in the center. Slow cooling causes precipitation with removal of a center acting as an electron trap - probably $V'_{Cd}$, thus shifting the conductivity cut-off to lower $p_{Cd}$, an effect already reported by de Nobel. Annealing at a lower $p_{Cd}$ therefore may give better results.

High-temperature measurements of the Hall effect of a crystal grown from a Ge doped melt showed the properties of undoped crystals. There are reasons

that the crystals did not contain Ge. New crystals are being grown on which these experiments will be repeated.

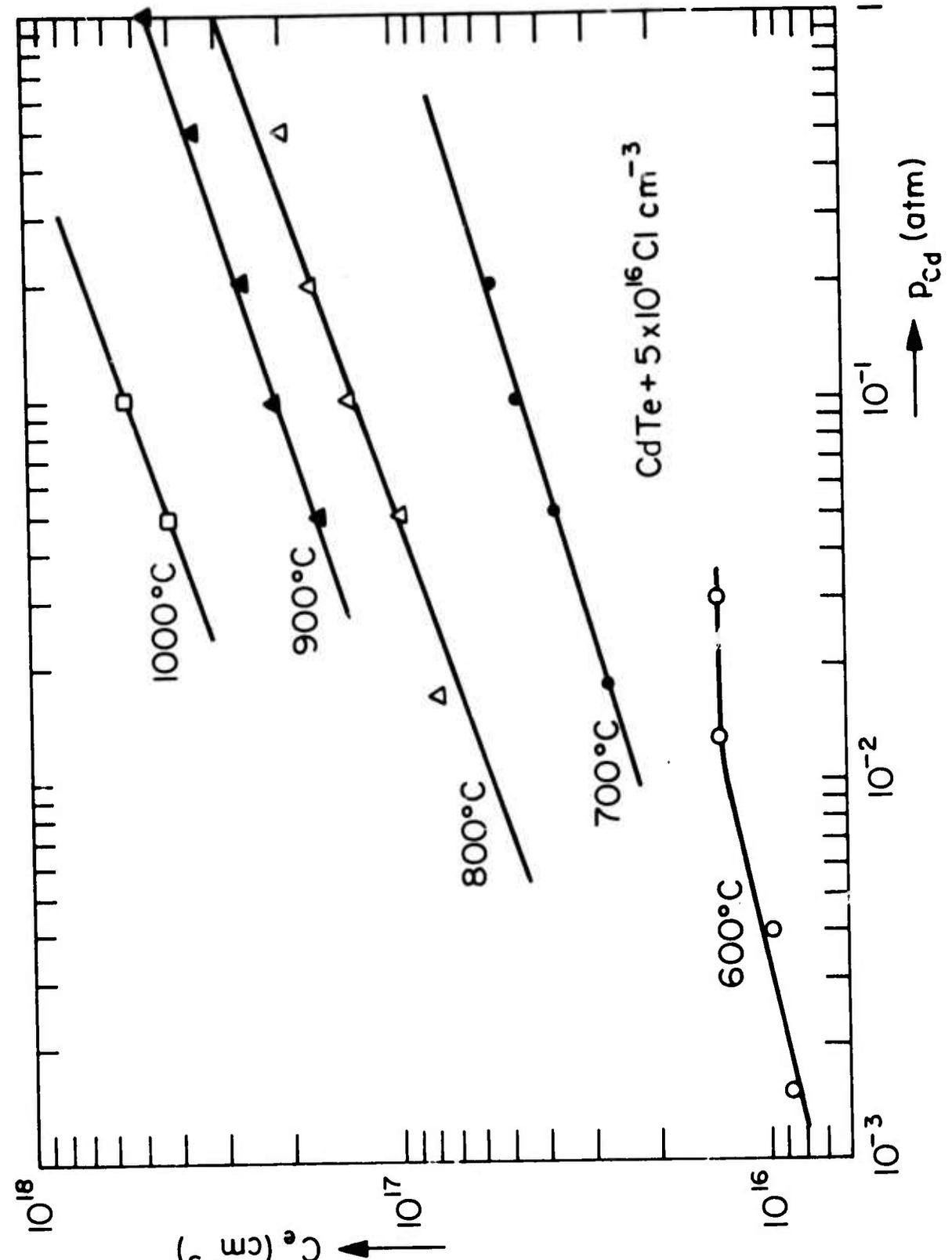


Figure 1a Carrier concentrations in CdTe + $5 \times 10^{16}$ Cl $cm^{-3}$ determined by high-temperature Hall effect measurements.

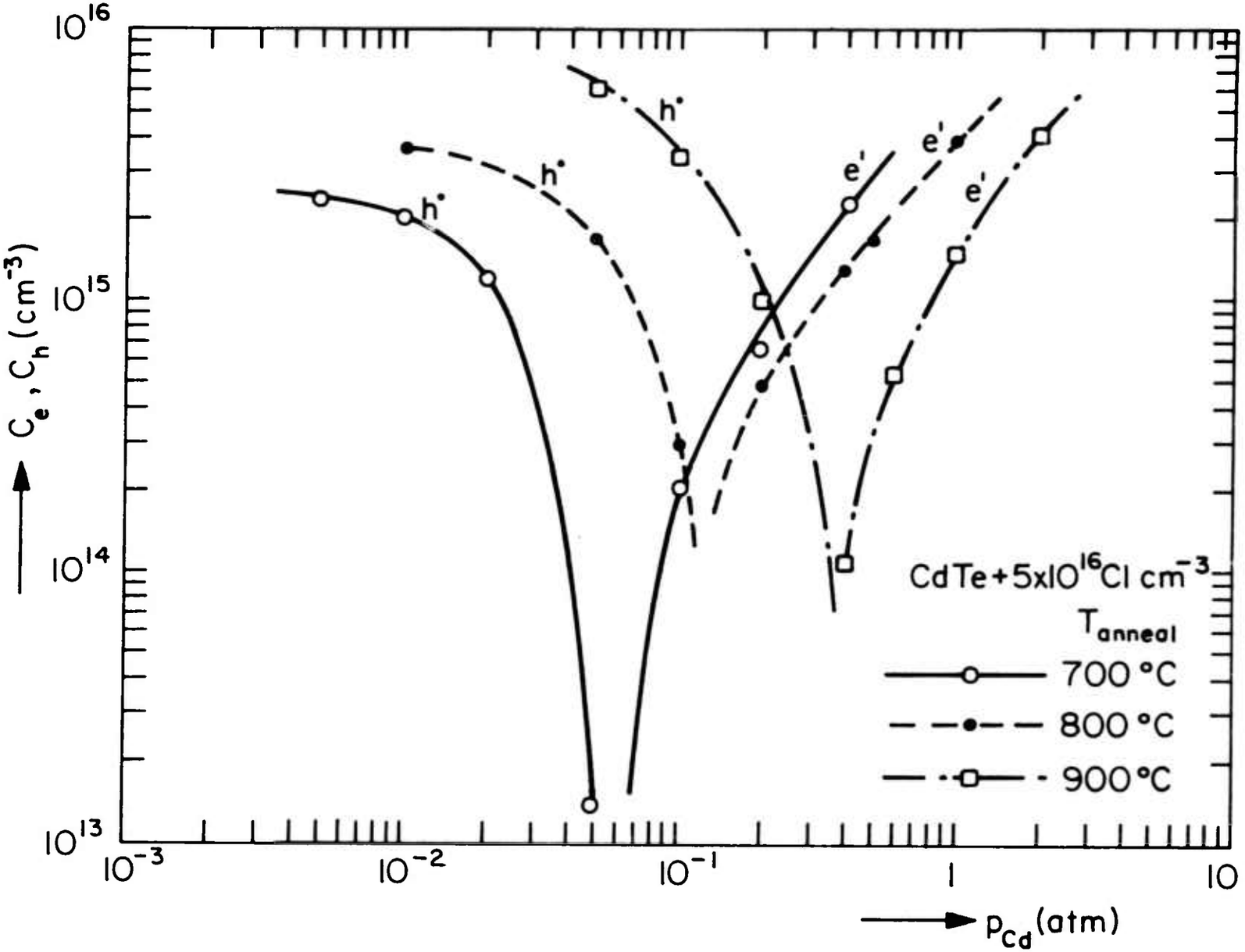


Figure 1b Carrier concentrations as f($p_{Cd}$) anneal for cooled crystals CdTe + 5 × $10^{16}$Cl $cm^{-3}$.

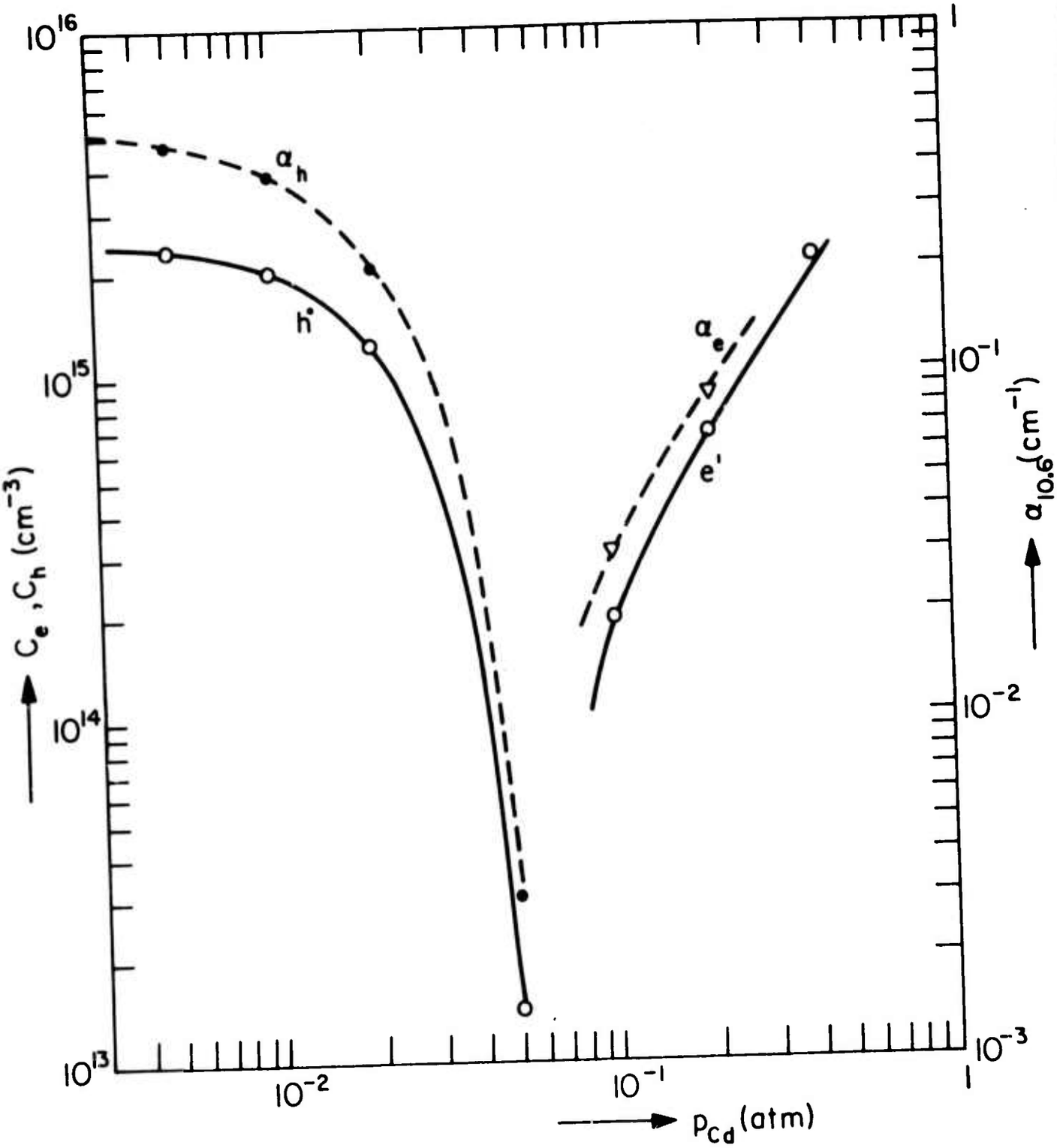


Figure 1c Carrier concentrations and the absorption coefficient $\alpha_{10.6}$ for the crystals of Figure 1b cooled after annealing at 700°C.

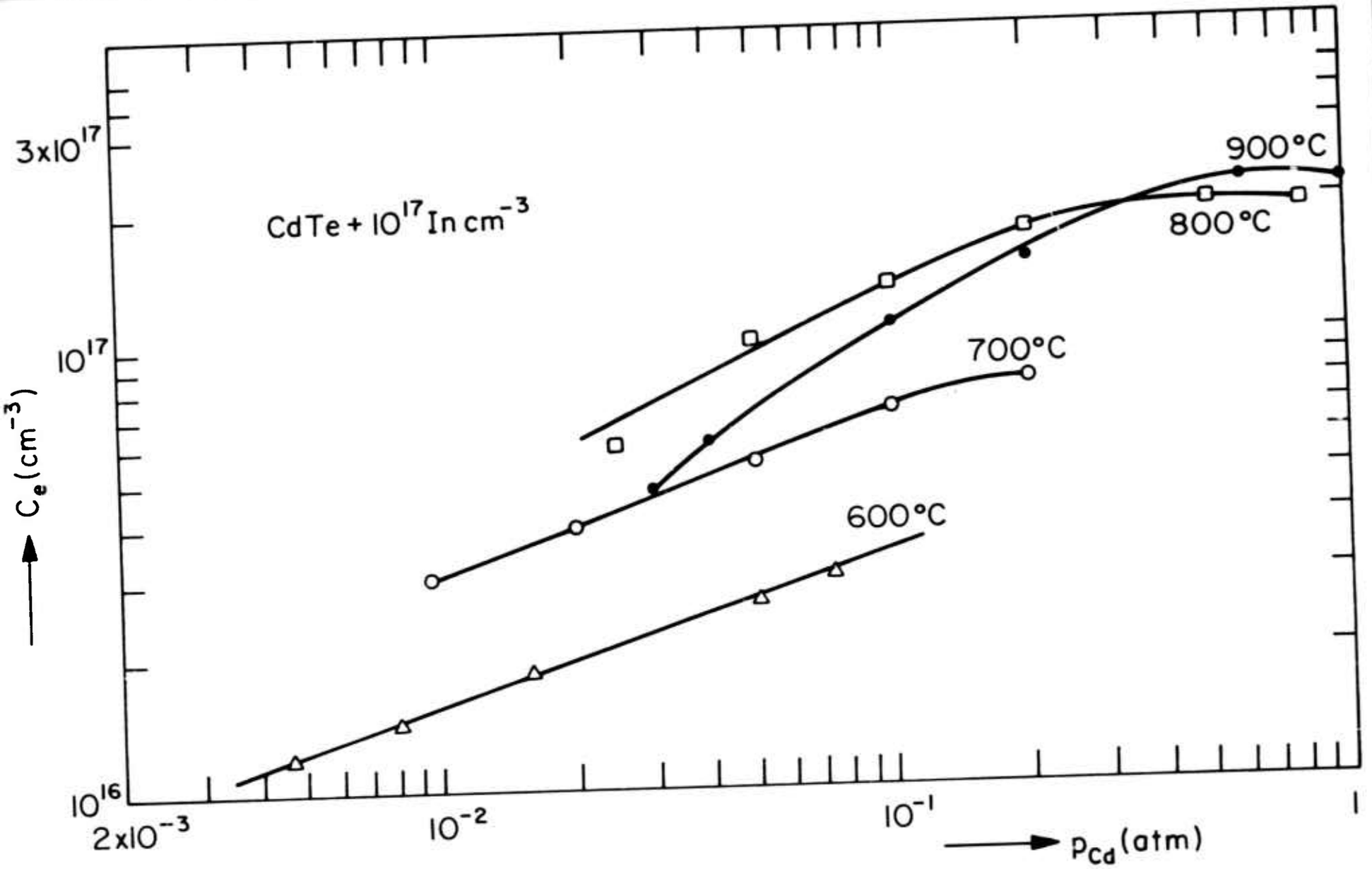


Figure 2a Carrier concentrations in CdTe + $10^{17}$ In $cm^{-3}$ determined by high-temperature Hall effect measurements.

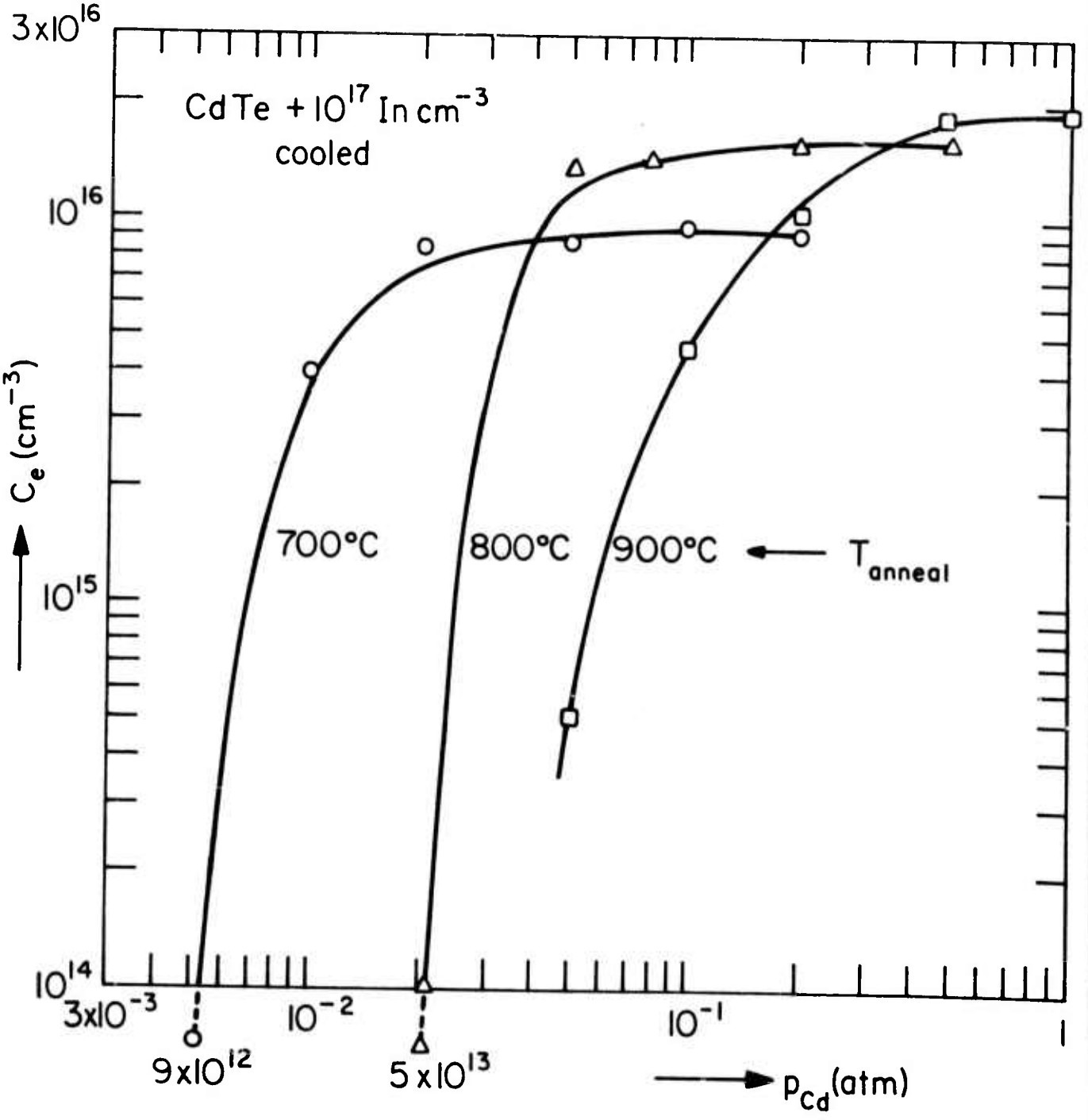


Figure 2b Carrier concentrations as $f(p_{Cd})$ anneal for cooled crystals CdTe + $10^{17}$ In $cm^{-3}$.

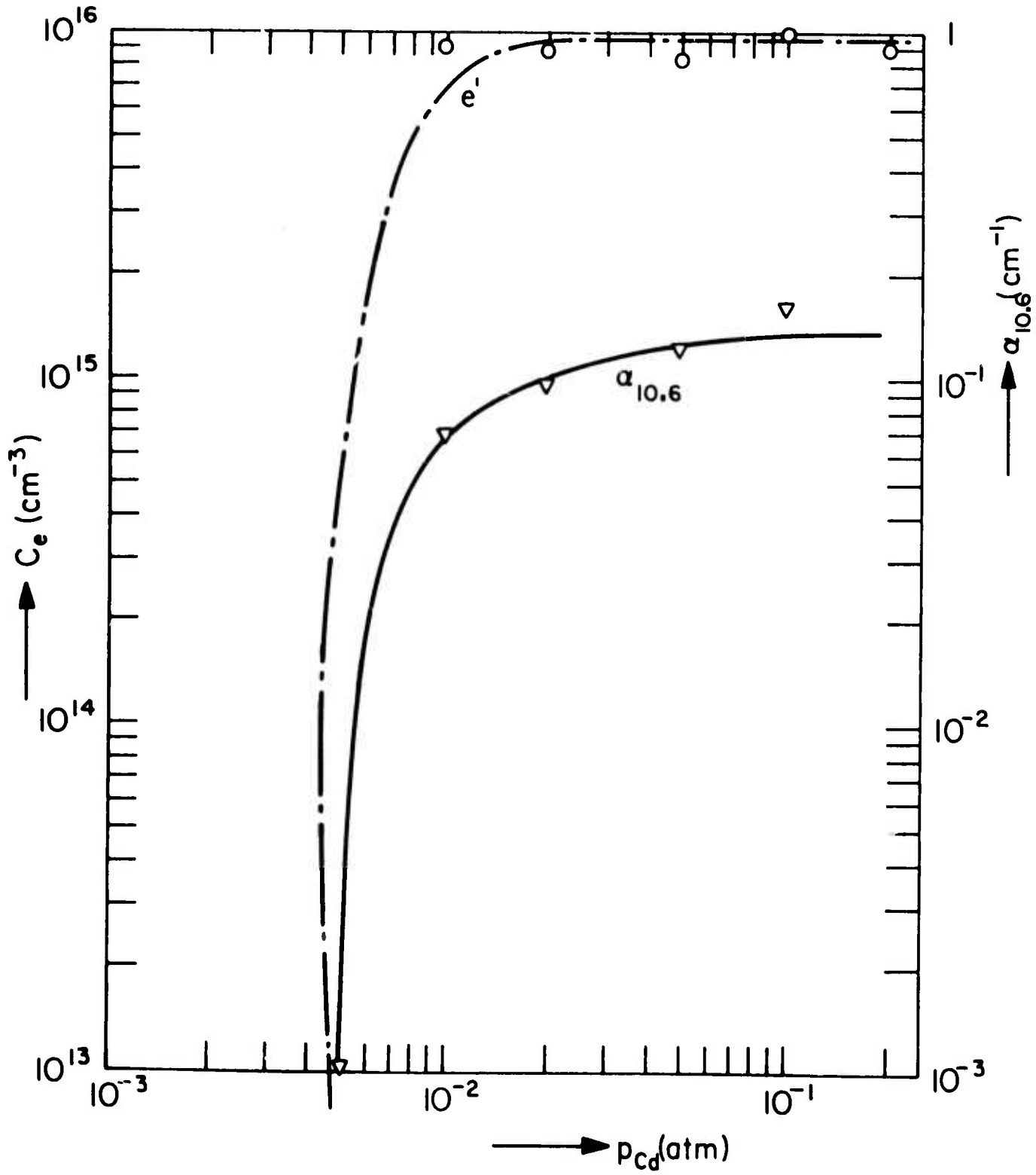


Figure 2c Electron concentration and the absorption coefficient $\alpha_{10.6}$ for the crystals of Figure 2b cooled after annealing at 700°C.

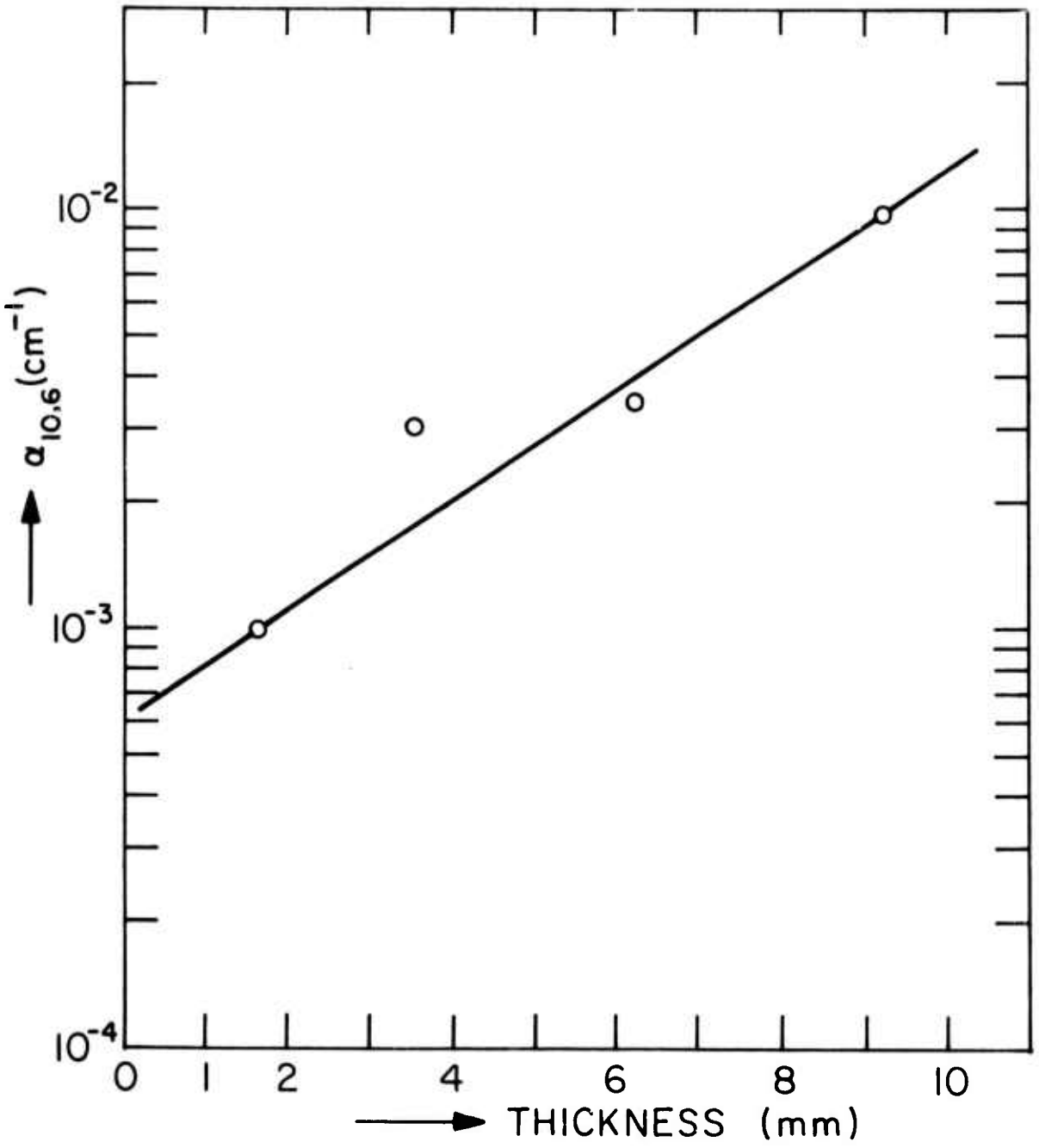


Figure 3 Absorption coefficient $\alpha_{10.6}$ for crystals of CdTe + $10^{17}$ In $cm^{-3}$ of various thickness, quenched after an anneal at 700°C at $p_{Cd}$ = $5 \times 10^{-3}$ atm.

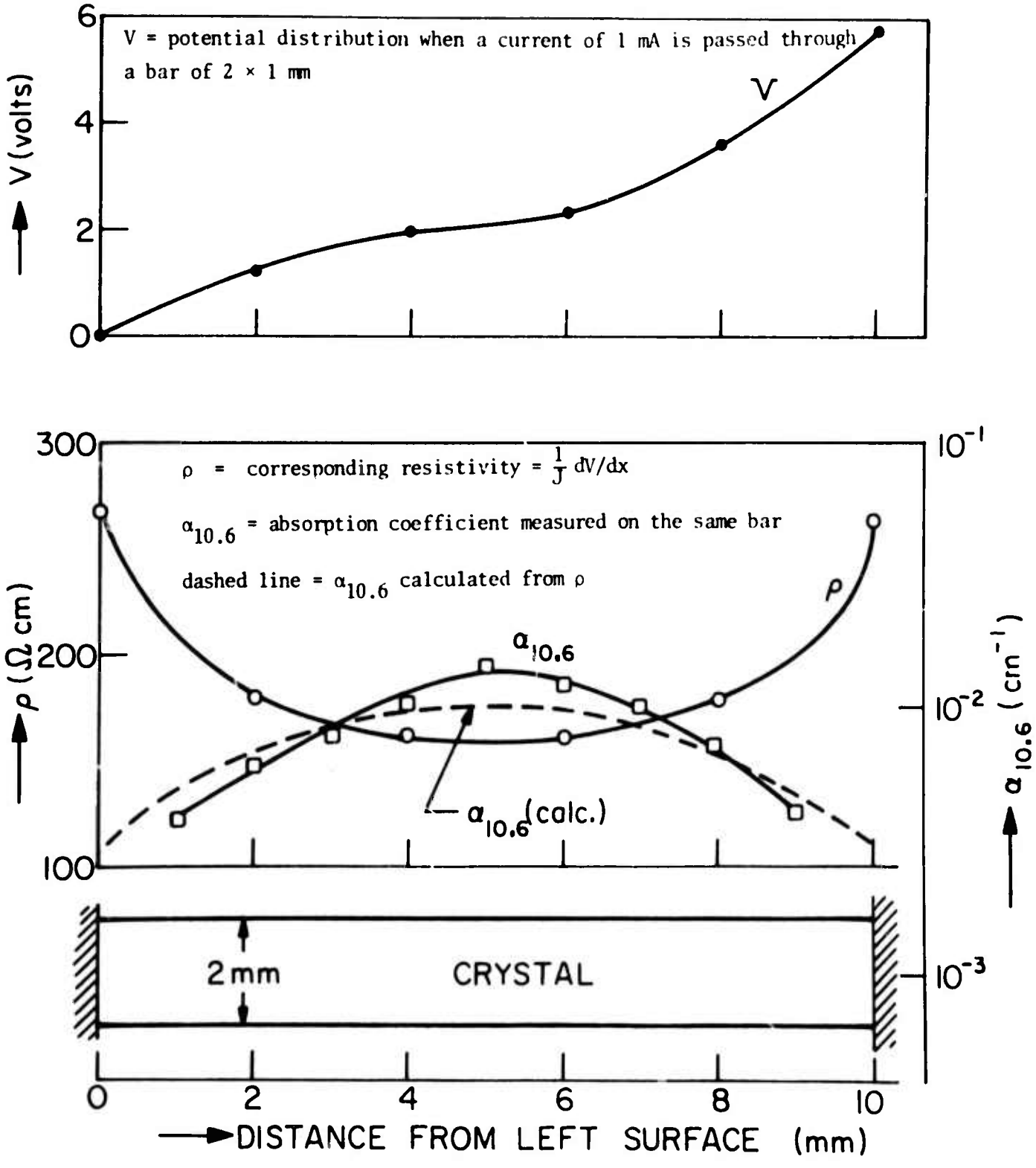


Figure 4 op Properties along a line through the center connecting the center of opposite faces for a cube of CdTe + $10^{17}$ In cm$^{-3}$ quenched after a 95 hour anneal at 700°C at $p_{Cd}$ = $5 \times 10^{-3}$ atm.

e.1 Theoretical Studies of Absorption Mechanisms in IR Window Materials

R. W. Hellwarth and M. Mangir

In this quarter we have searched for an experiment which can give accurate enough data for the application of our method to measure the relative contribution of the nonlinear dipole moment to multi-phonon absorptions as compared to the contribution of anharmonic forces.

As we have reported previously, this method requires the experimental measurement of $\int_0^\infty \omega\varepsilon_2(\omega)d\omega$ at two temperatures. For materials that are currently of interest, the ZnSe, CdTe, GaAs, etc., there is very little and incomplete data. Only for LiF we have found extensive and precise data on $\varepsilon_2(\omega)$ and our complete results will be published in August 15, 1974 issue of Physical Review B.

Accurate measurement of $\varepsilon_2(\omega)$ in the infrared, especially around $\omega_{TO}$ is very difficult and relies on indirect measurements like Kramers-Kronig analysis or double-pole fit of the reflection spectrum. We have come up with an experiment where the integral $\int_0^\infty \omega\varepsilon_2(\omega)d\omega$ can be obtained directly from the experimental data rather than measuring $\varepsilon_2(\omega)$ and making the indicated integration. Since this experiment would involve measurement of index of the refraction of the material (see Appendix) as a function of frequency in the infrared at two different temperatures, potentially it can give more accurate and precise experimental values.

We have also searched the literature for accurate measurements of index of refraction in infrared, but again there isn't experimental data within the frequency range of

of interest and for the materials of interst. L. W. Tilton and E. K. Plyler[1] had measured n for LiF, but only at room temperature; nevertheless the numbers derived from their results agree with the number we have used for our paper.

We also made some numerical calculations for ZnSe, to determine the frequency range and accuracy required in measuring n, to obtain the desired integral with 1% accuracy.

Reference

1. L. W. Tilton and E. K. Plyler, J. of Research of the NBS 47, 25 (1951).

Appendix

In the part of the frequency spectrum between electronic band absorption and lattice absorption, using Kramers-Kronig relation, we can write

$$\varepsilon_1(\omega)=\varepsilon_\infty+\frac{A\omega^2}{B\omega^2-C}+\frac{2}{\pi}P\int_0^\infty\frac{\omega'\varepsilon_2'(\omega')d\omega'}{\omega^2-\omega'^2}$$

where $\varepsilon_1(\omega)$ is the real part of dielectric constant, $\varepsilon_\infty$ is the high frequency dielectric constant, the second term with constants A,B,C determined experimentally represents the dispersion due to electronic band absorption, and $\varepsilon_2'(\omega)$ is the imaginary part of the dielectric constant due to the lattice absorption. P stands for principal part of the integral.

We can approximate the integral as

$$P\int_0^\infty\frac{\omega'\varepsilon_2'(\omega')d\omega'}{\omega^2-\omega'^2}=\frac{1}{\omega^2}\int_0^\infty\omega'\varepsilon_2'(\omega')d\omega'+\frac{1}{\omega^4}\int_0^\infty\omega'^3\varepsilon_2'(\omega')d\omega'+\ldots$$

If $\omega>3\omega_{TO}$ the terms neglected decrease very rapidly, because they are of the order of $(\frac{\omega_{TO}}{\omega})^{2m}$, m=1,2,3...

In this frequency region $(3\omega_{TO}<\omega<\frac{1}{5}\frac{E_{gap}}{\hbar})$ $n^2>>k^2$, where n and k are the real and imaginary parts of the complex refractive index.

Within these approximations

$$n^2(\omega)\cong\varepsilon_1(\omega)\cong\varepsilon_\infty+\frac{A\omega^2}{B\omega^2-C}+\frac{2}{\pi}\frac{1}{\omega^2}\int_0^\infty\omega'\varepsilon_2'(\omega')d\omega'+\frac{1}{\omega^4}\int_0^\infty\omega'^3\varepsilon_2'(\omega')d\omega'$$

So an accurate measurement of n as a function of frequency will enable one to obtain the desired integral.

f.1 Wavelength and Temperature Dependent Calorimetry Measurements on GaAs

W. H. Steier, C. P. Christensen, R. Joiner

In the past quarter we have completed construction of an improved laser calorimeter designed around a Model 500L Apollo $CO_2$ laser. The laser is line-tunable over the range 9.4μ - 10.8μ with 20 watts output at 10.6μ. Experimental data obtained with the new calorimeter has been found to be quite consistent with results obtained with the older system. This measuring set is now available to other staff members working on the contract for the measurement of materials under investigation.

A large-diameter GaAs sample has been obtained from W. Allred of Crystal Specialties, and we have found its absorption spectrum to be nearly identical to that of the lowest loss samples measured previously. We now have six low-loss samples from different laboratories which exhibit very similar absorption spectra.

A summary of our GaAs investigations was prepared during the last quarter and has been submitted for publication. A copy of the manuscript is attached.

# INVESTIGATION OF INFRARED LOSS MECHANISMS IN HIGH RESISTIVITY GaAs

C. P. Christensen, R. Joiner, S. T. K. Nieh and W. H. Steier

Department of Electrical Engineering
University of Southern California
Los Angeles, California 90007

## ABSTRACT

The absorption coefficient of GaAs has been measured by calorimetry as a function of wavelength in the 9-11$_\mu$ band and as a function of temperature. The samples measured were the best available material growth by several laboratories and by several techniques. The results suggest that infrared loss near 10$_\mu$ in these samples is dominated by an intrinsic absorption mechanism.

# INVESTIGATION OF INFRARED LOSS MECHANISMS IN HIGH RESISTIVITY GaAs*

C. P. Christensen, R. Joiner, S. T. K. Nieh and W. H. Steier

Department of Electrical Engineering
University of Southern California
Los Angeles, California 90007

## Introduction

GaAs has found extensive application in optical devices designed for the 10 μ wavelength region. Modulators, mirror substrates, and laser windows have been very successfully fabricated from high-resistivity GaAs, and the material has received recent attention as a prospective window material for very high power $CO_2$ lasers. In the latter application it is extremely important that the material exhibit very low IR absorption, since thermal beam distortion is a severe problem.

IR absorption in GaAs has been the subject of several investigations (1)-(4). In these studies, absorption coefficients at 10.6 μ ranging from $6 \times 10^{-3}$ $cm^{-1}$ to $2 \times 10^{-2}$ $cm^{-1}$ were reported for high-resistivity GaAs samples. It has not been shown, however, whether this loss is intrinsic to GaAs at 10.6 μ or is due to some impurity or imperfection in the crystal and could thus be reduced by more careful material preparation. Homology arguments (1) and extrapolation of loss measurements at longer wavelengths (2) suggest that intrinsic absorption due to

* Research supported by the Advanced Research Projects Agency of the Department of Defense under Contract No. F19628-72-C-0275, monitored by Air Force Cambridge Laboratory.

lattice vibrations or a nonlinear electric moment should be of about the measured order of magnitude. However, the structure of the absorption spectrum near 10 μ and the temperature dependence of IR loss in high resistivity GaAs has not been obtained in previous studies. These measurements are useful in understanding the IR loss mechanisms in high-resistivity GaAs and may find application in the design of $CO_2$ laser devices utilizing GaAs as well.

The following sections describe experiments constructed to measure the wavelength and temperature dependence of infrared absorption in seven high resistivity GaAs samples. The samples were obtained from four different laboratories and are intended to be representative of the best currently available high resistivity GaAs. A more detailed sample description is given in Table I. Absorption in these low-loss samples was measured using calorimetric techniques with a line tuneable $CO_2$ laser as the infrared source.

## Experiment

The experimental apparatus used in the calorimetric absorption measurements is schematically shown in Figure 1. Grating G is used to line tune $CO_2$ laser, L, and also as the laser output coupler. Laser oscillation was obtained on 48 lines covering the wavelength range between 9.2 μ and 10.9 μ, and the power levels used in the experiments were typically 3 to 5 watts. A spherical mirror was used to focus the laser output to a spot approximately 1 mm in diameter, and the GaAs sample was placed at the focus. For room temperature measurements, the sample was supported by two plexiglas fingers and shielded from room air currents

by a plexiglas tube. The samples were typically a few millimeters thick with transverse dimensions of approximatel 1 cm. The sample temperature was monitored by a thermocouple inserted into a small hole drilled about 0.050" into the edge of the sample. Silicon heat sinking compound was used to assure good thermal contact between thermocouple and sample. Thermocouple voltages were monitored with a microvoltmeter, which was then connected to one channel of a dual-channel stripchart recorder. Laser flux passing through the sample was measured with a thermopile detector and displayed on the second recorder channel.

For loss measurements at elevated temperatures, the sample was mounted with four brass fingers at the center of an oven constructed from an open steel tube. The steel tube was heated electrically and thermocouples were used to measure both the temperature of the oven wall and the temperature of the sample relative to the oven wall.

In the absorption measurements, the laser was allowed to irradiate the sample for a period of several minutes, and the sample temperature vs. time was recorded on a stripchart recorder. The slopes of this temperature curve during irradiation and during cooling after irradiation (at the same T ) and the transmitted laser power were used to compute the absorption coefficient using the formula (5).

$$\beta = \frac{\left|\frac{dT}{dt}\right|_h + \left|\frac{dT}{dt}\right|_c}{P_{tr}} \cdot \frac{2n}{n^2+1} \cdot \frac{mC}{\ell} \qquad (1)$$

where $\left.\frac{dT}{dt}\right|_h$ = slope of the temperature curve during irradiation

$\left.\frac{dT}{dt}\right|_c$ = slope of the temperature curve after irradiation

$P_{tr}$ = transmitted power

n = refractive index = 3.3

m = sample mass

$\ell$ = sample length

C = GaAs specific heat = 0.27 j/g$^{o}$C

Prior to measurement, samples were chemically polished with "Mirrolite" polishing agent (Materials Development Corporation), cleaned with trichloroethylene, acetone, and methyl alcohol, and finally rinsed in deionized water. Preparation in this manner left the GaAs surface free from dirt and irregularities larger than approximately 25$\mu$ .

Experimental Results and Discussion

Results of the spectral measurements are summarized in Figure 2. In general the lowest loss materials studied had a $\beta$ of about $9 \times 10^{-3}$ $cm^{-1}$ at 10.6$\mu$ which decreased to about $5 \times 10^{-3}$ $cm^{-1}$ at 9.3$\mu$ . One of the most interesting aspects of these results is the great degree of similarity in both amplitude and structure among the spectra of the five low loss samples. This is particularly surprising in view of the wide variety of growth techniques and doping conditions which characterize these samples. The similarity in these spectra would seem to indicate that the loss in these samples is either dominated by an intrinsic absorption mechanism such as multiphonon absorption or that there exists an extrinsic absorption mechanism common to all the samples. One

common denominator for all the samples of Table I is high temperature growth.

The temperature dependence of the observed absorption was measured at 9.28$\mu$ and 9.68$\mu$ (near the minimum and the maximum in the absorption) for samples WA-1000 and 55-1A. Loss in both samples showed a similar temperature dependence, and the temperature dependence was identical at both wavelengths. The results of the 9.28$\mu$ measurements are shown in Figure 3. It is evident from those data that the absorption shows markedly different temperature dependence in two thermal regimes. Below 280°C absorption varies very slowly with temperature; however, above 280°C the temperature dependence is nearly exponential.

In the high-temperature regime the observed loss is apparently due to the rapidly increasing number of free carriers in the material. Hall measurements performed on these samples indicate that the material is n-type, so that we can write $\beta(T) = n_e(T)\sigma_e(T)$ where $n_e$ and $\sigma_e$ are the electron density and absorption cross section. The electron density as a function of T is known from the Hall measurements which show $n_e$ equal to $10^7$ cm$^{-3}$ at 20°C and a carrier activation energy of 0.7 eV. The temperature variation of $\sigma_e$ can be estimated from the Drude theory of free carrier absorption

$$\sigma_e = \frac{4\pi e^2 \tau}{ncm^*} \cdot \frac{1}{1+\omega^2\tau^2} \cong \frac{4\pi e^2}{ncm^*\omega^2} \cdot \frac{1}{\tau}$$

where e, $m^*$, and $\tau$ are respectively the charge, mass, and collision time of an electron, and $\omega$ is the optical frequency. Thus, if $\tau$ is dominated by electron-phonon collision rates, it is reasonable to assume a $T^{3/2}$ temperature dependence for $\sigma_e$. Spitzer and Whelan (6) have

measured the room temperature $\sigma_e$ for electrons in GaAs and find $\sigma_e \cong 10^{-16}$ cm$^2$ at 9.3$\mu$ . The calculated free carrier absorption for the samples studied, using the above parameters, is shown as a dashed line in Figure 3, and is in good agreement with the experimental results above 280°C.

The weak temperature dependence found in the absorption data below 280°C might lead one to propose that the observed loss is due to a fundamental local-mode vibration rather than a multiphonon process, since a simple theory would predict a temperature variation proportional to $T^{(m-1)}$ for m-phonon absorption at high temperatures. However, Bendow(7) and McGill, et al. (8) have pointed out that shifts in the optical phonon frequency greatly reduce the temperature dependence of multiphonon absorption. The expression for multiphonon losses is of the form (7), (8)

$$\beta = \beta_o \left[(F+1)^{\omega/\Omega} - F^{\omega/\Omega}\right] e^{-\gamma\omega/\Omega} \qquad (2)$$

where $\Omega$ is the TO phonon frequency, $\omega$ is the optical frequency, and $F = (e^{\omega/\Omega} - 1)^{-1}$. The constant $\gamma$ has been shown to be inversely proportional to $\Omega$ (6) and $\gamma = 7.0\mu$ in GaAs at 20°C (2). An estimate of the temperature dependence of $\Omega$ can be obtained from Raman scattering results, although TO phonons other than Raman phonons can contribute to multiphonon IR losses. The Raman data of Chang et al. (9) gives $d\Omega/dT = 0.016$ cm$^{-1}$/°K. The calculated temperature dependence of multiphonon absorption in GaAs, using Eq. (2) and including phonon frequency shifts, is shown in Figure 3. There is clearly good agreement between this calculated result and the experimental

data at temperatures below 280°C.

As indicated in Figure 3, irreversible increases in absorption were brought about by heating in the calorimetric oven. Sample absorption was observed to increase each time the sample was subjected to a 400°C temperature cycle. The sample was repolished before each measurement to eliminate surface contamination. Figure 4 shows the shift in bulk abosrption experienced by Sample 55-1A after four heating cycles. Hall measurements made after the four cycles indicated little change in carrier concentration or mobility. To further investigate these low temperature annealing effects, a second sample (54-4A) was sealed in an evacuated quartz ampoule, heated to 400°C for two hours and allowed to slowly cool. This thermal cycle was intended to approximate that used in the calorimetry experiments, but Sample 54-4A showed no increase in bulk absorption after heating (see Figure 4). This suggests that irreversible effects in the calorimetry experiments were due to contamination of the sample by the oven. Since the oven design incorporated large amounts of steel and the thermocouples and sample supports contained copper, we suspect either iron or copper contamination. Copper is a very likely candidate since it diffuses extremely rapidly in GaAs. The diffusion length for Cu corresponding to a one-hour heating at 400°C is about 2 mm, which in most cases is greater than the sample thickness.

A final annealing experiment was performed with Sample 55-1A. After four 400°C anneals in air, the sample was sealed in a quartz ampoule containing only powdered GaAs, heated to 1100°C for 15

minutes and quenched in water. This annealing step resulted in further increases in IR absorption, although it is difficult to ascertain the mechanism responsible for the increased loss. The absorption spectrum after the high temperature annealing cycle is shown in Figure 4.

Summary

In summary, our experiments on GaAs have yielded the following results:

A. Samples from several laboratories grown by different techniques and compensated by different methods all show identical absorption spectra with $\beta$ varying from $5 \times 10^{-3}$ at $9.3\mu$ to $9 \times 10^{-3}$ at $10.6\mu$. The results are shown in Figure 1 and Table I.

B. The degree of structure seen in the spectra of Figure 1 is consistent with a resonant process such as intrinsic multiphonon absorption or a vibration associated with a bulk or surface impurity.

C. The order of magnitude of the observed $\beta$ in the $10\mu$ range is consistent with measurements at other wavelengths assuming an exponential frequency dependence which is characteristic of multiphonon loss (2).

D. The dependence of $\beta$ upon temperature can be explained by free carrier generation above $280^{\circ}C$ and is consistent with multiphonon absorption at lower temperatures.

This evidence seems to support multiphonon absorption as the primary loss mechanism at room temperature in low-loss GaAs. While the evidence is not conclusive, it appears the absorption we have observed in the lowest loss samples is intrinsic to GaAs.

Acknowledgement

The authors wish to thank Prof. J. M. Whelan for obtaining several of the samples and for helpful discussion, and Prof. W. G. Spitzer for several suggestions and comments. Mr. Sharad Joshi performed the Hall measurements. This work would not have been possible without the cooperation of the companies listed in Table I.

References

1. C. A. Klein and R. I. Rudko, Appl. Phys. Lett., 13, 129 (1968).

2. F. A. Horrigan and T. F. Deutsch, Raytheon Research Div., Quarterly Technical Reports, Nos. 1 and 2, Contract No. DA-AH01-72-C-0194, 1972 (unpublished).

3. J. Comly, E. Garmire and A. Yariv, J. Appl. Phys., 38, 4091 (1967).

4. R. Weil, J. Appl. Phys., 40, 2857 (1969).

5. R. Weil, J. Appl. Phys., 41, 3012 (1970).

6. W. G. Spitzer and J. M. Whelan, Phys. Rev., 114, 59 (1959).

7. B. Bendow, Appl. Phys. Lett., 23, 133 (1973).

8. T. C. McGill, R. W. Hellwarth, M. Mangir and H. V. Winston, J. Phys. Chem. Solids, 34, 2105 (1973).

9. R. K. Chang, J. M. Ralston and D. E. Keating, Proc. of the Intnl. Conf. on Light Scattering Spectra of Solids, New York University, 1968, p. 369.

| Sample | Room Temperature Mobility ($cm^2/V$ sec) | Resistivity (ohm-cm) | Growth Technique |
|---|---|---|---|
| Bell Labs 55-1A | 6000 | $1.4 \times 10^8$ | Float Zone, Un-doped |
| EMC 6012B | ---- | $2.2 \times 10^7$ | Czochralski Cr-doped |
| EMC 6050T | ---- | $3.2 \times 10^7$ | Czochralski Cr-doped |
| USC WA1000 | 3000 | $10^8$ | Horizontal Bridgeman un-doped |
| IBM WORM-1 | ---- | high $\rho$ | Horizontal Bridgeman with Oxygen remelt* |
| Bell Labs 44-3A | 5550 | $4.6 \times 10^8$ | Float Zone, Carbon-doped |
| Bell Labs 55-4A | 5700 | $2.5 \times 10^8$ | Float Zone, Un-doped |

TABLE 1. GaAs samples used in calorimetric loss measurements.

*In this sample, oxygen was purposely introduced into the boat, and after growth the sample was remelted.

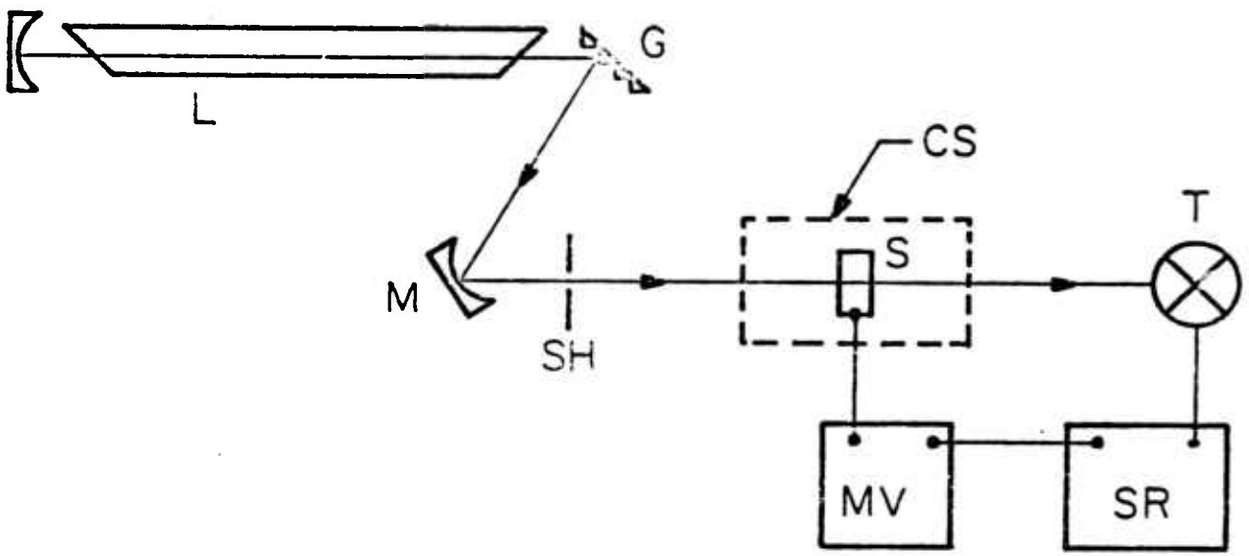


FIGURE 1

Schematic experimental arrangement. L-$CO_2$ laser, G-grating, M-spherical mirror, SH-shutter, CS-calorimeter shielding, S-sample, T-thermopile detector, MV-millivoltmeter, SR-stripchart recorder.

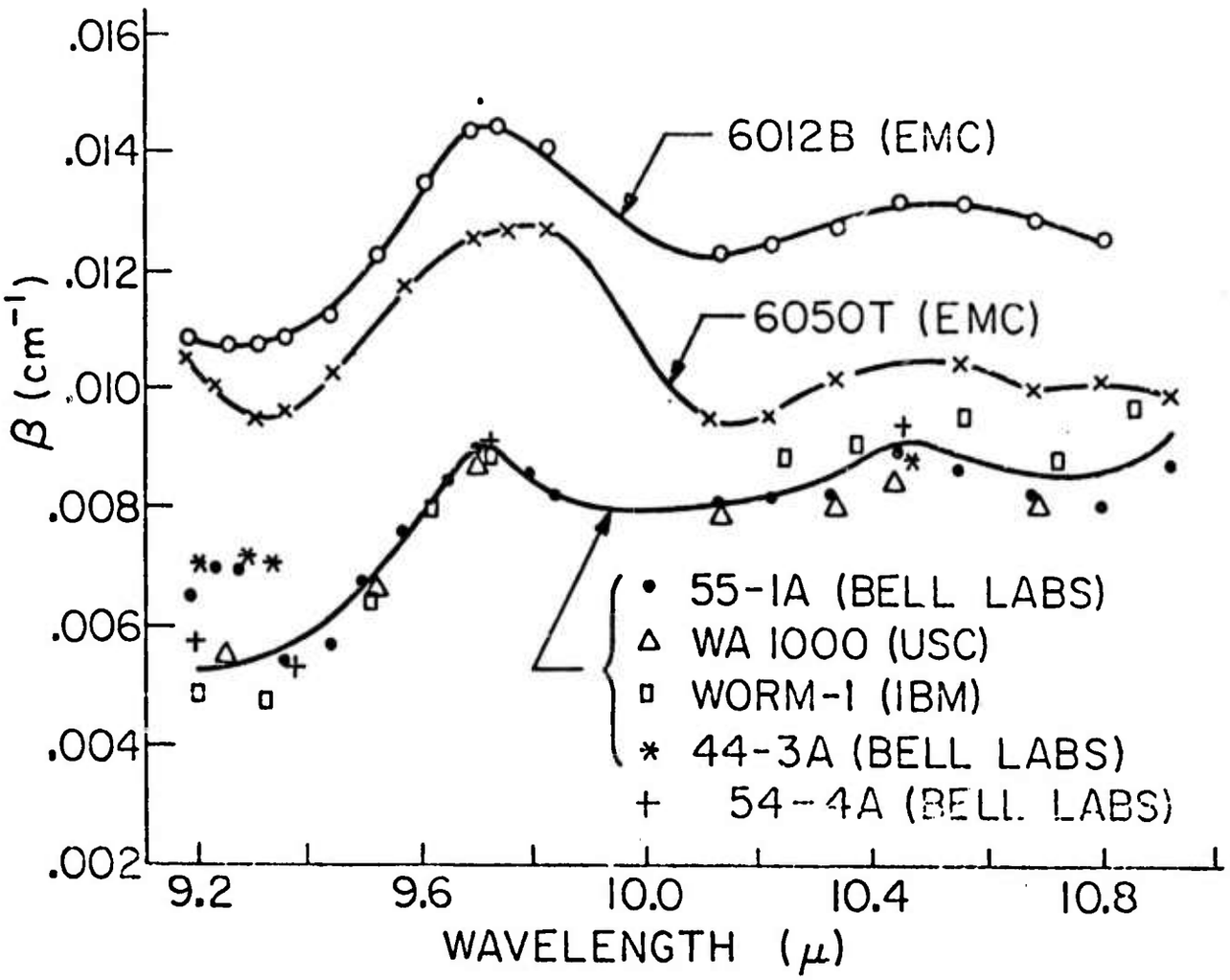


FIGURE 2
Absorption spectra for the samples described in Table 1.

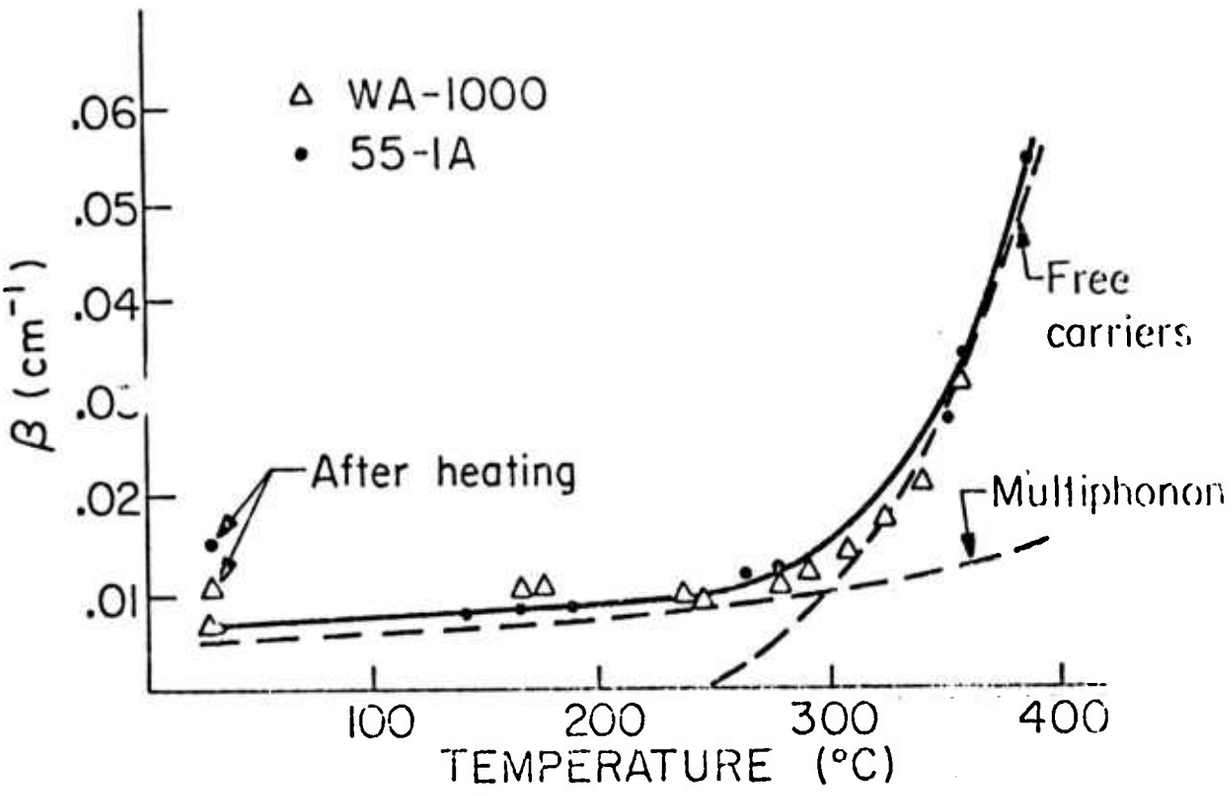


FIGURE 3

Absorption as a function of temperature for samples WA-1000 and 55-1A. Experimental points were obtained at a wavelength of 9.28 . Dashed lines show the theoretical temperature dependence of free carrier and multiphonon absorption in these samples.

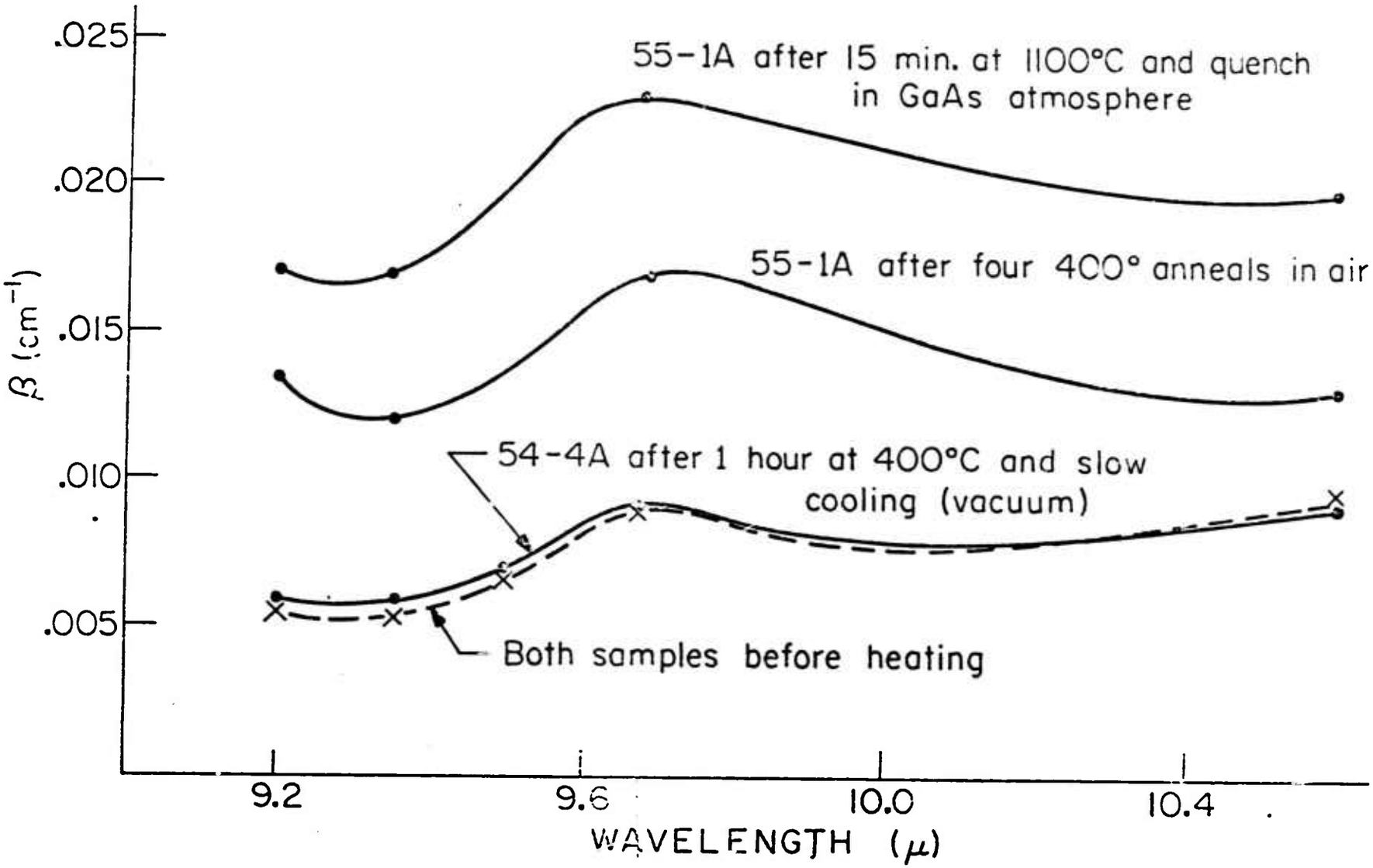


FIGURE 4
Annealing effects observed in GaAs

## f.2 Alkali Halide Surface Studies with Acoustic Probe Techniques

J. H. Parks, D. A. Rockwell, T. S. Colbert

During this quarter our research effort included the application of acoustic surface wave techniques to measure the depth dependence of surface properties, and a fluid coupling analysis of surface wave energy transfer to a KCl surface. In this quarterly report, we review work performed in these two areas and also discuss plans for continuing these studies during the next contract period. During this past quarter we participated in an ARPA research review of surface studies at which we presented the overall results of our current contract period. A technical paper has been submitted for publication to Applied Physics Letters which discusses the application of acoustic surface waves to detect radiative absorption. A broader treatment of the theory and experimental analysis, and also a paper describing the fluid coupling technique are both being prepared for publication.

### f.2.a Surface Wave Studies of Depth Dependence

In past reports we have established the reliability of

(a) applying acoustic surface waves to quantitative measurements of radiative absorption,[1] and

(b) coupling an acoustic surface wave to a nonpiezoelectric surface via a fluid layer[2] in order to extend absorption measurements to alkali halide materials.

These accomplishments represent two important elements in the

development of a technique to measure the surface depth dependence of radiative absorption processes. During this past quarter the direction of our research has been focused on the analysis and experimental methods to extend these techniques to measure this depth dependence.

The phase change signal shown in Fig. (1) was obtained by acoustic surface wave techniques and represents our current capability. This data trace was the result of radiative absorption by a KCl sample at 10.6μ. This material was supplied to us by the Hughes Research Laboratory after being polished and surface etched in HCl. The noise in the signal arises primarily through the fluid coupling process. The relationship between this induced phase variation and the KCl radiative absorption parameters is obscured experimentally by the presence of heat diffusion, and analytically by the absence of an explicit model describing the details of the radiative process.

We present here a model which in the simplest form represents the experimental observation of a surface absorption which is at least an order of magnitude larger than the measured bulk absorption. Consider a depth dependent absorption mechanism resulting in an exponential decay of incident radiation determined by an absorption coefficient $\beta$. In this model, the coefficient $\beta$ is assumed to vary in depth from a value $\beta_S$ at the surface to a smaller value $\beta_B$ representing the bulk coefficient. The simple form of this variation is shown in Fig. (2) in which $\beta_S$ is taken as constant over some characteristic depth d. Figure 2 shows the variation of the relative temperature with depth below the surface after 1 msec which

results from a two-$\beta$ model calculation using parameters $\beta_S$, d, $\beta_B$ given in the insert. These values are comparable to experimental results which measure a surface absorption $\sigma \simeq \beta_S d$ of $\sigma \simeq 2 \times 10^{-3}$. The heat source characterized by this variation of $\beta$ produces a temperature gradiant which is significantly greater than that generated by a single $\beta = 10 cm^{-1}$ also shown in Fig. (2). The retention of this gradiant even in the presence of heat diffusion suggests the feasibility of probing the depth variation of the temperature with a surface wave probe.

The model described above provides a relationship between the absorption process and the resulting temperature distribution. This is a necessary analytical link which can be used to then relate the phase change signals to the absorption parameters. This latter analysis is presently under consideration and will be presented in more detail in a later report. The problem is to include the depth variation of the temperature distribution in the calculation for the induced phase change. As a first step, we have experimentally measured the induced phase change for three different acoustic wavelengths (25$\mu$, 65$\mu$ and 102$\mu$) in Y-cut quartz. It is reassuring to observe the pronounced wavelength dependence shown in Fig. (3) even for a 10 msec pulse for which the calculated temperature distribution has a halfwidth of $\sim$135$\mu$. This is the first observation of such a depth dependence using this technique. Although this effect is not related to a surface absorption, it does indicate the feasibility of applying the acoustic probe technique to measure a temperature gradiant arising from such an absorption. In

addition, this effect in Y-cut quartz provides a controlled experiment which can be used to develop the details of a more complex analysis necessary for quantitative measurements in alkali halide materials.

The data taken to date on KCl indicates two results:

(1) Analysis using a single absorption coefficient model yields a value for $\beta$ of $\sim 5 \times 10^{-2} cm^{-1}$. Since this analysis assumed negligible heat diffusion and included only a single acoustic wavelength, such a value for $\beta$ merely represents a lower limit for $\beta_S$ and an upper limit for $\beta_B$. Clearly no estimate for the characteristic depth d is possible.

(2) As suggested by Fig. (2), which also shows the energy depth profile for a surface wave in KCl of $\lambda_s \simeq 10\mu$, this probe technique may possibly resolve a temperature depth profile following absorption of a 1 msec $CO_2$ laser pulse. Note that Fig. (1) shows, sizeable phase change signals can be obtained for KCl with an incident laser energy of $\sim$200 mJ in a 100 msec pulse. Since the heat diffusion length will decrease by a factor of 10 using a 1 msec pulse, induced phase change signals of comparable magnitude could be induced by short pulses with a peak power of $\sim$20 watts. This is well within the present technical capability and points out that data which reduces the effects of heat diffusion to a greater extent is attainable with 100 $\mu$sec pulses of $\sim$100-200 watts peak power. Fluid coupling transducers are presently being fabricated by Dr. David White and Mr. Ray King of China Lake NWC which will allow a step variation of acoustic wavelength for studies on KCl surfaces. These transducers will yield measurements which

span a depth of ∿10-75μ below the surface and will be used shortly in the initial surface studies with long $CO_2$ pulses. This will be adequate to establish limits on the absorption parameters but a new laser system with the above capabilities will be necessary to obtain more detailed information.

f.2.b. Surface Wave Energy Transfer to KCl Surfaces via Fluid Coupling

A study has been carried out to investigate how surface waves are most efficiently coupled to KCl surfaces by a fluid layer. In particular it is of interest to consider what optimum piezoelectric material should be used to excite the initial wave. This analysis extends the original formalism[3] describing a fluid layer wave to include a calculation of the percentage acoustic energy propagating in the KCl surface wave. Three common piezoelectric materials were considered: Y-cut Quartz, Lithium Niobate, and Bismuth Germanium Oxide (BGO). The results are sensitive to the number of layer wave modes propagating and show the following qualitative behavior:

(i) For fewer than about 7 modes propagating, as in the case of thin fluid layers less than 50μ thickness, Y-cut Quartz and Lithium Niobate are very comparable and significantly better than BGO. The percentage of energy in KCl can be as great as 50% depending on the number of modes.

(ii) For a larger number of modes, BGO offers a greater advantage. A layer wave with this piezoelectric is capable of leading to 10% of the layer wave energy in KCl propagation independent of the mode number.

These results do not account for the boundary value problem of acoustic energy losses incurred by entry and exit from the layer wave fluid region which can be excessive. However, these results do suggest that Y-cut Quartz is an adequate choice considering the availability and price of the material, as well as the ease of fabrication for our purposes.

## References


1. F. A. Kroger, J. H. Marburger et al., Electronic Sciences Laboratory, University of Southern California, "IR Window Studies", Quarterly Technical Reports No. 3 AFCRL TR-73-0325 and No. 7 AFCRL TR-74, Contract No. F19628-72-C-0275, ARPA Order No. 2055.

2. ibid., Quarterly Technical Reports No. 4 AFCRL TR-73-0414, No. 5 AFCRL TR-73-0680, and No. 6 AFCRL TR-74-0060.

3. P. W. Staecker and W.C. Wang, J. Acoust. Soc. Am. 53, 65 (1973).

LASER INDUCED
PHASE VARIATION

10.6μ – KCl
OPTOVAC

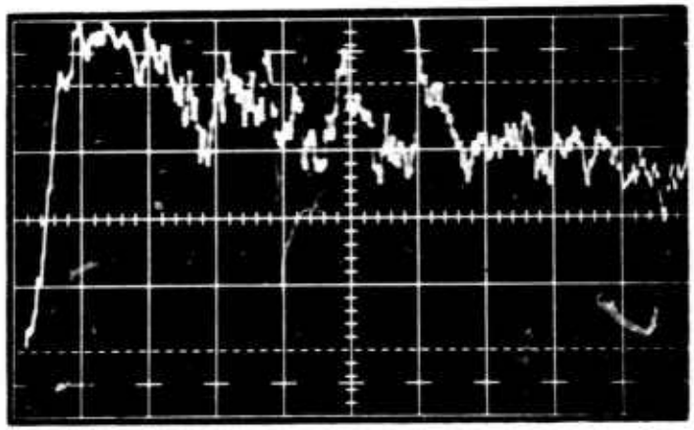

200 msec/DIV
10 mv/DIV

$P_{TR} = 2 \pm .15$ W

$\tau_p \simeq 100$ msec

$\nu = 123.8$ MHz

$\lambda_s \simeq 8\mu$

$\Delta\phi_p \simeq 10$ mrad

FIGURE 1

# TEMPERATURE DEPTH PROFILE ON KCl AT t = 1 MSEC

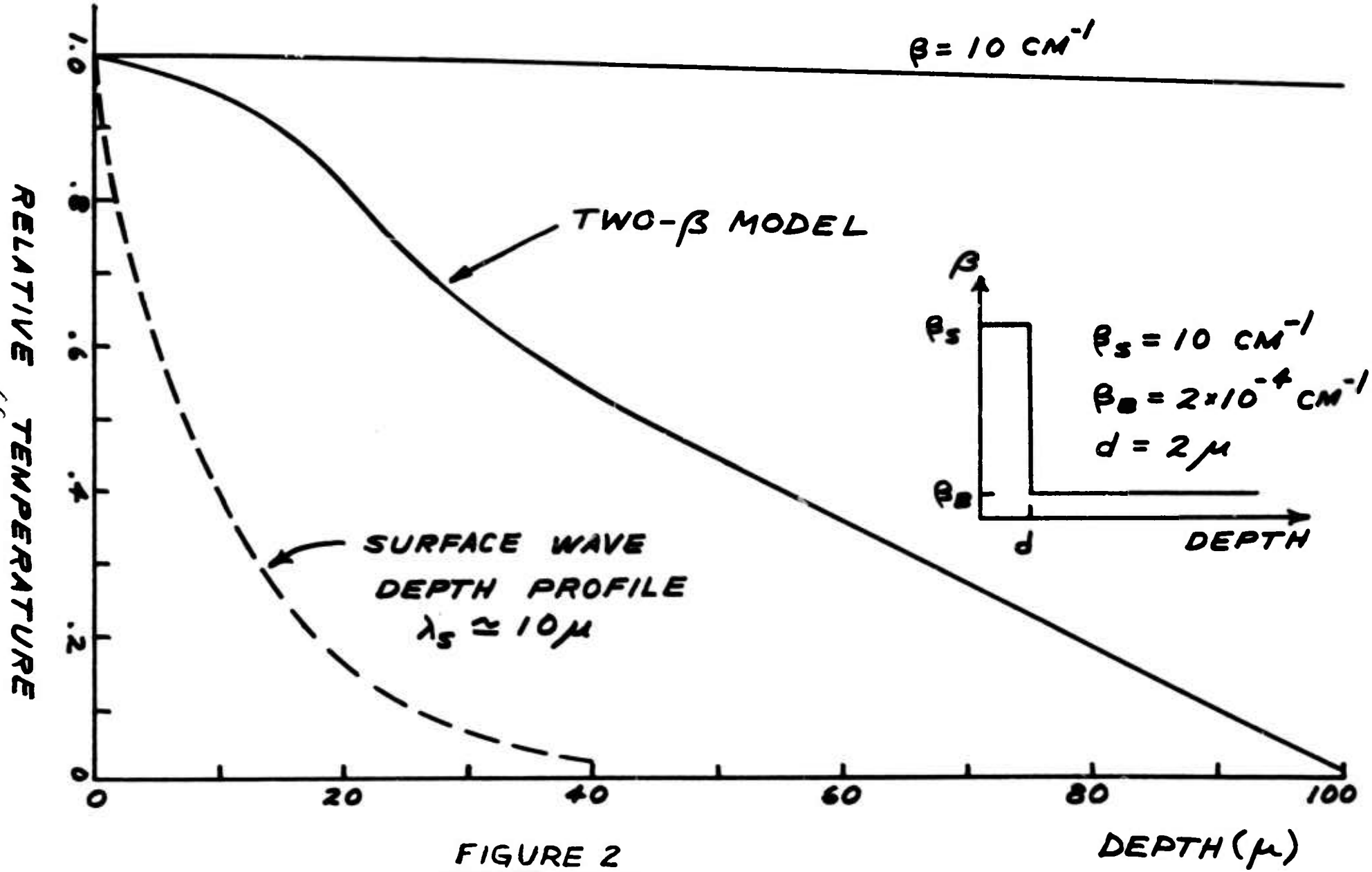


FIGURE 2

# ACOUSTIC WAVELENGTH DEPENDENCE OF INDUCED PHASE CHANGE

$$\Delta\phi = \frac{2\omega}{V_0} f_B \int_0^L \{\epsilon_\lambda - \alpha_v \Delta T_\lambda\} d\lambda$$

Surface wave of wavelength $\lambda$ probes the induced thermoelastic strain $\epsilon_\lambda$ and the temperature variation $\Delta T_\lambda$.

$\omega_0 = 2\pi \cdot (123\ MHz)$

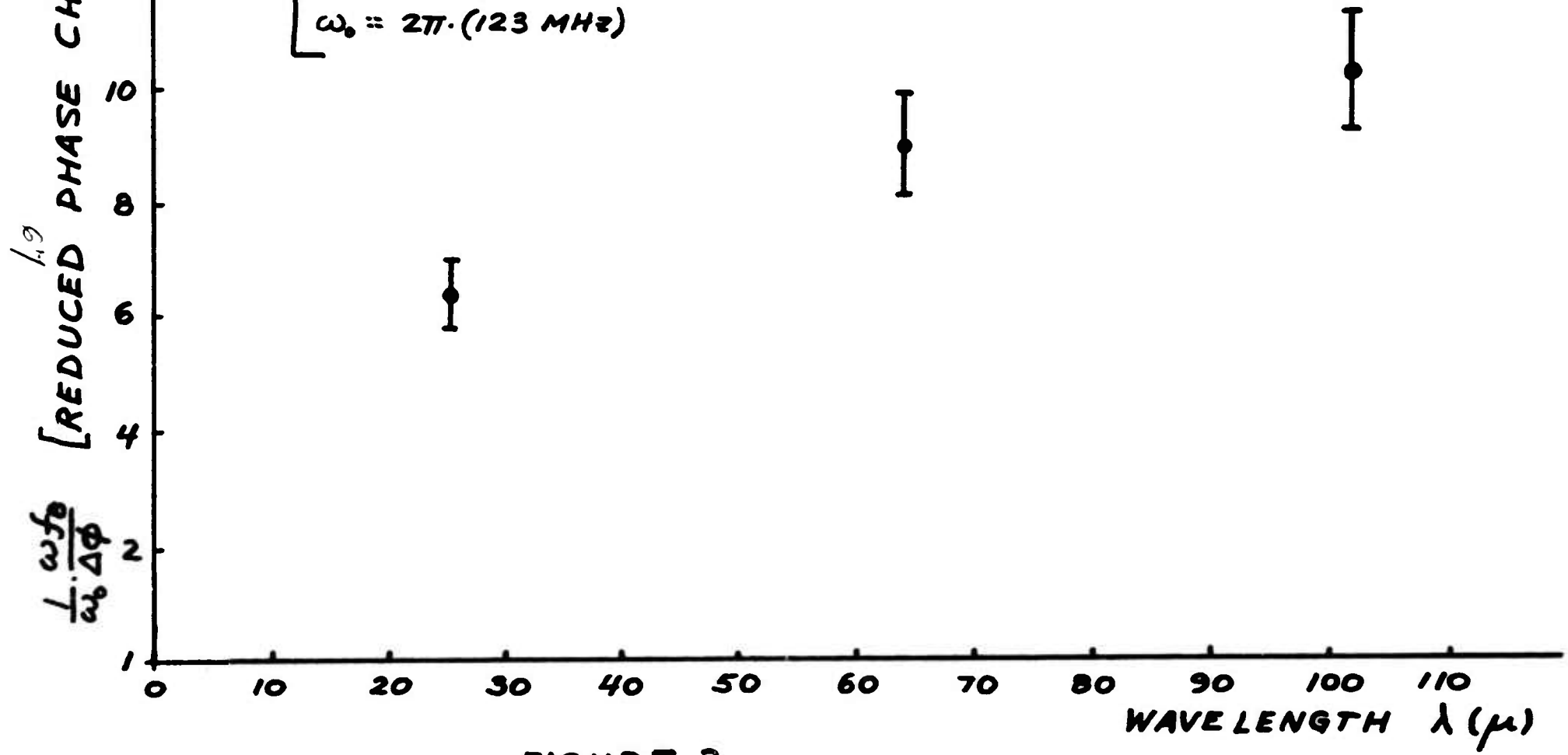


FIGURE 3

## f.3 Absorption Studies of CdTe and ZnSe

B. V. Dutt and W. G. Spitzer

In the last quarterly report we indicated the initiation of a study of the absorption processes in CdTe and ZnSe for both undoped and intentionally doped material. The following is a brief summary of our initial infrared transmission measurements in the range 250cm$^{-1}$ to 10,000cm$^{-1}$. In each case where a specific sample or material is discussed the source of the material is indicated in parentheses.

CdTe:

(1) Annealing of CdTe (Hughes) and CdTe-Cl with $5 \times 10^{16}$Cl/cc (II-VI, Inc.) samples at 885°C under a $p_{Cd}$ 0.8 atm decreased the transmission at 250-500cm$^{-1}$ slightly. This is probably due to the formation of $Cd_i^{\cdot}$ causing free electrons.

(2) Annealing (Hughes and II-VI, Inc. material) at 885°C under $p_{Te_2}$ = $5.10^{-2}$ atm resulted in samples, that are inhomogeneous and highly absorbing and opaque at frequencies 250cm$^{-1}$-500cm$^{-1}$.

(3) A survey of the literature (B. M. Vul, et al., Sov. Phys. Semiconductors, V4, No.1, P. 50, 1970 and V. Capek et al. Phys. Stat. Solidi (b), 56, 739 (1973) indicates that Te-doped CdTe shows p-type conduction. The earlier results of de Nobel Philips Res. Reports 14 (1959) and the recent results of Professor F. A. Kroger's group (see section d.2) indicate p-type conduction on the lower $p_{Cd}$ side of the phase diagram.

We therefore carried out absorption measurements at room temperature and at liquid nitrogen temperature on Te-annealed CdTe with a view to obtain free carrier absorption cross-section in p-type CdTe. Our experiments are at a preliminary stage.

(4) In-doped CdTe (II-VI, Inc.) with $1 \times 10^{17}$In/cc which is annealed in high $p_{Cd}$ or $p_{Te_2}$ at 885°C is less transparent than the as-received material. The In-doped material annealed in Te-atmosphere is more transparent than undoped similarly annealed material.

Local Mode Studies:

(1) Li alloyed on the surface of CdTe and diffused in gives a strong absorption band centered at 270cm$^{-1}$ (see Figure 1). Samples of 3 mil thickness are opaque in this region. Suspecting the possibility of a second phase (such as $Li_2Te$) we performed reflectivity measurements in this range and found no indication of a second phase.

(2) We are now modifying a P.E. 301 spectrometer to extend the low temperature local mode measurement capability down to $\sim$ 70cm$^{-1}$. The

extension is necessary to see localized vibrational modes due to Si or Al in CdTe. The frequencies estimated in an isotropic approximation occur around $200cm^{-1}$ which is slightly below our present lower limit of $\sim 220cm^{-1}$. We have grown a polycrystalline ingot of Si-doped CdTe and we plan to grow Al-doped material very shortly.

Crystal Growth: In view of the slow growth rates (typically 3-5mm/day) involved in the travelling heater method (THM), we have changed to either (1) freezing in a gradient or (2) horizontal Bridgman technique. Some of the initial growth efforts using THM yielded polycrystalline CdTe doped with chromium. Using the freezing in a gradient technique we obtained an ingot of Si-doped CdTe. Also, the horizontal Bridgman technique was used to grow In-doped material. These materials have not yet been evaluated as to microstructure, homogenity, transmission, electrical characteristics, etc.

Within the next few weeks we intend to grow separate ingots doped with Si, P, Ge, Cr and Al.

ZnSe

Undoped Material: Some preliminary measurements of undoped material have been initiated and we find that laser calorimetry at 10.6μ gives an absorption coefficient of $4.1 \times 10^{-4}cm^{-1}$ on polycrystalline ZnSe (Raytheon grown, supplied by II-VI, Inc.). We plan to do laser calorimetry measurements on Zn and Se annealed samples of the polycrystalline material.

Al-doped Material: Untreated, as-grown Al-doped material (Eagle Picher Co.) shows low carrier density as inferred from the absence of free carrier absorption in the infrared. Al-ions are supposed to go on zinc sites in ZnSe and act as shallow state single donors; these donors may be compensated by native acceptors, like $V''_{Zn}$. It is also likely that the donors and acceptors may form complexes which are either singly negatively charged $(Al_{Zn}\text{-}V_{Zn})'$ or neutral, involving two substitutional Al-ions and a doubly charged zinc vacancy $(2Al_{Zn}\text{-}V_{Zn})^{x}$. The charge compensation in its most general form is

$$\left[Al_{Zn}^{\cdot}\right] = \left[e'\right] + 2\left[V''_{Zn}\right] + \left[\left(Al_{Zn}V_{Zn}\right)\right]'$$

If by annealing the crystal in a zinc-rich atmosphere, the concentration of $V''_{Zn}$ can be reduced then one anticipates partial relative increase of the role of electrons. Under sufficiently zinc-rich conditions the $\left[V''_{Zn}\right]$ could become a minority species with charge compensation mainly by electrons: $\left[Al_{Zn}^{\cdot}\right] \approx [e']$. This corresponds to a saturation limit of the electron concentration equal to [Al] assuming no carriers are excited into the conduction band from other unintentional impurities or native donors such

as $Zn_i^{\cdot}$ .

Based on the above arguments and previously reported work (A. Mitsuishi, et al., Suppl. Prog. Theor. Phys, Vol. 45, p. 21, 1970), we carried out some preliminary measuremnts and the results are as below:

1. As reported by Mitsuishi, et al., we find 6 absorption bands due to Al in ZnSe at 339, 342, 346, 359, 388 and 393cm$^{-1}$. The band at 359cm$^{-1}$ was identified as the one due to isolated substitutional $Al_{Zn}$. The remaining five bands were not well identified . Assigning these to the ($Al_{Zn}$-$V_{Zn}$) complex,the so-called A-center or self-activated luminescent center (see e.g. Aven and Prener, The Phys. and Chem. of II-VI Compounds, or articles by S. Shionoya and J. Schneider in II-Vi Semiconducting Compounds by D. G. Thomas) poses problems from symmetry considerations as indicated by Mitsuishi et al. The $T_d$ site symmetry of $Al_{Zn}$ will be lowered to $C_S$ if $Al_{Zn}$-$V_{Zn}$ pairs form. This would lead to lifting of the triple degeneraty of the $Al_{Zn}$ mode and one expects three bands besides the isolated $Al_{Zn}$ band at 359cm$^{-1}$. But the experimental data shows 5 other bands in addition to the 359cm$^{-1}$ band. The bands may involve more than one defect center or more than one Al per defect.

(2) Annealing of the ZnSe-Al crystals (Eagle Picher Co.) at 885°C in $p_{Zn} \simeq 1.8 \times 10^{-3}$ atm for 5-1/2 hours resulted in a sample that is opaque in the low frequency range 250cm$^{-1}$-1000cm$^{-1}$ for a 19.5 mil thickness. Absorption measurements at room temperatures and liquid nitrogen temperatures at higher frequencies show free carrier absorption with the absorption coefficient being proportional to $\nu^{-3}$. We have been unable to locate any reference to free carrier absorption measurements in ZnSe, either for doped or undoped and for n-type or p-type materials.

(3) Annealing of ZnSe-Al at 885°C in $p_{Se_2} \approx 5 \times 10^{-2}$ atm for 5-1/2 hours resulted in a reduction of the intensity of the bands due to aluminum except for the one band at 359cm$^{-1}$, as compared with the bands in the as-grown material.

(4) Besides the above arguments regarding compensation of the positively charged $Al_{Zn}^{\cdot}$ donors the compensation can also be met by doping with acceptors in concentrations comparable to the donor concentration. With this in mind we diffused Cu into ZnSe-Al under Zn-rich conditions. The Cu was introduced from an electrolytically deposited layer formed by using an aqueous solution of $CuSO_4$ as the electrolyte. Absorption measuremnts on this doubly-doped ZnSe-Al, Cu shows the 359cm$^{-1}$ band and three new bands. (See Figure 2) As outlined above these bands could arise from the formation of $Al_{Zn}$-$Cu_{Zn}$ pairs.

(5) We performed absorption measurements for ZnSe-$^7$Li and ZnSe-$^7$Li + $^6$Li samples prepared here by Li diffusion and find some major differences with the earlier reported work in which Li was introduced as a dopant during crystal

growth.

To pursue the results obtained above, we plan to carry out the following measurements for ZnSe-Al with a view to identify the defect center or centers causing the 5 bands mentioned above and also a complete free carrier study to determine the free carrier absorption cross-section. The experiments will be as follows:

(1) Annealing of the crystals (ZnSe-Al) at various temperatures, under different partial activities of the components and for different Al doping levels followed by both Hall measurements and infrared absorption measurements at room temperatures and liquid nitrogen temperatures on these variously annealed samples to determine the free carrier absorption cross-section.

(2) Electron irradiation of the samples previously annealed in different Zn-rich atmospheres, and infrared measurements on these.

(3) To help identify the nature of defect centers of Al-doped material, we plan to diffuse Li into this material and carry out infrared measurements.

(4) We wish to pursue the work on Li-doped ZnSe with the isotopes $^{6}Li$ and $^{7}Li$ separately and mixed to identify the absorption band and their influence, if any, on 10.6μ absorption level.

Fig. 1: ZnSe-Al

(1) ZnSe-Al, as grown, t = 18 mils, LNT.

(2) ZnSe-Al, annealed in $P_{Se_2} \sim 5 \times 10^{-2}$atm for 5½ hours with the crystal at 885°C. t = 19.5 mils, LNT.

(3) AnSe-Al, Cu diffused at 885°C for 40 hours at $P_{Zn} \sim 2 \times 10^{-3}$atm, t = 4.5 mils, LNT.

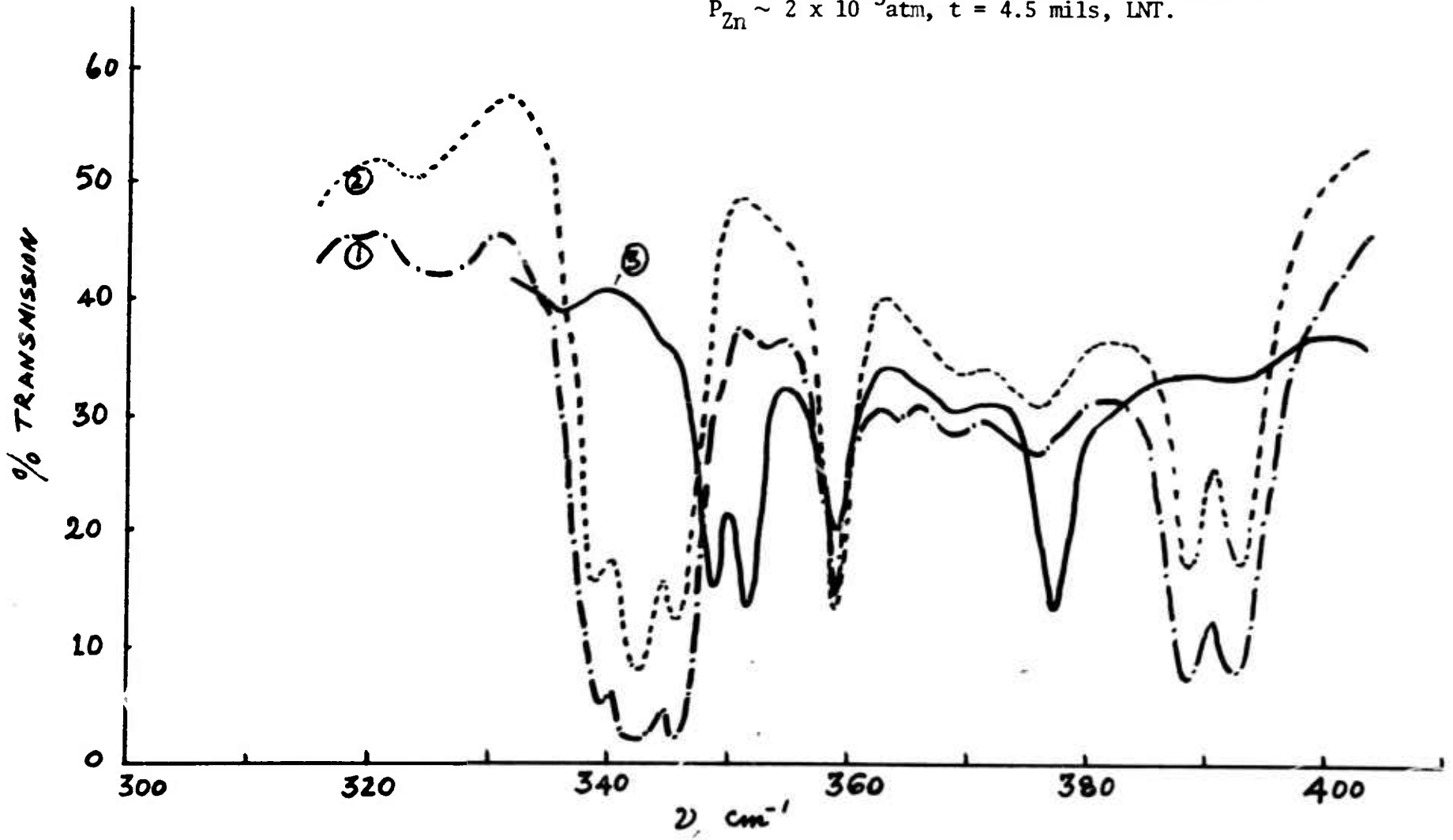

Fig. 2: Li-doped CdTe

(1) $^{7}_{Li}$ diffused CdTe-Cl (Cl: 5 x $10^{16}$/cc), t ≃ 5 mils at room temperature.

(2) Same sample as (1) thinned to 3 mils at Liq. $N_2$ temp.

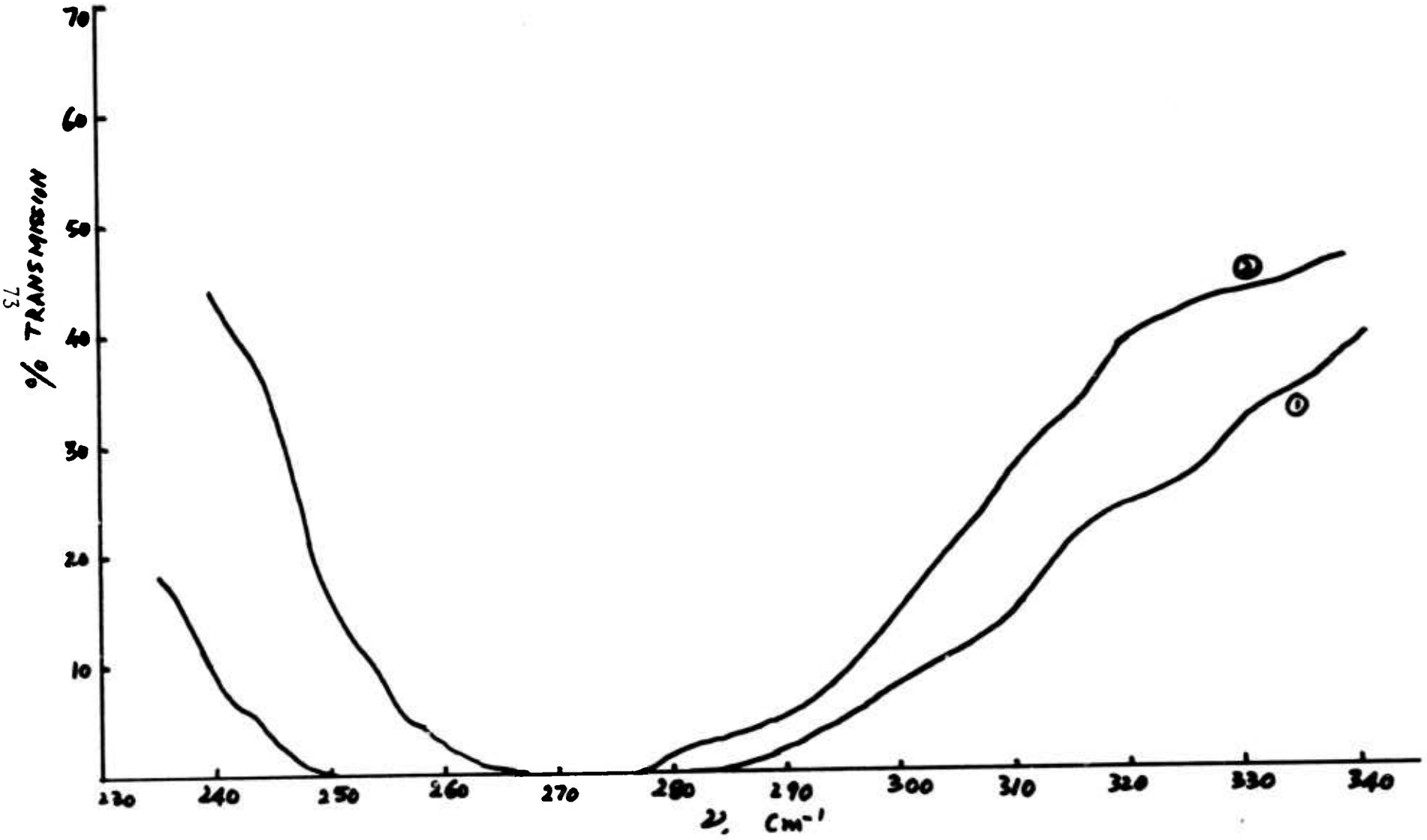

g.1 Characterization of Optical Performance of IR Window Systems

M. Flannery - J. H. Marburger

During this reporting period, we continued our analysis of the diffraction theory of thermal lensing begun in QPR #6. Our narrative review of this theory, including results obtained under this contract, is continued below following the updated table of contents. Figure 9.1 in the sixth quarterly report contained a minor error, and we reproduce below a corrected version.

Simultaneously with the preparation of this review, we have been extending the diffraction theory of thermally distorted windows to anisotropic (crystalline) windows. We have verified that a window made of a slab of material of cubic symmetry will exhibit cylindrically symmetric elastic properties in the plane stress approximation if oriented in a [111] direction. That this might be the case was suggested in unpublished work of Horrigan (Raytheon) which was brought to our attention by Bendow (AFCRL). Our analysis will be described in detail in a subsequent report.

Another project initiated during this period is being conducted in support of the acoustic surface wave IR absorption measurement technique of Parks. In this technique, the "surface temperature" of a sample is detected by measuring the temperature induced change in phase velocity of an acoustic surface wave launched across the heated (illuminated) sample surface. In fact the detected phase change depends not only on the surface temperature, but also on the temperature within about one acoustical wavelength of the surface. This suggests that measurements made at different acoustical wavelengths contain information about the depth dependence of the temperature, and therefore also about the depth dependence of the heat source, or absorption coefficient. The question is, how can this information be extracted?

The relation between detected phase difference $\varphi(q)$ and temperature T is approximately

$$\varphi(q) = \int_0^\infty \exp(-qz)\ F(z)\ dz$$

where q is the acoustical penetration factor (wave number) and F(z) is a known linear functional of the temperature at depth z. If F (z) were known, the absorption coefficient at depth z could be obtained in a relatively straightforward way. Now F(z) is clearly the inverse Laplace transform of $\varphi(q)$, so that

$$F(z) = \frac{1}{2\pi i} \int_c \exp qz\ \varphi(q)\ dq\ ,$$

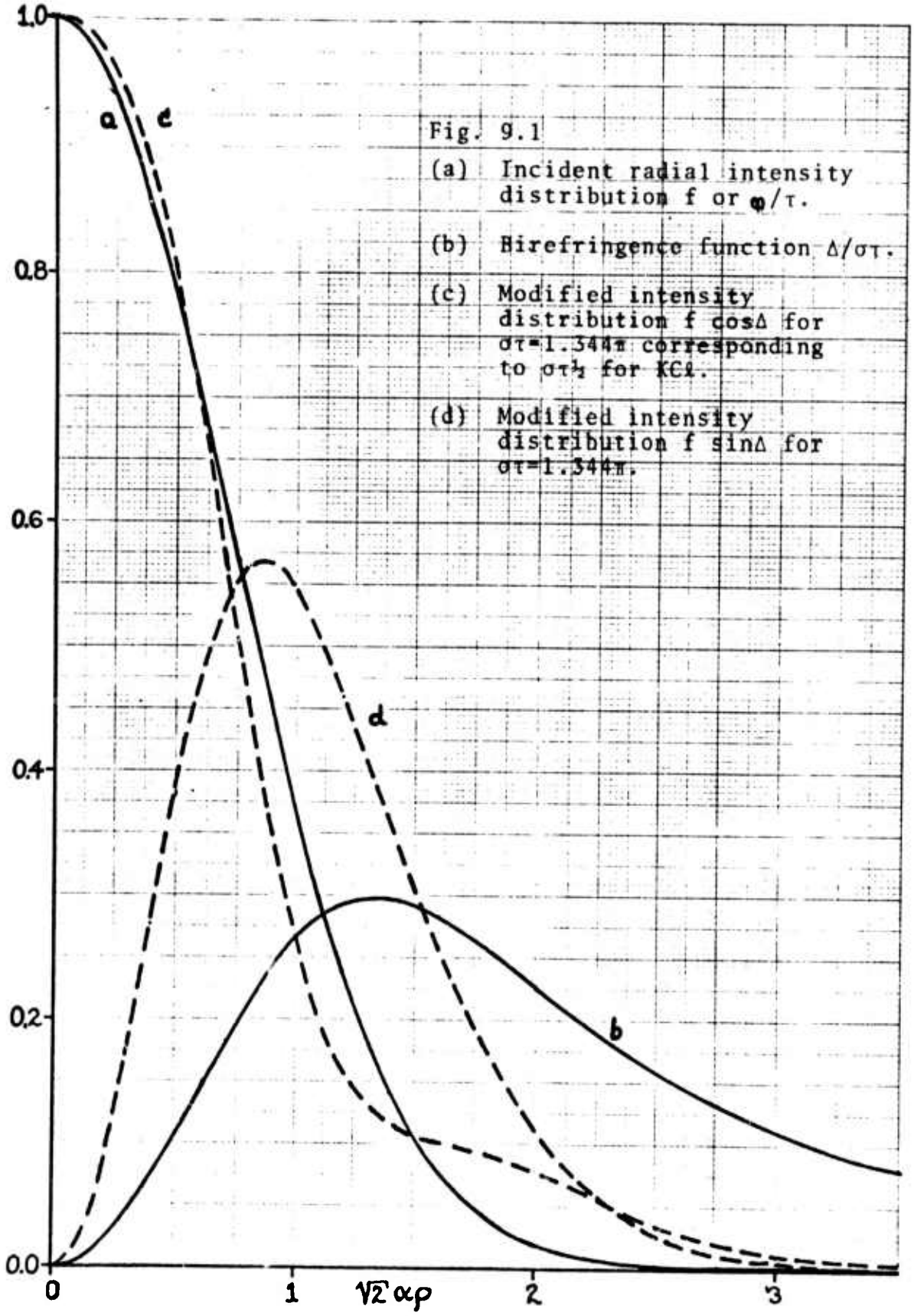


Fig. 9.1

(a) Incident radial intensity distribution f or $\varphi/\tau$.

(b) Birefringence function $\Delta/\sigma\tau$.

(c) Modified intensity distribution f cos$\Delta$ for $\sigma\tau=1.344\pi$ corresponding to $\sigma\tau_{\frac{1}{2}}$ for KCl.

(d) Modified intensity distribution f sin$\Delta$ for $\sigma\tau=1.344\pi$.

Where c is a contour obtained from a path parallel to the imaginary q axis and (loosely speaking) to the right of all singularities of $\varphi(q)$ in the complex q plane. While $\varphi(q)$ is known only on the real axis (and only approximately even there), it is nevertheless possible to model its behavior in the complex plane. For example, one may represent $\varphi(q)$ by a Padé approximant (a ratio of two polynomials) and evaluate the inverse transform by summing the residues at the poles of the resulting integrand. This method is feasible only if $\varphi(q)$ is known in some detail over a wide range of q values.

A simpler method, which is more appropriate when $\varphi(q)$ is known for only a few q values, is to replace the unknown F(z) by a trial function whose transform can be fit to the $\varphi(q)$ data by variation of parameters. This method is particularly suitable for temperature distributions arising from a monotonically decreasing absorption coefficient near the surface. The resulting temperature distribution can be modeled easily with a few-parameter function whose Laplace transform can be performed analytically. Preliminary wavelength dependent data have just become available, and the results of a trial function fit will be reported in the next quarterly report.

List of Sections of Review of Diffraction Theory of Thermal Lensing in Thin Windows (Sections 1 through 10 appear in QPR #6)

1. Diffraction Integral for Beams
2. Vector Corrections
3. Aberration Matrix for Thin Windows
4. Aberration Matrix for Cylindrical Anisotropy and Inhomogeneity (Thin Windows)
5. Diffraction Field for Cylindrical Anisotropy
6. Diffracted Beam Geometry for Specific Incident Polarization States
7. Relation to Notation of Bendow and Gianino
8. General Properties of Radia Dependence of Transmitted Intensity
9. Aberration Functions for a simple Window Model
10. Focal Intensity with No Birefringence for Simple Window Model
11. Influence of Birefringence on Focal Intensity for Simple Window Model
12. Influence of Birefringence on off-axis Intensity for Simple Window Model
13. Effect of Refocusing in Simple Window Model

14. Aberration Matrix for Non ideal Window Systems
15. Approximate Methods for Non ideal Systems I
16. Approximate Methods for Non ideal Systems II
17. Strategy for computing Aberration Matrix
18. Computation of the Aberration Matrix for cylindrical symmetry
19. Crystal symmetries which lead to cylindrical symmetry in the plane stress approximation
20. Remarks on other orientations of crystalline Windows
21. Approximate computation of the Aberration Matrix for non-cylindrical symmetry
22. Diffraction Field for Acentric System: Thermal slewing

## 11. Influence of Birefringence on Focal Intensity for Simple Window Model

If the birefringence parameter $\sigma$ is not zero, then Eq. (10.1) must be replaced by (8.2):

$$|E(0,\rho)| = \frac{E_i}{\rho} \left| \int_0^1 \rho' d\rho' \exp\left[ i\tau \exp(-2\alpha^2\rho'^2) \right] \right.$$
$$\times \cos \tfrac{1}{2}\sigma\tau \left\{ \left[ \frac{1 - \exp(-2\alpha^2\rho'^2)}{\alpha^2\rho'^2} \right] - 2\exp(-2\alpha^2\rho'^2) \right\}$$
$$\left. \times \exp(-\alpha^2\rho'^2) \right| . \qquad (11.1)$$

Figure (11.1) shows how the characteristic focal intensity degradation time $\tau_{\frac{1}{2}}$ is influenced by nonzero values of $\sigma$ when the truncation has the optimum value $\alpha = 1.1224$, or $h = 0.0805$. Of the materials in common use for $\lambda = 10.6\,\mu m$ optical elements, only KCl shows a substantial degradation due to birefringence. Several materials useful in the 2 to 5 $\mu$m regime show quite large degradation, as anticipated by Bendow and Gianino. The manner in which the focal intensity decreases with time is shown in Figure (11.2) for several values of $\sigma$. Notice that as $\sigma$ increases, the oscillations in focal intensity become more pronounced and have shorter period. The period is roughly inversely proportional to $\sigma$, as anticipated in section 8, but accurate analytical estimates of the times for maxima and minima are difficult because of the complexity of (11.1). Notice that in the focal plane ($z = \rho$) the field depends

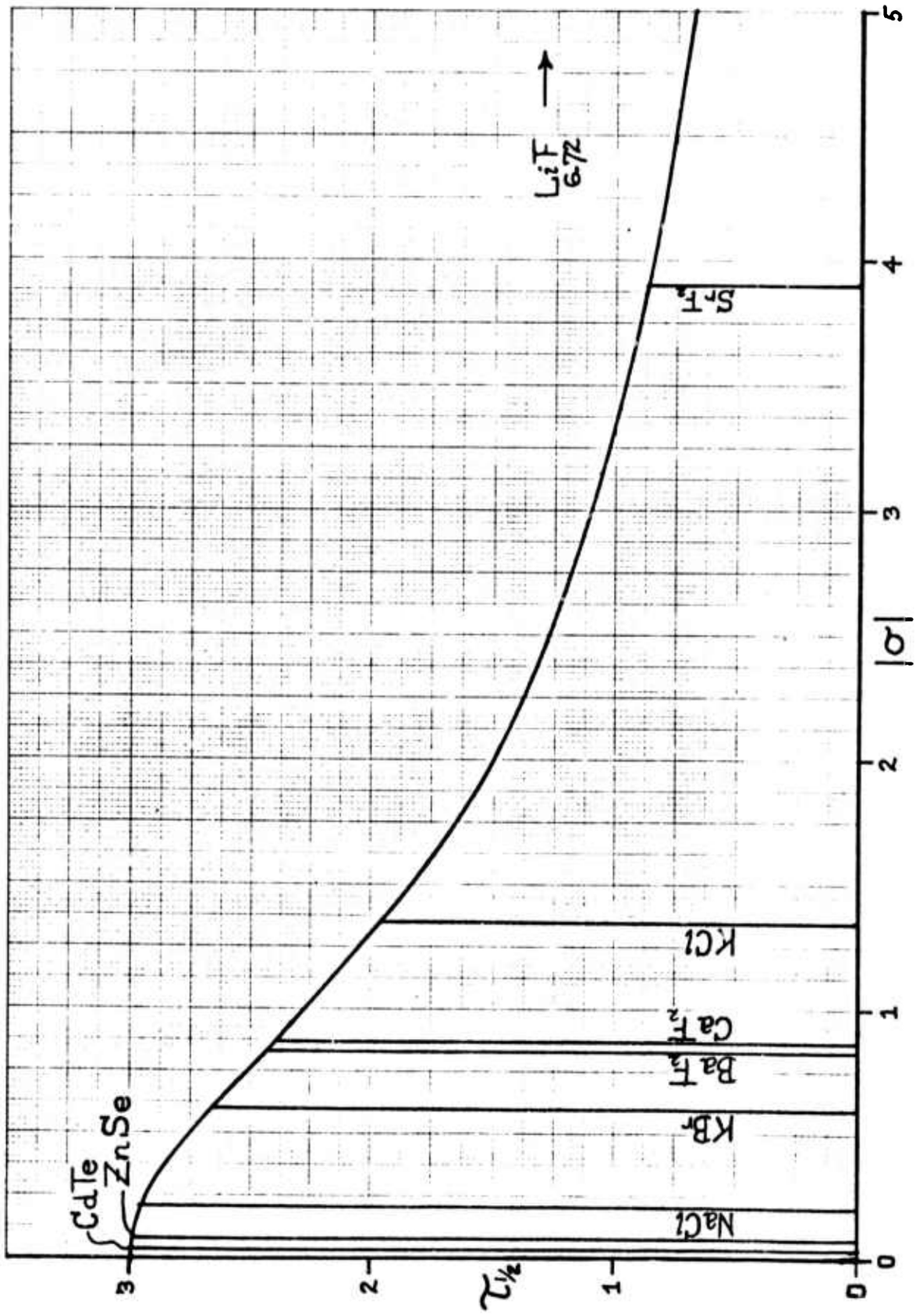


Fig. i1.1 Focal half-intensity degradation time as a function of birefringe.

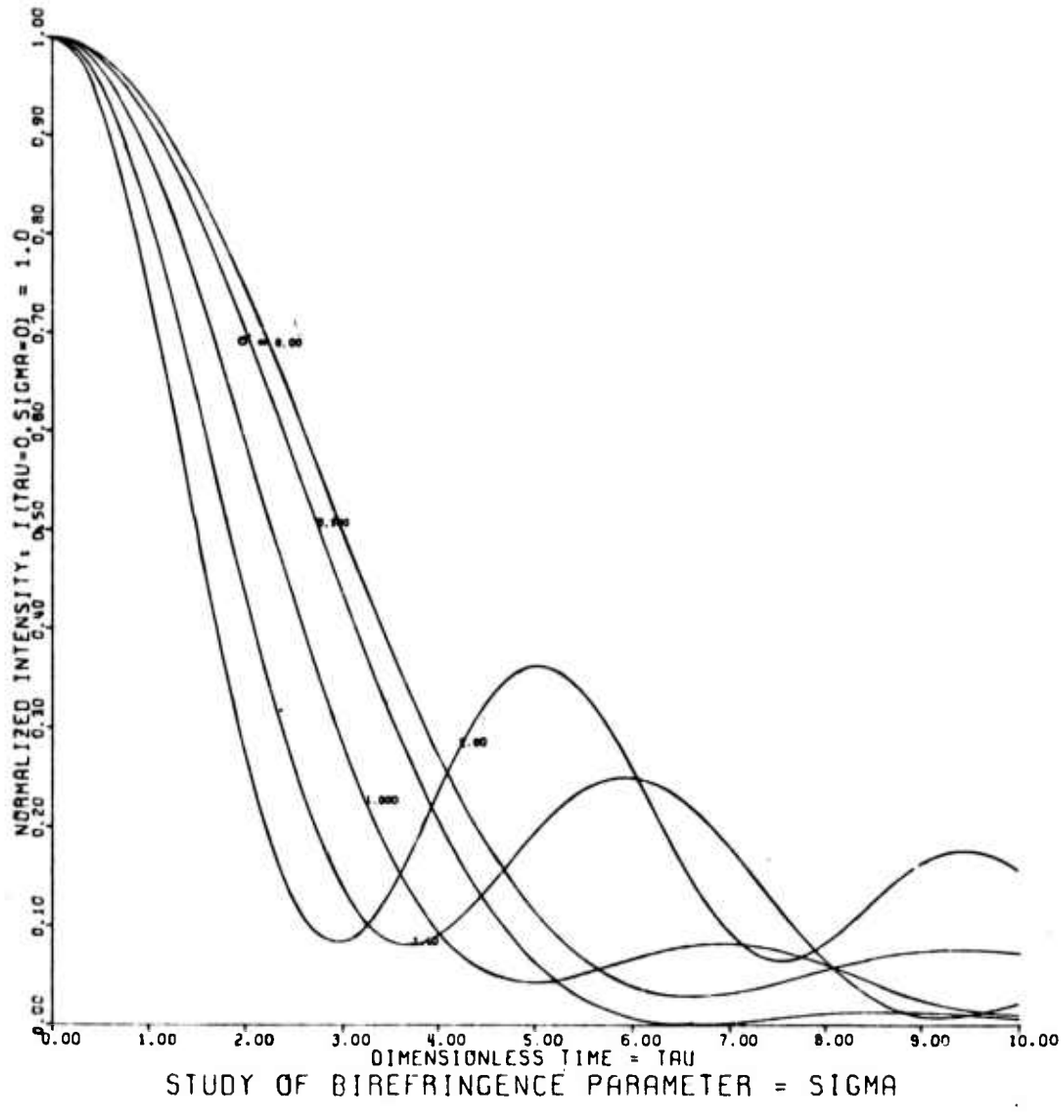


Fig. 11.2 Focal intensity evolution in time for several values of $\sigma$.

only upon the magnitudes, and not the signs, of both $\sigma$ and $\tau$

## 12. Influence of Birefringence on Off-Axis Intensity for Simple Window Model

At off-axis points in the focal plane, the fields may be computed from (6.4), (8.7) and (8.8). Figure 12.1 shows the evolution of a typical radial intensity profile for $\sigma = 2$ and optimum truncation. At $\tau = 0$, the profile is very nearly gaussian, as one expects for this nearly untruncated case. But as time passes, the axial intensity decreases and the power oscillates between a central peak and an off axis "ring". That the ring arises from birefringence effects is seen clearly in Figures 12.2 and 12.3 where the total intensity is resolved into contributions from $|E_o|^2$, $|E_2|^2$ and the interference term $-2\,\mathcal{R}e\,(E_o E_2^*)$ appropriate for linear incident polarization. Notice that the odd looking shoulder on the profile at time $\tau = 1.5$ is composed of the relatively structure free components $E_o$ and $E_2$.

It is of interest to examine the validity of the approximate formula for the location of the off axis ring

$$\rho_m = 3.1\,\mathcal{R}/\rho'_m \quad , \tag{12.1}$$

derived in section 8. Recall that $\rho'_m$ is the radius ($\rho = r/d$) at which the factor in the integrand of (8.8) multiplying $J_2(\rho\rho'/\mathcal{R})$ has its maximum value. The integrand, omitting the factor $J_2 \exp i\varphi$, is easily evaluated, and is shown in Figure 12.4 for the cases for which Figures 12.2 and 12.3 were computed. (For those cases, $\mathcal{R} = R/kd^2$ was set equal to unity, corresponding to focusing at the Rayleigh range of the window aperture). The inferred values of $\rho_m$

$$\rho_m = 4.13 \quad \text{for} \quad \tau = 1.5$$

$$\rho_m = 4.77 \quad \text{for} \quad \tau = 3.0$$

are indicated in Figures 12.2 and 12.3. Better agreement is obtained for smaller values of $\sigma\tau$.

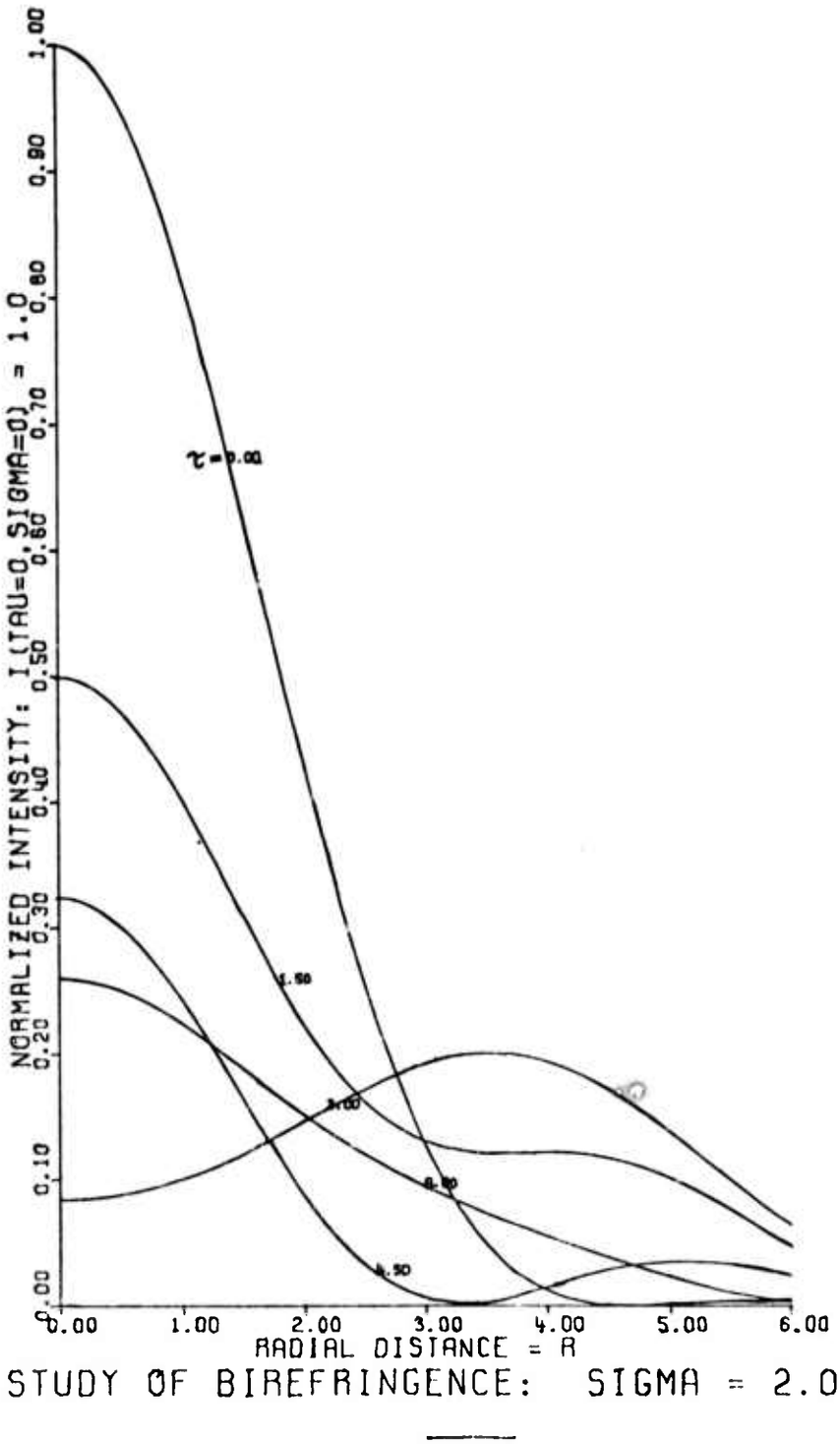


Fig. 12.1 Focal plane intensity along the x-axis for a beam linearly polarized in the x-direction.

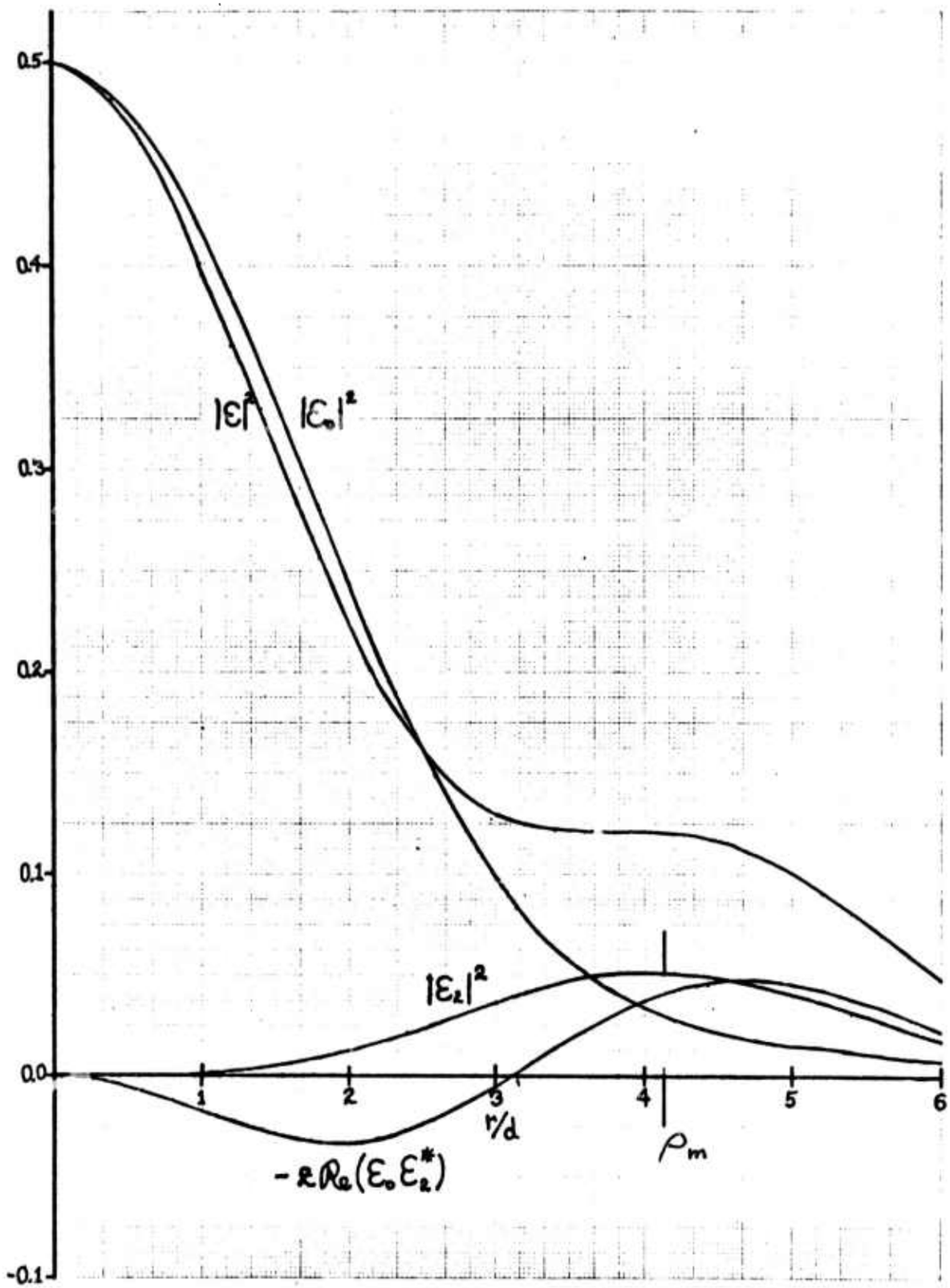


Fig. 12.2 Decomposition of the $\tau=1.5$ curve of Fig. 12.1 into components: $|E|^2=|E_0|^2+|E_2|^2-2Re(E_0E_2^*)$

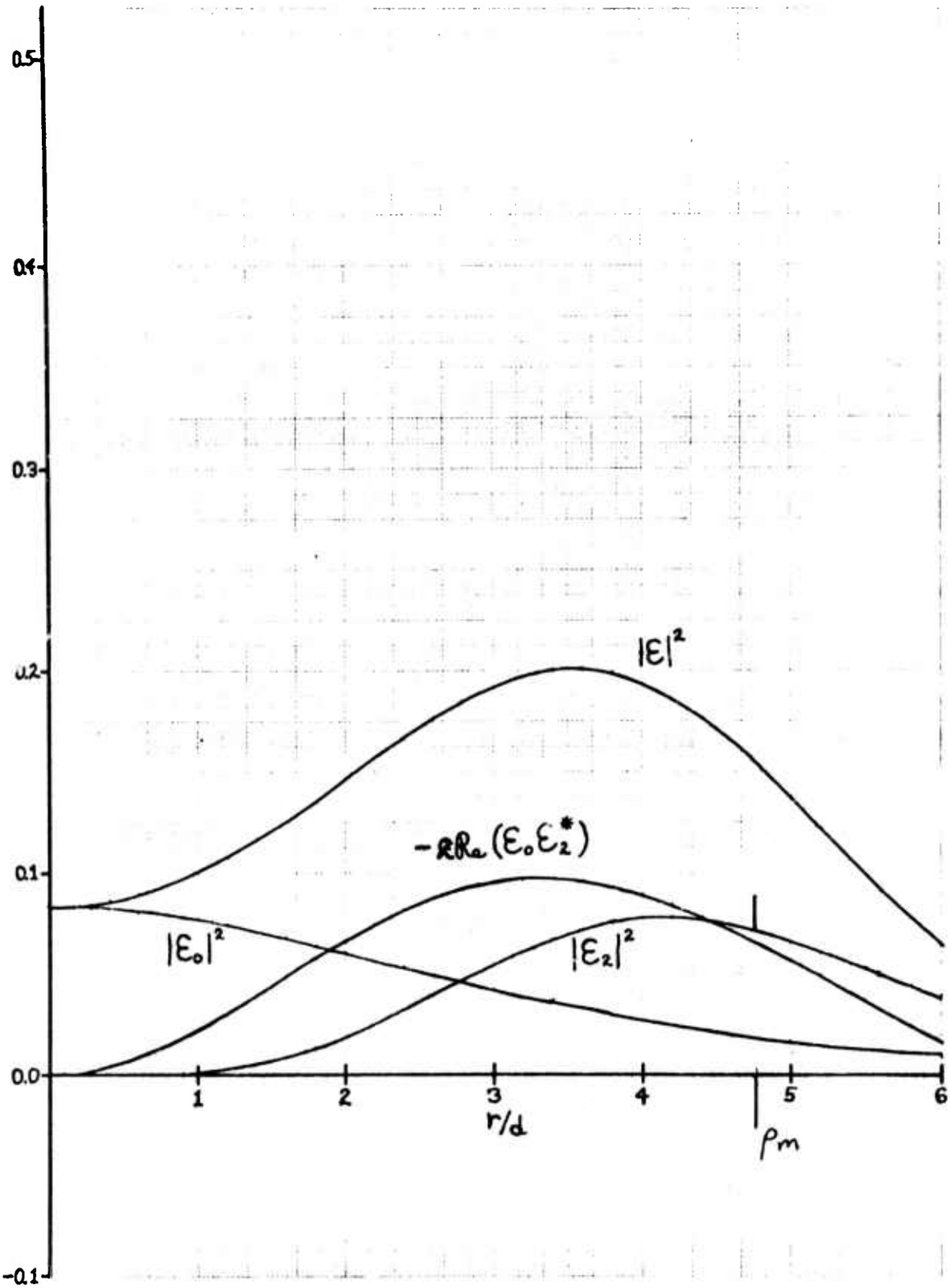


Fig. 12.3 Decomposition of the $\tau$=3.0 curve of Fig. 12.1 into components: $|E|^2=|E_0|^2+|E_2|^2-2Re(E_0E_2^*)$

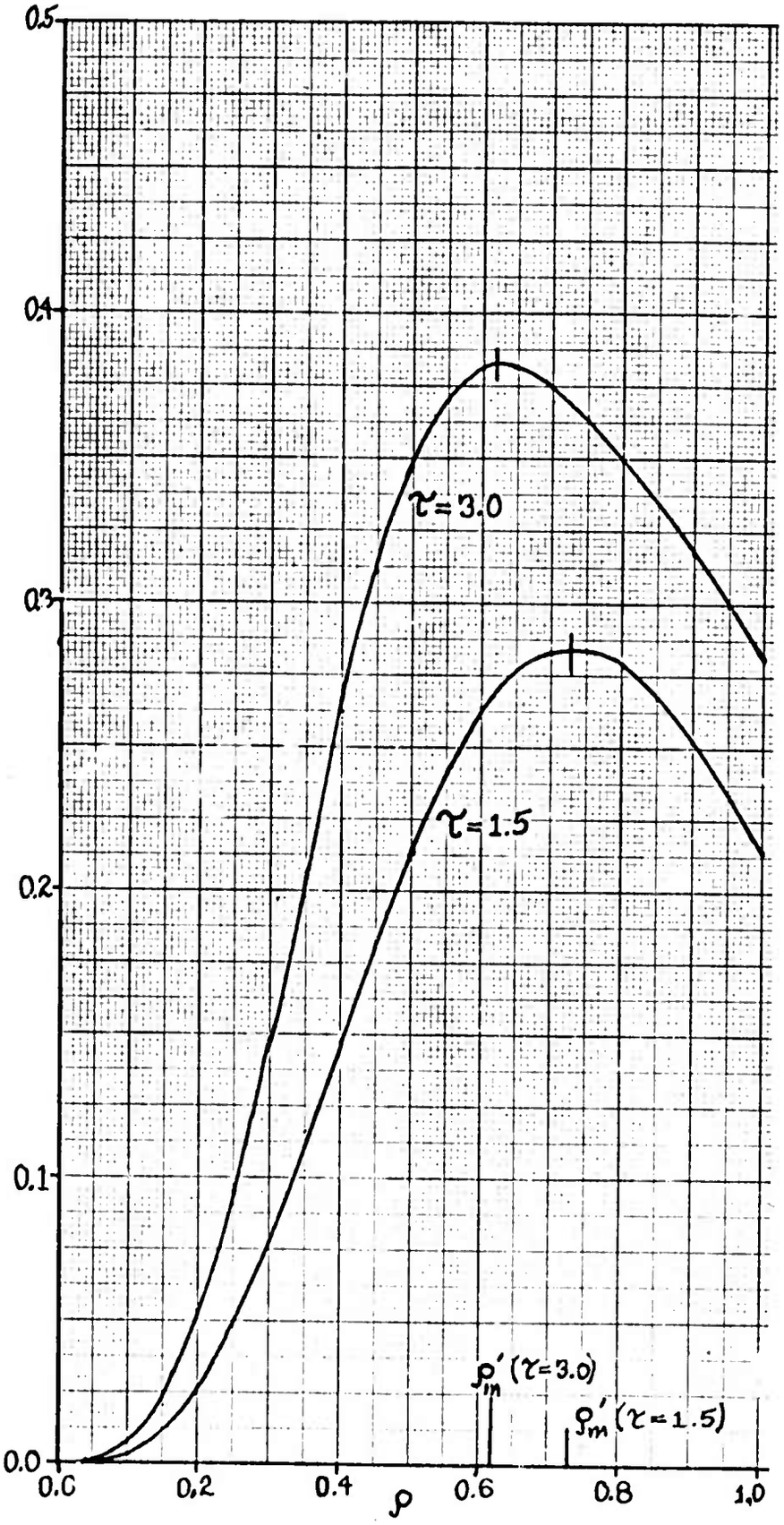


Fig. 12.4 Integrand of Equation (8.8) omitting the factor of $J_2 \exp i\varphi$.

## h.1 Initial Investigation of the Role of Inclusion Damage in the Failure of 10.6μm Optics

M. Bass, L.G. DeShazer, K.M. Leung, A.G.J. Balbin-Villaverde, U.O. Farrukh

During this quarter, the $CO_2$ TEA laser was operated; we began to characterize the absorptivity and scatter in the samples and an expression giving the probability that a defect which can be damaged be present in the irradiated volume was derived.

### h.1.a Operation of the $CO_2$ TEA Laser

During this quarter, the high-voltage power supply was received and installed. An exhaust system was installed to remove the exhausted gas and any ozone build-up from the TEA laser. Using all the available diagnostic equipment on hand for analysis, we had great difficulty discovering why the TEA laser did not operate. Near the middle of this quarter it was found that the cathode-anode separation was ~1/4" larger than it was supposed to be. This error was traced to incorrect machining during the construction of the electrode mounts. When the cathode-anode separation was modified to the prescribed 1.7 cm by inserting spacers between each electrode and its mount, a uniform main discharge was obtained with proper gas mixture and discharge voltage. As a result, with an optical cavity consisting of one 10 m radius, 100% reflective mirror and one flat 80% output mirror, the $CO_2$ TEA laser could be used as a source of pulsed 10.6μm laser light.

Absolute energy measurements of the laser output were performed using a ballistic thermopile (TRG 100). With the intracavity aperture open, the multimode output was 0.5 joules. This output was optimized with the input conditions indicated in Table 1. We noted that the laser output on a pulse to pulse basis was very repro-

ducible. A preliminary measurement of the $TEM_{00}$ output with intracavity aperture restricted to 0.6 cm diameter gave 20 mJ.

Since several of the electronic components of the laser broke down towards the end of this quarter, we were unable to optimize the $TEM_{00}$ mode output. We found that one trigger resistor was shorted out and the contacts for six of the energy storage capacitors were no longer reliable. Replacement of these discharge-circuit components have been located and are being sent to us.

Our assembly work on the TEA laser has shown the reliable electrical contact between the electrode holders and the storage capacitors is a necessary condition for a TEA laser of this design to operate. In the following months, we will optimize the $TEM_{00}$ mode output and attempt to operate the laser in single longitudinal mode by inserting an uncoated germanium etalon in the cavity.

h.1.b Characterization of Samples

Eighteen(18) samples have been acquired. Table 2 tabulates some preliminary information for these samples. We have characterized some samples by optical microscopy and calorimetry. In general, there are common scratches due to polishing on all sample surfaces. We are scheduled to characterize the scattering in our samples with the scatterometer at the Naval Weapons Center at China Lake. This should occur in mid-July. A crude scatterometer consisting of a He-Ne laser, a sample mount, a beam blocking stop and a photomultiplier is being assembled at USC to permit us to see if visible scatter and 10.6μm damage are correlated. When the damage measurements are completed we hope to be able to identify a relationship between scatter and 10.6μm laser induced damage.

h.1.c Spot-size Effect of Laser Induced Damage due to Bulk Damage

Laser-induced damage to dielectric surfaces are a function of the spot size of the laser-beam [1,2]. In our current studies we are investigating laser-induced damage to the bulk. Therefore, we calculated the expected spot-size dependence for bulk damage, following the calculation for surfaces.

The basis assumption is that the bulk defects, such as inclusions, are randomly distributed throughout the given material. If the laser beam encloses a certain volume V inside the material then the probability that n defects would be encountered is given by

$$P(n) = [(\rho V)^n/n!] \exp(-\rho V) \quad (1)$$

where $\rho$ is the density of defects. The probability that one or more defects are hit by the laser pulse is found by summing Eq. (1) over n and excluding n=0 or

$$P(V) = 1 - \exp(-\rho V) \quad (2)$$

Changing the volume V by changing the optical setup of the laser system will change the probability of encountering defects which is expressed mathematically

$$dP(V) = \rho dV \exp(-\rho V) \quad (3)$$

Let the intensity threshold of damage be $I_{th}$ and the peak intensity value be $I_p$.

If a pure Gaussian-profile laser beam is focused inside a given material, then the volume enclosed by a surface of constant intensity $I_{th}$ is given by [2]:

$$V_q = \tfrac{1}{2}\pi k W_o^4 \{ -\beta[1+(\beta^2/3)]\, \ell n[q(1+\beta^2)] + 2/3\,(\beta^3/3 + 2\beta - 2\tan^{-1}\beta) \} \quad (4)$$

where $q = I_{th}/I_p$,

$I_p$ = intensity at the waist,

$\beta = \left(\frac{1-q}{q}\right)^{1/2}$,

$W_o$ = Gaussian width at the waist where the electric field drops to 1/e of the peak value.

A plot of the $V_q/\pi k W_o^2$ vs q is given in Figure 1 [3].

Let $r_o$ be the mean separation of bulk defects. Thus

$$r_o = \int_0^\infty r\,dP(V) \quad (5)$$

where $V = \frac{4\pi}{3} r^3$. Eq. (5) could be best described as follows: Let us have $N_T$ points located throughout a given space of volume V with a density of points symbolized by $\rho$. Because of the randomness of the location of these points, all reference points are equivalent. Thus the mean distance is given by

$$r_{mean} = \frac{1}{\Sigma_{\ell=0}^{\infty} N_\ell} \Sigma_{\ell=0}^{\infty} N_\ell\, r_\ell \quad (6)$$

where $N_\ell$ is the number of particles in a volume $\Delta V_\ell$. That increment of volume $\Delta V_\ell$ has a mean distance $r_\ell$ from the reference point. Statistically the quantity $N_\ell/\Sigma_{\ell=0}^{\infty} N_\ell$ is replaced by dP(V) which is the change in probability of finding one or more particles in an increment of volume dV. The summation sign is replaced by an integral sign and Eq. (5) is then obtained.

After integrating Eq. (5) we express the bulk defect density $\rho$ in terms of the expected value $r_o$ or

$$\rho = \frac{3}{4\pi} \frac{1}{r_o^3} \left( \frac{\Gamma(1/3)}{9} \right)^3 \qquad (7)$$

where the gamma function $\Gamma(1/3) = 2.67893$. Substituting Equations (7) and (4) in Eq. (2) gives the probability of hitting one or more defects when the intensity threshold is $I_{th}$ or:

$$P(q, W_o) = 1 - \exp\left( - \frac{3}{4\pi} \frac{1}{r_o^3} \left( \frac{\Gamma(1/3)}{9} \right)^3 V_q \right) \qquad (8)$$

which is a general expression for any intensity ratio $q = I_{th}/I_p$, $W_o$ or $r_o$.

Table 1. Dimensions and Optimum Performance Details of the Multimode $CO_2$ TEA Laser.

| | |
|---|---|
| Discharge length | 41 cm |
| Discharge height | 5 cm |
| Discharge width | 1.7 cm |
| Discharge volume | 348 $cm^3$ |
| Cavity length | 120 cm |
| Mirror radius of curvature | 10 meters |
| Reflectivity of plane output window (Ge) | 80% |
| Storage capacitance | 0.08 μf |
| Trigger capacitance | 500 pf |
| Charging voltage | 23 kv |
| Input energy | 21 J |
| Output energy | 0.5 J |
| Efficiency | 2% |
| Flow rates (l/mm) ratio, $He:CO_2:N_2$ | 8.7:2.4:2.6 |
| Output energy density E/v | 1.4 J/l |

Table 2. Sample Materials for Inclusion Damage Studies

| Material | Sample No. | Size (mm x mm) | Thickness (mm) | Refractive Index n | Absorption ($cm^{-1}$) | Source |
|---|---|---|---|---|---|---|
| ZnSe | ZRMB | 45 x 68 | 3.5 | 2.43 | -- | Raytheon/M. Bass |
| ZnSe | ZRD-734 | 25 x 27 | 7.4 | 2.43 | 0.0046 | Raytheon/AFML |
| ZnSe | ZR II-VI | 25 dia. | 2.0 | 2.43 | -- | II-VI/Raytheon |
| KCl | KG-10 | 38 dia. | 12.0 | 1.49 | 0.0008 | Harshaw/AFML |
| KCl | KIC-4a | 25 x 25 | 4.0 | 1.49 | 0.0034 | International Crystal |
| KCl | KIC-4b | " | " | " | -- | " |
| KCl | KIC-4c | " | " | " | -- | " |
| KCl | KIC-4d | " | " | " | -- | " |
| KCl | KIC-4e | " | " | " | -- | " |
| KCl | KIC-65a | 39.5 x 39.5 | 6.5 | " | -- | " |
| KCl | KIC-65b | " | " | " | -- | " |
| KCl | KIC-65c | " | " | " | -- | " |
| KCl | KIC-65d | " | " | " | -- | " |
| KCl | KH-5a | 25 dia. | 5.0 | " | 0.0023 | Harshaw |
| KCl | KH-5b | " | " | " | -- | " |
| KCl | KH-5c | " | " | " | -- | " |

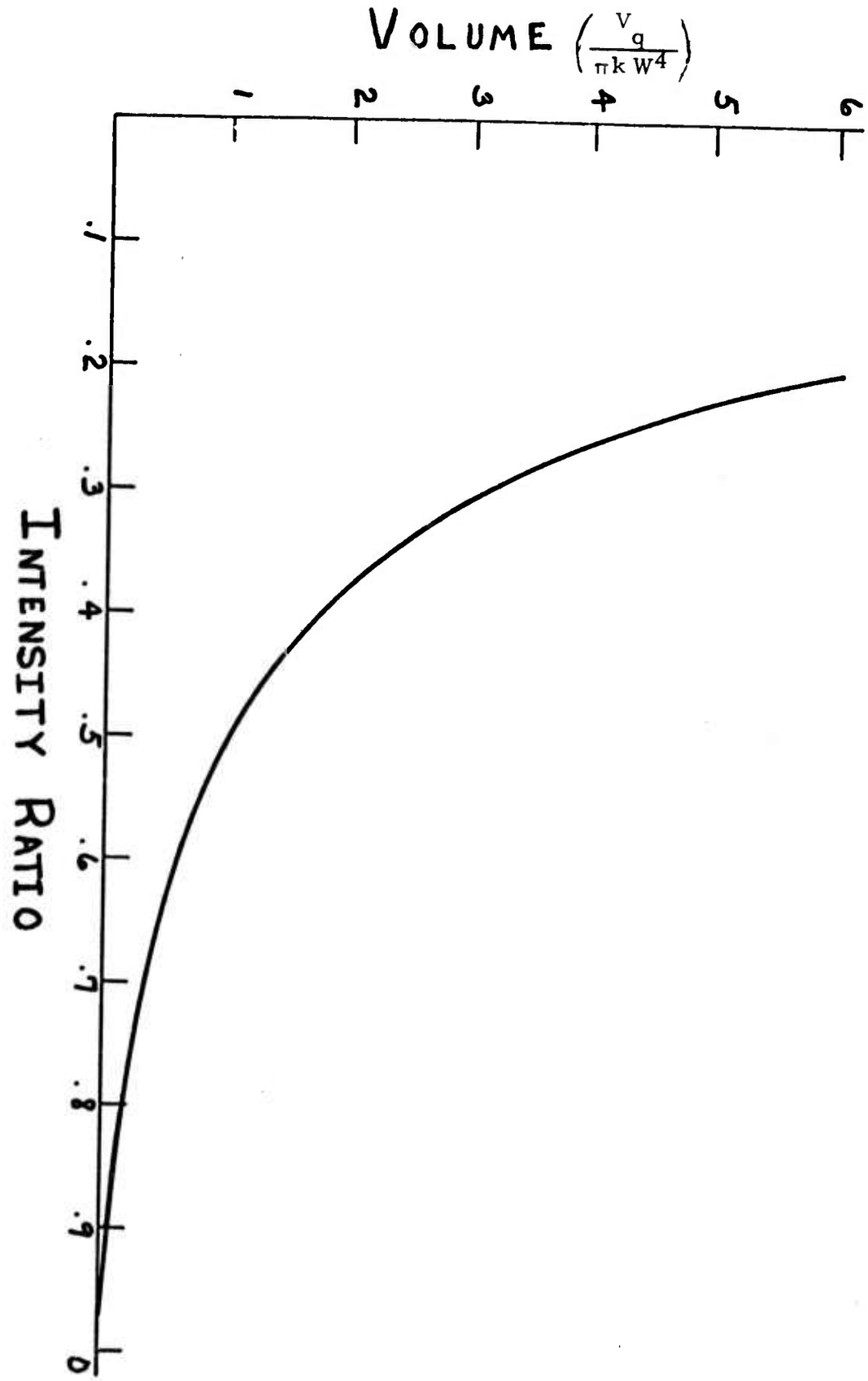
VOLUME $\left(\frac{V_q}{\pi k W^4}\right)$
1
2
3
4
5
6
INTENSITY RATIO
.1
.2
.3
.4
.5
.6
.7
.8
.9
0

Figure 1.

## REFERENCES


1. L.G. DeShazer, B.E. Newnam and K.M. Leung, Appl. Phys. Lett. 23, 607 (1973).

2. U.O. Farrukh, "Diffraction of Focusing of Truncated Gaussian Beams," U.S.C. Dissertation, 1974, p. 126.

3. Reference 2, p. 131.

## 3. DISCUSSION

A calorimeter combined with a tunable $CO_2$ laser was constructed and is available for general use between 9.4 and 10.8μm. Using this apparatus, a sixth sample of melt-grown GaAs was measured and was found to show an infrared absorption spectrum almost identical in structure and intensity to that of five previously studied samples. An apparatus to grow epitaxial layers of GaAs under electrochemical pumping and oxygen activity monitoring was used both to regulate and monitor the water content in hydrogen and then regulate and monitor the oxygen content of the gallium melt. Better epitaxial growth at low temperatures occurs with then without oxygen pumping.

The apparatus to grow thick layers of GaAs from liquid gallium at higher temperatures was completed and a first run has been made.

Attempts to deform GaAs at room temperature led to fracture on {110} without noticeable deformation or twinning; this shows that twinning is not a deformation mechanism under these conditions. Electron diffraction patterns of CdTe obtained in the electron microscope showed anomalous streaks and extra diffuse reflexions similar to those observed earlier with GaAs with an intensity increasing with temperature. Both are due to thermal diffuse scattering (and not to precipitates, as proposed in the literature).

Measurements have been done to relate the properties of CdTe, pure and doped with indium at high temperature in equilibrium with a vapor of well-defined cadmium pressure to those of the crystals after rapid cooling to room temperature. Free electrons present as a result of a deviation from stoichiometry at high temperature and high cadmium pressure are no longer formed after cooling; electron microscopy shows the presence of precipitates, probably cadmium. With lower supersaturation dislocation rings are found, indicating that the excess of cadmium was present mainly as interstitials. Electrons due to foreign donors (indium remain in the sample, either partly or totally. Further studies are required to decide on this point.

Weakly doped crystals from high $p_{Cd}$' free holes when cooled from low $p_{Cd}$ (= $p_{Te_2}$) with a narrow transition range at intermediate $p_{Cd}$.

Indium doped crystals show after cooling free electrons when cooled from a cadmium pressure above a critical limit, and no free carriers below this limit down to the phase boundary. A lowest absorption coefficient at 10.6μm of $9.9 \times 10^{-4}cm^{-1}$ was found for cooling rapidly a thin sample from 700°C, $5 \times 10^{-3}$ atm. cadmium. Thicker samples which could not be cooled so rapidly showed a larger absorption coefficient and a correspondingly larger carrier concentration. This

effect is due to a shift of the conductivity cut-off to lower $p_{Cd}$ with slower cooling and is attributed to precipitation of native electron traps, $V_{Cd}'$. Cooling after annealing at 700°C at $p_{Cd} < 5 \times 10^{-3}$ atm. may not show this effect but may give a higher absorption due to tellurium precipitation. The optimum conditions are being determined. In addition, attempts are being made to introduce deep trapping levels of a different nature by suitable doping.

High density CdTe has been made by hot pressing in the presence of $CdCl_2$ as a liquid sintering aid, but with and without the use of a seal to present early escape of the sintering agent.

Optical studies have been carried out on pure polycrystalline ZnSe, and single crystalline ZnSe + Al. The latter, when annealed under zinc vapor shows considerable electron conductivity and free carrier absorption $\propto \lambda^3$. Local mode studies show several absorption bands, one of which can be assigned to $Al_{Zn}^{\bullet}$. Assignments for the others are as yet uncertain. The method to measure the dielectric constant of GaAs, CdTe and ZnSe has been refined; final values will be reported in the next progress report.

The discrepancy between the theoretically predicted low 10.6μm absorptio coefficient of KBr and the value actually found is attributed to impurities, probably $BrO_3^-$. Efforts are being made to prove this and to achieve improvement by decomposition of the bromate ion. Attempts to attach the bromate ion with $C_2F_4$ (the latter made by thermal decomposition of teflon) have been abandoned because of decomposition of the $C_2F_4$ and the danger of explosions due to this decomposition. Reduction of bromate by liquid potassium led to coloration by F center formation and an increase rather than a decrease of the 10.6μm absorption. A favorable effect may still occur after removal of the F centers by subsequent bromination.

Acoustic probe studies of alkali halide surface coupled by a liquid to a piezoelectric material were continued with Y-cut quartz, lithium niobate and Bi-Ge oxide as piezoelectric materials. All could be used, but the easily available Y-quartz appears to be the best candidate. The measured phase change depends on the temperature distribution near the surface up to a depth of one acoustic wavelength. A theory to analyze the results is presented.

The characterization of optical performance on the basis of the diffraction theory of thermal lensing was extended to anisotropic crystalline windows. Cubic crystals oriented in 111 direction give cylindrical symmetry of the elastic properties in the plane stress approximation. The influence of birefringence in the focal intensity and off-axis intensity was investigated.

An experiment is designed which yields the information required to determine the relative contributions of the non-linear dipole moment and anharmonic forces to multi-phonon absorption.

The TEA laser for optical damage studies was put in operation. It has an output of 0.5 Joule in multimode pulse mode. The $TEM_{oo}$ power, not yet optimized, was 20 mJ at an intracavity aperture diameter of 6 mm. The spot size effect of inclusions on bulk damage was calculated for a random distribution of inclusions.